The Role of Biosphere-Atmosphere-Ocean Interactions in the Climate of West Africa During the Middle Holocene

by

Michelle Marie Irizarry-Ortiz

B.S. in Civil Engineering, University of Puerto Rico (1999)

Submitted to the Department of Civil and Environmental Engineering
in partial fulfillment of the requirements for the degree of

Master of Science in Civil and Environmental Engineering

at the

MASSACHUSETTS INSTITUTE OF TECHNOLOGY

June 2001

Author . . . .
Department of Civil and Environmental Engineering
May 21, 2001

Certified by . . . . . ,. . . . .
Elfatih A. B. Eltahir
Associate Professor
Thesis Supervisor

Accepted by . . . . . . ___ . . . .
Oral Buyukozturk
Chairman, Department Committee on Graduate Students
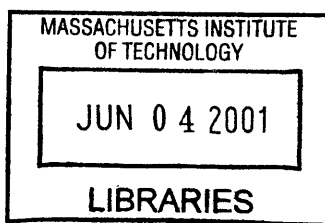
The Role of Biosphere-Atmosphere-Ocean Interactions in the Climate of West Africa During the Middle Holocene

by

Michelle Marie Irizarry-Ortiz

Submitted to the Department of Civil and Environmental Engineering
on May 21, 2001, in partial fulfillment of the
requirements for the degree of
Master of Science in Civil and Environmental Engineering

Abstract

In previous studies, a zonally symmetric, synchronously coupled biosphere-atmosphere model (ZonalBAM), which includes explicit representation of ecosystem dynamics, has been developed and validated based on current forcings over the region of West Africa. Here, we use ZonalBAM to study the response of the coupled biosphere-atmosphere system to changes in the Earth's orbital forcing during the Middle Holocene (6K yrs BP) and the relative contribution of vegetation and ocean feedbacks.

Simulations in which vegetation conditions were prescribed to the current distribution, show that an orbitally-induced increased seasonality in insolation for the Middle Holocene, by itself, results in a 1.1° northward shift in the location of the southern margin of the Sahara as compared to current solar forcings. When vegetation dynamics are allowed, a 2.4° northward shift is simulated. However, when dynamic vegetation is initialized according to *Hoelzmann et al.*'s [1998] map of palaeovegetation, a 5.1° northward shift is simulated, bringing results more consistent with palaeoevidence. Contrary to other studies, these results suggest that multiple climate equilibria could have coexisted over the region of West Africa during the Middle Holocene. Furthermore, based on previous studies on the current climate over the region [*Wang and Eltahir*, 2000b], we hypothesize that transitions between these different equilibria could have taken place during the Middle Holocene causing the southern desert margin to migrate between 18.1° N and 21.4° N and shaping low frequency climate variability.

In spite of a cold bias in the simulated sea surface temperature (SSTs) for the current climate, the addition of an interactive mixed layer ocean model (MLOM) to ZonalBAM provided some insight into how changes in the SSTs in the South Eastern Tropical Atlantic (SETA) could have resulted in enhancement of the monsoon circulation during the Middle Holocene. We hypothesize that the addition of an oceanic component into Mid-Holocene simulations could result in a more northward position of the southern desert margin, bringing our simulations in much better agreement with reconstructions.

Thesis Supervisor: Elfatih A. B. Eltahir
Title: Associate Professor

Acknowledgments

To my mom, Ada, whose dedication and support throughout my life and education made me the person I am today.

Contents

7

List of Tables

10

List of Figures

11

14

15

18

Chapter 1

Introduction

1.1 Background and Motivation

Located in the region between ˜15° N and ˜30° N over the African continent (Figures 1-1 and 1-2) and spanning an area of about 9,000,000 km² [*Tucker and Nicholson*, 1999], the Sahara Desert is currently the largest desert in the world. It is bounded by the transitional zones of the Sahel in the south and the Mediterranean in the north. The desert border is defined by the location of the 200 mm/yr precipitation isohyets. Today, this region is a harsh deserted environment where life-supporting resources are scarce. But, some 6000 years before present, during the Middle Holocene, it was thriving with catfish, hippos, elephants, giraffes, and other water-dependent animals. Lake levels were high [*Fontes and Gasse*, 1991; *Gasse and Van Campo*, 1994; *Petit-Maire and Guo*, 1997], wetlands were abundant [*Hoelzmann et al.*, 1998], and sand dunes were generally dormant [*Sarnthein*, 1978].

Climate reconstructions based on proxies such as pollen assemblages, lake sediments, and marine cores support this picture (Table 1.1) [*Street and Grove*, 1976; *Ritchie et al.*, 1985; *Lézine*, 1989; *Pachur and Hoelzmann*, 1991; *Street-Perrott and Perrott*, 1993]. Bones found in dry riverbeds, pottery, utensils, pictures, and carvings left by ancient civilizations show the transition from sedentary to pastoralist lifestyles and remain as evidence of how climate shapes the human life [*UNESCO*, 1962; *Petit-Maire et al.*, 1990]. It is based on this evidence that the scientific study of climate

change serves its purpose: Understanding the causes behind past climate change is key in predicting the future impact of both natural and anthropogenic forcings, which will ultimately influence the fate of the human race.
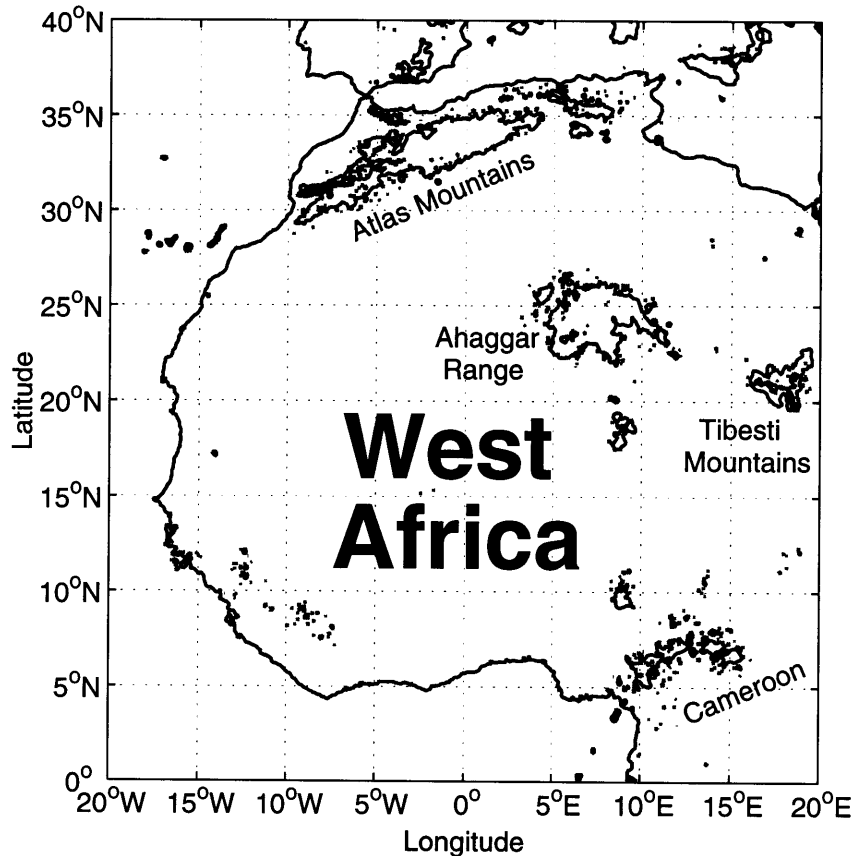
Figure 1-1: Region of West Africa showing the location of the main topographical features.

Before attempting to use a climate model to simulate future climates, it should be able to appropriately reproduce conditions existing under current forcings. However, in order to increase our confidence in the model's ability in simulating climate change, it must successfully reproduce the main features of past climates for regions where there are enough observations available to allow for comparison. The Middle Holocene (6K yrs BP) has been widely chosen as a case study for model validation since the effects of insolation on climate can be isolated for the period. There is evidence that during the Middle Holocene, CO_2 concentrations were close to the preindustrial

value, the ice sheets had already retreated to their current extent [*Peltier*, 1993], and the SSTs were not significantly different from the current [*Ruddiman and Mix*, 1993; *Felzer et al.*, 1998]. Additionally, but most importantly, the vast amount of proxies available for climate reconstruction over the region of West Africa during the period presents a unique opportunity to test model results against observations. Synthesis of Mid-Holocene data in the region are required in order to test the ability of climate models to simulate conditions under forcings different from the current.

This constitutes the basic motivation behind this research: to understand the mechanisms behind past climate change as a basis for extrapolation into studies of future climate change. With the purpose of gaining a deeper understanding of the mechanisms behind climate change over the West African region, we attempt to validate the utility of our climate model, ZonalBAM, in reproducing past changes, using the Middle Holocene as a basis for comparison with the current climate.
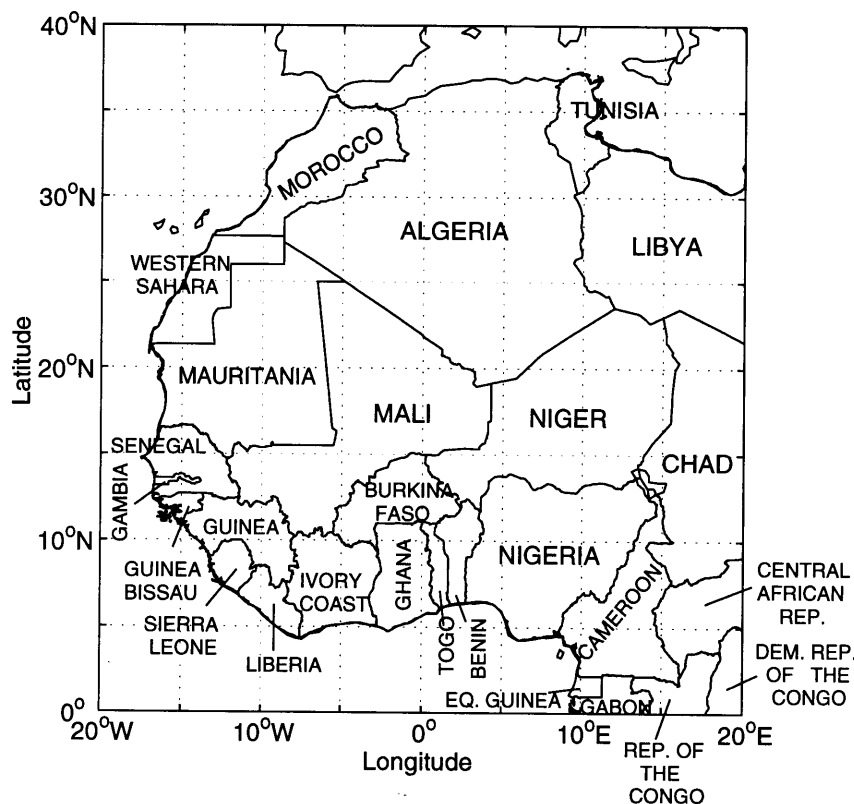
Figure 1-2: Political map of West Africa.

21

Location	Long.	Lat.	Reconstructed prec. (mm/yr)	Reference
Lake Chad, Nigeria	16°30′ E	13°44′ N	(300 to 350) +current	*Kutzbach*, 1980
West Nubian Basin, Sudan	25°30′ E	18°30′ N	total: 500 to 900	*Hoelzmann et al.*, 2000
Oyo depression	26°11′ E	19°16′ N	total: 300	*Ritchie et al.*, 1985 *Lézine*, 1989
Chemchane, Mauritania	12°13′ W	20°56′ N	total: 400	*Lézine*, 1989

Table 1.1: Reconstructed total annual precipitation in North Africa for the Middle Holocene.

1.2 Orbital Theory

Before attempting to fully understand the mechanisms underlying the expansion of the Sahara Desert to its current extent it is important to start by analyzing how the driving force of the climate system, namely the energy balance, changed during the period. This is achieved by invoking the astronomical theory developed by the Serbian scientist Milutin Milankovitch in the 1920s.

The geometry of the Earth's orbit can be defined by the three classical astro-insolation parameters based on the pioneering studies of Milankovitch, namely the obliquity, eccentricity, and precession (Figure 1-3). These parameters vary in time, mainly as a result of the gravitational forces exerted on the Earth by other planets. As a consequence, three timescales of climate change are produced, affecting the latitudinal and seasonal distribution of incoming solar radiation at the top of the Earth's atmosphere. Based on astronomical considerations, these parameters can be obtained as a summation of sinusoidal terms whose amplitudes, frequencies, and phases have been most recently estimated by *Berger* [1978a,b]. Furthermore, these can also be evidenced on proxy records of climate such as the oxygen-isotope content of foraminifera and in the chronology of tropical reef development.
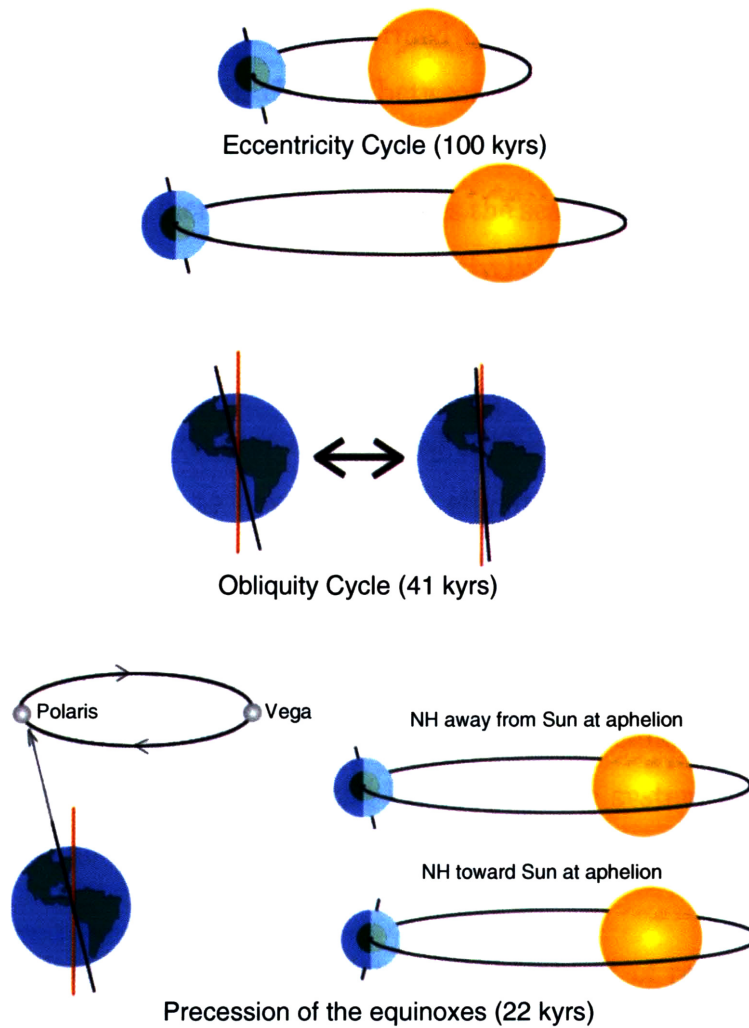
Figure 1-3: Classical astro-insolation parameters, and their associated periodicities, based on the works of Milankovitch in the 1920s.

Precessional cycles reflect secular changes in the Earth's perihelion –the season when the Earth is closest to the Sun. Precession can be separated into two components: axial and elliptical precession. Axial precession results from the torque of the Sun and Moon on the Earth's Equator causing the Earth's axis of rotation to wobble with a period of 26 kyrs. Elliptical precession, which results from planetary effects on the entire Earth's mass, causes the Earth's elliptical orbit to rotate independently about one of its focus. The resulting effect is that the equinoxes and solstices shift slowly around the Earth's orbit with a period of 22 kyrs.

Obliquity refers to the degree of tilting of the Earth's axis of rotation with respect to the plane of the ecliptic –the plane formed by the Earth's orbit around the Sun. The obliquity of the Earth's axis changes between 22° and 25° with a period of 41 kyrs as a result of planetary effects on the position of the ecliptic in space. The climatic effect of obliquity is that increased tilt amplifies the seasonality at high latitudes since a greater tilt would expose polar regions to relatively more radiation than the tropics.

Eccentricity is related to how the shape of the Earth's orbit changes in time with a period of 100 kyrs. It results from the gravitational pull of the Sun and planets. At one extreme the orbit approaches a circle and at the other a more elongated ellipse. More elliptical orbits tend to have a greater climatic influence on the seasons, but this effect mainly acts as a modulator of the precessional cycle producing periodic effects every 19 kyrs and 23 kyrs [*Cronin*, 1999].

So, from this limited perspective, the periodicity inherent in these parameters would result in periodic climate changes significant over milenial-timescales. However, due to the existence of feedbacks in the Earth's climate system and recently more important, due to anthropogenic effects, the response of the climate system is highly non-linear.

The Middle Holocene (6K yrs BP) has been the object of recent study since the effects of insolation on climate can be isolated for the period, while the extent of the ice sheets [*Peltier*, 1993] and global SSTs [*Ruddiman and Mix*, 1993] were similar to today's. The period of maximum insolation resulting from changes in the Earth's orbit in fact occurred during the Early Holocene (9K yrs BP). However, since the Laurentide and Scandinavian ice sheets were still present at 9K yrs BP and CO_2 concentrations were significantly different from preindustrial levels, the Middle Holocene has been widely chosen for comparison with current forcings. During the Middle Holocene (6K yrs BP), the insolation anomaly was about 6 % (~25 W/m^2) greater in the Northern Hemisphere summer and 6 % less in the Northern Hemisphere winter, mainly because perihelion occurred near the autumnal equinox (rather than close to winter solstice as today) and the Earth's axial tilt was larger than at present (24.10° versus 23.45°). Precessional cycles have been found to be the most important pa-

rameter influencing low and middle latitude seasonality, and consequently, climatic processes such as tropical wetland activity, equatorial upwelling, and tropical monsoons [*Prell and Kutzbach*, 1987]. Nevertheless, the effect of increased tilt on monsoon circulations has been found to be of secondary importance [*Park and Oglesby*, 1990].

It is of current scientific interest to understand the mechanisms through which these insolation changes enhanced the monsoon climate of West Africa during the period resulting in a significant rainfall increase, as has been widely recorded. Palaeontological, geochemical, and sedimentological proxy records suggest significantly wetter conditions over the Sahel/Sahara region during the Middle Holocene (6K yrs BP). Evidence exists of grass/savannah vegetation expanding as much as 500 km further north (to at least 23° N) and lakes showing significantly wetter conditions to about 30° N as compared to current conditions. The great amount of palaeodata available and the vast number of studies performed for the region, present a unique opportunity to test a model's performance when subject to different forcings.

1.3   Literature Review on Palaeoclimatic Evidence

The importance of using models in which the components of the climate system are synchronously coupled has been stressed by several studies as the key to more accurately reproduce the palaeoclimate [*Broström et al.*, 1998; *Hoelzmann et al.*, 1998; *Braconnot et al.*, 1999; *Foley et al.*, 2000]. However, efforts in this direction have been limited both by computational constraints and the lack of a quantitative set of boundary and initial conditions for the period.

Advances in the use of proxies for the reconstruction of past climates have allowed scientists to get more insight into the mechanisms of past climate change and have served as significant tools for model evaluation [*Kohfeld and Harrison*, 2000] and development. Several palaeoenvironmental datasets have been developed recently. With recent advances in the spatial coverage, quality, time resolution, dating control and interpretation of observations, these datasets are becoming more and more useful in model evaluation. However, their use as boundary and initial conditions for model

simulation is limited due to the spatial generalization and regridding required, processes through which detailed features in the data could be lost. For example, *Martin* [1998] has demonstrated that in AGCMs, the biome-based inference of vegetation characteristics is not equivalent to the cell-by-cell estimation of these parameters.

In the subsequent sections these proxy-based reconstructions of the Mid-Holocene climate over West Africa are presented based primarily on the component of the climate system they describe.

1.3.1 Vegetation and Soils

Several studies using atmospheric general circulation models (AGCMs) in which only changes in insolation were taken into account, have consistently underestimated [*Kutzbach and Guetter*, 1986; *Yu and Harrison*, 1996; *Hall and Valdes*, 1997; *Masson and Joussaume*, 1997] the expected greening of the Sahara during the Middle Holocene. Their results suggest that some positive feedback mechanisms are needed to explain the full magnitude of the observed greening. Although the vegetation, soil, lake, wetland, and ocean feedbacks on climate have been omitted in these studies, these have been identified as the possible mechanisms through which orbital forcings could have been enhanced to produce the recorded significant rainfall increase. The reasoning behind this has been demonstrated by *Eltahir and Gong* [1996]. They have found that the strength of the monsoon circulation, bringing moisture from the ocean inland during summer, is controlled by the gradient of boundary-layer moist static energy between the land and the ocean. Consequently, changes over land or over the ocean will result in changes in the surface fluxes which feed the boundary layer with moist static energy, and will, therefore, affect its gradient.

From previous studies it has become evident that the inclusion of changes to the vegetation conditions during the Middle Holocene is important in order to get a better match between the simulated and reconstructed climate. Therefore, the need for a detailed database of vegetation distribution and characteristics for the Middle Holocene has become critical. It would serve as both boundary/initial conditions and as a basis for the comparison of model simulations. The most recent efforts in

this direction include reconstructions of palaeovegetation by the BIOME 6000 project [*Hoelzmann et al.*, 1998; *Jolly et al.*, 1998, 1999; *Prentice et al.*, 1998], the National Climate Research Program of the German Government (hereafter called NCRPGG) [*Anhuf et al.*, 2000], and the Quaternary Environment Networks (hereafter called QEN) [*Adams*, 1997; *Adams and Faure*, 1997].

Using mostly pollen data from terrestrial and marine sediment cores, past vegetation cover has been reconstructed by these groups. These reconstructions show a significant shift from desert to grass/savannah vegetation in the Early- to Mid-Holocene as a result of wetter conditions in the region, consistent with a monsoon enhancement. As an example, *Jolly et al.*'s [1998] biome reconstruction from continental pollen data, show that the Sahara/Sahel boundary was as far north as 23° N in eastern and central northern Africa, respectively. Their pollen data from marine cores suggest a more southward position of this boundary in coastal western Africa, probably between 15° N and 19°N [*Rossignol-Strick and Duzer*, 1979; *Hooghiemstra*, 1989]. Similarly, the most northward location of this boundary in western Africa during the period, was identified as 20° N in NCRPGG's reconstruction based on pollen data alone [*Anhuf et al.*, 2000]. However, evidence on the existence of vegetation in the margins of the today hyperarid Tanezrouft Desert, located in southern Algeria and the border zone of Mali (~23° N and ~1° E) in the middle of the Sahara, suggest that conditions were significantly greener even further north [*Petit-Maire et al.*, 1990].

According to *Hoelzmann et al.* [1998], the most reliable method for reconstructing local vegetation is based on pollen records. However, since pollen preservation in arid to semiarid areas is generally poor, supplemental data is required [*Street-Perrott and Perrott*, 1993]. The addition of charcoal and plant macrofossil data from several archaeological sites in the region has been used by *Hoelzmann et al.* [1998] and *Jolly et al.* [1999] to supplement the pollen data in the BIOME 6000 project. A map of the vegetation distribution at 6K yrs BP has been produced by the BIOME 6000 project by determining the diversity and abundance of taxa belonging to different plant functional types (pfts). Based on the relative abundance of each pft, biomes have been assigned between 5 types and tabulated in terms of the percentage of

the area occupied in a 1°X1° grid. Additionally, percentages of wetland and lake areas are included in the dataset, which is available through the internet. Their vegetation distribution is similar to that of the QEN, except for small discrepancies due to differences in the vegetation classification. BIOME 6000's more complete reconstruction shows grassland extending to at least 23° N in the western and eastern Sahara, and up to 26° N in the region north of Lake Chad in the central Sahara [*Broström et al.*, 1998; *Hoelzmann et al.*, 1998]. In addition, lake reconstructions represent a good alternative when other data sources are scarce. Evidence of this is shown in *Jolly et al.*'s [1998] reconstruction of lake-levels from the coastal region of West Africa, where they found conditions wetter than present to at least 21° N, instead of the 19°N found based on marine pollen data alone. Several studies [*Kutzbach et al.*, 1996; *Doherty et al.*, 2000; *Texier et al.*, 2000; *Carrington et al.*, 2001] also suggest the possibility that the distribution of vegetation north of ~20°-25° N was not as spatially continuous as has been inferred from the interpolation between a limited number of sites, and that local moisture recycling may have played an important role in maintaining regional-scale patches of vegetation/lakes/wetlands rather than a uniform continental-scale vegetation shift.

In the equatorial region, data from the BIOME 6000, shows a reduction in the West African rainforest and precipitation near Cameroon when compared to the present [*Jolly et al.*, 1998], consistent with a more northerly position of the monsoon front during summer as a result of a more seasonal climate near the Equator. However, data compiled by the QEN [*Hamilton*, 1988] show that rainforest extent during the period was greater than today.

Consistent with the greener vegetation distribution in the Sahel/Sahara region during the Middle Holocene, a higher organic content in the soils of the region is evident in several locations [*Petit-Maire and Riser*, 1983; *Haynes*, 1985]. This change resulted in a higher soil moisture capacity and a decreased surface albedo, the latter of which could have contributed to the monsoon enhancement by affecting the energy balance at the surface. Additionally, evidence on generally dormant sand dunes [*Sarnthein*, 1978], and consequently, lower aerosol dust loadings in the Eastern Equa-

torial Atlantic [*de Menocal et al.*, 2000] during the period, are consistent with higher precipitation and soil moisture conditions.

In addition to the direct inference of vegetation conditions, several methods to translate pollen data into quantitative estimates of climatic variables, such as temperature and precipitation, exist [*Guiot*, 1990; *Vincens et al.*, 1993]. As an example, *Street-Perrott and Perrott*'s [1993] reconstruction from pollen data show wetter conditions in the coastal areas of West Africa and in Chad at 6K yrs BP. Other efforts in this direction have similarly yielded very sparse data, which is not useful for the comparison of model simulations. Therefore, several climate modelers [*Jolly et al.*, 1998] have used an alternative approach in which the simulated climatic variables are translated into vegetation types by the use of biome models, and the resulting maps are directly compared to observations of vegetation cover at a site.

1.3.2 Surface Waters

As demonstrated on the previous section, although pollen-based reconstructions of past climates are more reliable, their preservation is poor in arid to semiarid areas [*Street-Perrott and Perrott*, 1993]. Therefore, reconstructions based on lake-levels present a good alternative. Lakes in arid to semiarid areas are very sensitive to variations in their hydrological cycle. Therefore, these have served as the most common indicators of climate change during the Holocene. Additionally, they contribute to the local hydrologic budget and interact with the climate by modifying the characteristics of the land surface. Due to their high heat capacity they serve as buffers by limiting the range of temperature fluctuations. Also, their high water content favors evaporation over sensible heating.

The Holocene record of lake-level fluctuations in West Africa has been derived from various sources such as the distribution of nearby archaeological sites, the location of old shorelines, and the stratigraphy and geochemistry of sediment cores. The Oxford Lake-Level Data Bank, derived as part of the Cooperative Holocene Mapping Project [*COHMAP Members*, 1994], comprises records of lake status, a measure of relative water depth, for lake basins which have been closed for part, or all, of their Late

Quaternary history. In this data bank, lake status was originally determined at 1000-year intervals between 30K yrs BP and the present day (0K yrs BP = 1950 AD), and is given as a relative value with respect to the total altitudinal range of fluctuation. It is divided into low (0-15% of range, including dry lakes), intermediate (15-70% of range), and high levels (70-100% of range, including overflowing lakes). Figure 1-4 shows the difference in the lake-level status between the Middle Holocene and the current conditions. It can be noticed that lake-levels were higher to much higher than the present during the Middle Holocene. Neglecting the lagged response to climate change of groundwater recharge into lakes, changes in the lake area and depth can be seen as resulting from changes in the net water balance $(P - E)$. Additionally, since the changes shown in Figure 1-4 occurred simultaneously in such a vast area, the hypothesis for significantly wetter conditions over West Africa during the Mid-Holocene is strongly supported.
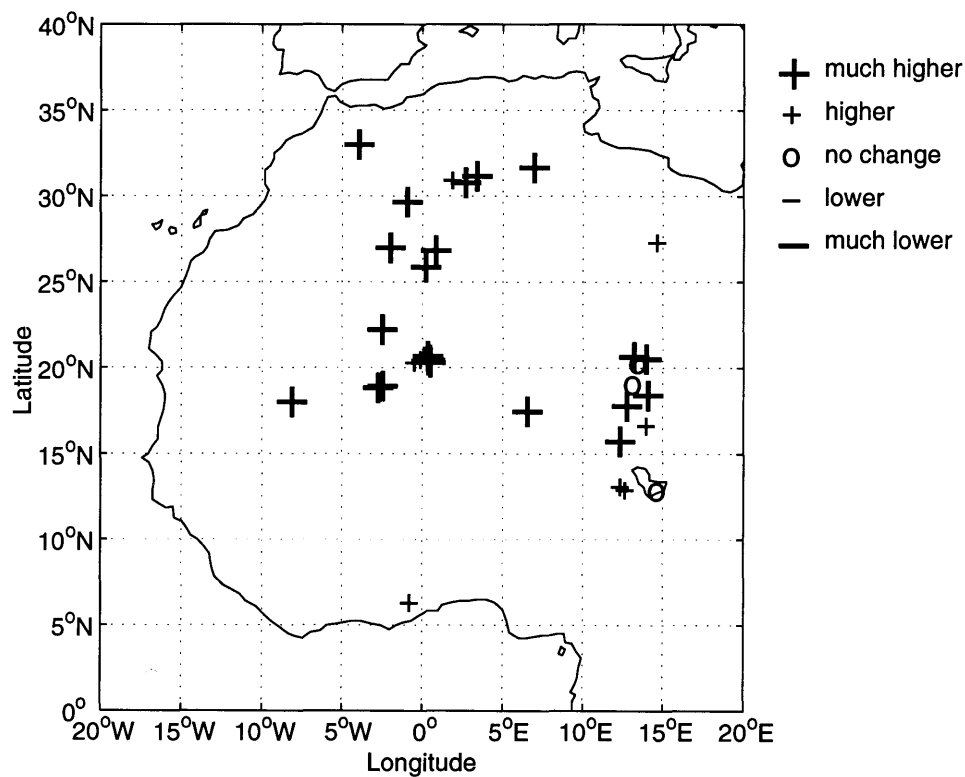
Figure 1-4: Difference in the lake level status between the Middle Holocene and the current climate based on reconstructions by *COHMAP* [1994].

Hoelzmann et al.'s [1998] reconstruction of palaeovegetation as part of the BIOME 6000 project, also includes the areal percentages occupied by wetlands and open-water lakes as well as the primary direction of surface drainage. Their dataset suggest that lake-levels were higher as far north as 30° N. They have found that the total areal percentage occupied by surface waters during the Middle Holocene was about 7.4%, which is more than a tenfold expansion as compared to their current extent. Wetlands occupied 4.6% (~750,000 km^2) of the total area in north Africa, with 1.1% in the west and 8.2% in the central and eastern portions. Similarly, lakes occupied 2.8% (~460,000 km^2) of the total land surface in north Africa, with 5.8% in the east and 0.5% in the west. The largest percentage of lakes in the eastern part of north Africa is due to the inclusion of Lake Mega Chad, which was fed by rivers from the eastern Tibesti Mountains (Figure 1-1) and occupied about 350,000 km^2 (as compared to its current extent of 20,000 km^2) [*Schneider*, 1967; *Pachur and Altmann*, 1997; *Kohfeld and Harrison*, 2000]. Their data also suggests a very extensive area of wetlands to the southeast of Lake Mega Chad similar to the scale of the lake itself, giving rise to an estimate of an additional 300-350 mm/yr of rainfall required for their sustenance. Additionally, large areas occupied by lakes were located in the Niger Basin (~15,200 km^2-56,000 km^2) [*Petit-Maire*, 1987, 1988, 1989], the Mali Desert (~7,600 km^2) [*Petit-Maire and Riser*, 1983], West Nubia (~7,000 km^2) [*Pachur and Rottinger*, 1997], and the Danakil Desert (~7,000 km^2) [*Gasse et al.*, 1974].

According to *Petit-Maire and Guo* [1997], the recorded water spots were located in nearly all the impervious closed depressions which could retain rainfall water or between dunes, but also in areas prone to feeding by regional aquifers. For example, evidence on small freshwater lakes were found at the region occupied today by the hyperarid Tanezrouft Desert (~23° N, ~1° E) in the middle of the Sahara, whose seasonal waters provided nomadic cattle herdsmen with freshwater and a place to stay for a few days or weeks [*Petit-Maire et al.*, 1990]. They found that the evidence for high lake-levels was scarcer, but still existent, from 24° N to 30° N due to the flatter landscape of the region which was not favorable for the formation of surface waters. They believe that the occasional precipitation that fell quickly infiltrated

31

or evaporated due to the high potential evaporation in the region. Their evidence suggests that two sources of rains fed these water bodies: one originating from the south (basically the monsoon rains), and one from the northwest corresponding to polar depressions and Atlantic cyclones which were predominant during winter and were more able to cross the barrier formed by the Atlas mountains (Figure 1-1).

Geomorphic and sedimentological evidence show that during the Middle Holocene, there was a major expansion of the surface drainage network as compared to today. The Sahara was drained by rivers and wadis, some of which can still be observed on satellite images [*Hoelzmann et al.*, 1998]. According to *Petit-Maire and Riser* [1987], some of these channels were occupied by perennial rivers, but most seemed to have been occupied episodically. Most large rivers are believed to have followed similar courses as today (e.g. Senegal and Niger Rivers), but the amount of water transported was significantly larger during the Mid-Holocene with increased inputs to the Mediterranean, which are consistent with large increases of freshwater input to the region [*Rossignol-Strick et al.*, 1982; *Rossignol-Strick*, 1985]. In the central Sahara, large drainage systems forming on the eastern Tibesti mountains flowed northward to the Mediterranean and southward to the region near Lake Mega Chad.

From these reconstructions, it is evident that on average conditions during the Middle Holocene were significantly wetter than today. However, several studies indicate that conditions during the Holocene were probably much more complex than previously thought. This issue will be discussed in more detail in Section 1.3.6. Limitations in the temporal resolution of lake-level reconstructions tend to obscure possible high-frequency fluctuations in the extent of the monsoon penetration. As an example, lake-level reconstructions by *Gasse and Van Campo* [1994], suggest dry events of minor amplitude around 6K yrs BP. They found a marked decline in the lake-levels of the Termite (16°05' N, 11°15' E) and Bougdouma sites (13°19' N, 11°40' E) at about 6.3-6K yrs BP.

1.3.3 Ocean Conditions

Reconstructions of sea surface temperature based on planktonic foraminifera from ocean sediment cores [*Morley and Dworetzky*, 1993; *Ruddiman and Mix*, 1993] show only small changes for the Middle Holocene. In general these reconstructions show slightly cooler SSTs along the Equatorial Atlantic and off the northwestern coast of West Africa. However, most of these changes are close to the standard error of the transfer function, and are, therefore, not statistically significant. Additionally, complex patterns of positive and negative anomalies were found in relatively small areas, making their interpretation more difficult.

Due to the large thermal capacity of the ocean, the insolation changes that took place during the Middle Holocene were probably not enough to cause large direct changes. Additionally, land ice and sea level were the same as current since the Laurentide and Scandinavian ice sheets had already retreated [*Kutzbach and Guetter*, 1986; *COHMAP Members*, 1988; *Peltier*, 1993; *Ruddiman and Mix*, 1993; *Felzer et al.*, 1998]. Atmospheric CO_2 concentrations were also close to their preindustrial levels. For all these reasons, SST anomalies are expected to be small as shown in reconstructions. However, it is believed that an orbitally-induced increased low-level flow into West Africa could have resulted in weaker trade winds and equatorial upwelling during the Middle Holocene producing a small localized warming of the Tropical North Atlantic (TNA: 10° N-25° N) [*Kutzbach*, 1981; *Ruddiman and Mix*, 1993]. An interplay between a small orbitally-induced direct cooling of the South Eastern Tropical Atlantic (SETA: 25° S-5° N and 15° W-15° E) region and the indirect warming of the TNA, expected due to weaker trade winds could at least partially explain the complicated patterns found in the SST anomalies during the Mid-Holocene.

Based on simulations with a synchronously coupled atmosphere-land-ocean-sea ice model, *Otto-Bliesner* [1999] has found that teleconnections between Sahel precipitation and ENSO SST anomalies were absent during the Middle Holocene with the Tropical Atlantic SSTs asserting the dominant influence. Faunal evidence on the Peruvian coast of stable, warm tropical water could indicate the absence of ENSO

for some millenia before 5K yrs BP [*Sandweiss et al.*, 1996]. However, interpretation of evidence on the subject is still subject to controversy.

1.3.4 Atmospheric Composition

In addition to pollen and lake-level based reconstructions, evidence on changes in the atmospheric composition can give additional clues about conditions in the West African region during the Middle Holocene. Interannual increases in the export of African dust aerosols to the subtropical Atlantic marine boundary layer by the African easterly jet have been related to negative annual precipitation anomalies in the source areas [*Prospero and Nees*, 1977; *Middleton*, 1987; *Moulin et al.*, 1997; *de Menocal et al.*, 2000], when diminished vegetation allows loose soils to be more easily transported. These precipitation anomalies have in turn been linked to changes in the vegetation conditions and sea-surface temperature anomalies in the Tropical Atlantic [*Druyan*, 1987; *Eltahir and Gong*, 1996]. A sharp increase in the terrigenous composition of a sediment core located off the coast of Mauritania, is centered at about 5-6 K yrs BP, consistent with the abrupt termination of the African humid period [*de Menocal et al.*, 2000], when generally dormant sand dunes became more active [*Sarnthein*, 1978].

Several reconstructions of past atmospheric CO_2 concentrations from ice cores show that these did not change dramatically over the course of the last 6000 years [*Neftel et al.*, 1982; *Lorius et al.*, 1984; *Barnola et al.*, 1987; *Raynaud et al.*, 1993; *Felzer et al.*, 1998] so that during the Middle Holocene (~265 ppmv) they were only slightly lower than preindustrial levels (~280 ppm). These slightly lower concentrations could have, at least in part, resulted from the additional storage provided by the denser vegetation in the monsoon regions [*Beerling*, 2000], although this is still subject to controversy.

Changes in methane are related to temperature- and moisture-related changes in the global extent of wetlands, since wetlands (such as swamps and peat bogs) are today the primary source of this gas. The great amount of subtropical wetlands during the Middle Holocene could have provided a larger source of methane during the period since biological wetland activity is greater in warm and humid environments.

Consistently, a relatively high atmospheric CH_4 concentration has been recorded for the Early to Mid-Holocene [*Petit-Maire et al.*, 1991; *Blunier et al.*, 1995].

1.3.5 Location of the Main Atmospheric Structures

Several studies have suggested that the Intertropical Convergence Zone occupied a more northerly position during the Middle Holocene summer in West Africa, consistent with a more northward penetration of the monsoon rains during the season [*Street and Grove*, 1976; *Jolly et al.*, 1998]. As an example, based on a macrophysical model, *Bryson* [1992] has found that the ITCZ was located ~1-2° further north than today during August –the month of maximum penetration, bringing rainfall to about 27° N. However, according to *Street and Grove* [1976], data is still insufficient to determine whether its mean position lay further north than now.

North of this location, precipitation nowadays occurs in the winter season associated with cyclonic storms. However, most of these systems are currently not able to penetrate inland due to the barrier formed by the Atlas mountain range, so that winter precipitation in the region is currently very rare (~150 mm/yr at 31° N: *Bryson*, [1992]). *Petit-Maire and Guo* [1997], *Cheddadi et al.* [1998], and *Texier et al.* [2000] have suggested that during the Middle Holocene, the Mediterranean cyclonic rain belt deepened and reached further southward than today making it easier for these cyclones to cross the Atlas barrier. This can be evidenced in the reconstruction of the level of a lake located over the Atlas Mountains in Morocco, which shows an arid event occurring at ~6K yrs BP, consistent with a more southward position or the weakening of the westerly jet stream winds [*Cheddadi et al.*, 1998]. The possibility of a southward displacement of the jet stream during the period is also consistent with the occurrence of high lake-levels in Algeria and Israel [*Street and Grove*, 1976], which could have resulted from more cyclonic activity being able to cross the Atlas barrier along with a few monsoon-related rains.

1.3.6 Variability of the Climate System

From the reconstructions of West African conditions during the Middle Holocene presented in the previous sections, it is evident that on average conditions during the period were significantly wetter than today. However, several studies suggest that the Holocene period was much more complex than previously thought with smaller-scale fluctuations reflecting possible causes different from the broad trends attributable to orbital forcing [*Street-Perrott and Perrott*, 1993]. Although the limited temporal resolution of lake-level reconstruction may obscure possible high-frequency fluctuations in the regional climate, several records suggest dry events of minor amplitude around 6K yrs BP. For example, *Gasse and Van Campo* [1994] found a marked decline in lake-level at about 6.3-6 K yrs BP on the Termite (16°05' N, 11°15' E) and Bougdouma (13°19' N, 11°40'E) sites. In their study they have identified a possible series of mechanisms explaining these fluctuations.

First, the reduction in albedo accompanying the recorded shift from desert to grass/savannah vegetation in the Middle Holocene in response to a higher water availability, could have provided an important positive feedback mechanism for monsoon enhancement. This mechanism of albedo reduction amplifying the positive rainfall anomaly has been identified by *Eltahir and Gong* [1996] as important in increasing the amount of net surface radiation, and consequently, the moist static energy fed into the land boundary layer which would result in a stronger monsoon. Additionally, large-scale forcings such as variations in the local and global ocean conditions (SSTs) could have provided another mechanism explaining these fluctuations.

Evidence on the complexity of the Mid-Holocene hydrology over the region has also been identified by *Maley* [1982], and *Lézine and Casanova* [1989] based on changes in the rainfall regime at Lake Mega Chad in the Sahel. High lake-levels were concurrent with minor local positive oscillations in a general trend of decreasing wetness in the subtropical Sahara. Similarly, *Lamb et al.* [1995] presents evidence on several century-scale arid events occurring probably during winter, rather than in summer as in tropical West Africa, in the montane Mediterranean zone of Morocco as reflected in

the low levels recorded during summer in a lake which is mostly fed by groundwater. These changes, however, are probably related to a southward displacement in the mid-latitude jet stream during the period.

1.3.7 Human Population

Petit-Maire [1994] has prepared a map of radiocarbon-dated data for the Sahara during the Holocene (Figure 1-5). It covers information on proxy markers of humidity such as surface waters, geochemical deposits, vegetative cover, and skeletal remains of aquatic and large land animals. Additionally, it includes information on prehistoric habitats describing the lifestyle of people during the period. Based on this evidence, they have been able to correlate the significantly wetter Sahara during the Middle Holocene with human occupation in the region. Based on the abundance of humidity evidence, they identified a hydrological optimum between 8.5 and 6.5K yrs BP. However, the distribution of human settlements, suggesting a semi-sedentary lifestyle, peaks about 1,000 years later, at a time (~6K yrs BP) when the Sahara started to expand. Evidence [*Petit-Maire et al.*, 1990] suggests that temporary shallow pools and vegetative cover, reaching even into the today hyperarid Tanezrouft Desert in the Sahara, provided seasonal freshwater for nomadic cattle herdsmen that could have lived there for a few days or weeks.

The lag between human occupation and humid conditions have been attributed by *Petit-Maire* [1994] to the delayed migratory response of vegetation, preys, and man, probably in that order, into previously hyperarid areas. Their evidence indicates that the progressive hydrological deterioration, which started from the Middle Holocene, induced wide migrations from the desert lowlands into the African highlands of the mountains, the Atlantic coast, and the banks of the Niger, Senegal, Euphrat, Tigris and Nile rivers where water availability was higher. Bones found in dry riverbeds, pottery, utensils, pictures, and carvings left by ancient civilizations show a transition from sedentary to pastoralist lifestyles and remain as evidence of how climate shapes the human life [*UNESCO*, 1962; *Petit-Maire et al.*, 1990].

The causes behind this hydrological deterioration were not understood until very

recently. Most evidence shows that these causes were natural and related to a decreased insolation amplified by vegetation dynamics. Possible anthropogenic impacts through deforestation did not play an important role mainly because the Neolithic population was relatively small and it is believed that they were careful in conserving the environment [*Petit-Maire*, 1994]. Conversely, these drier conditions are believed to have been the possible stimulus leading to the foundation of civilizations along the river banks.
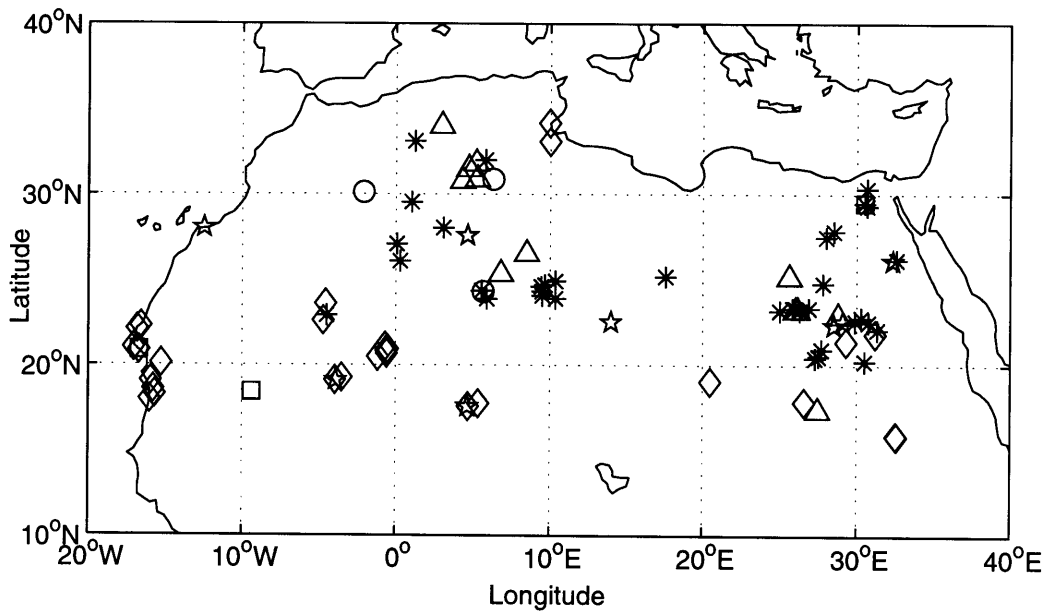
Figure 1-5: Radiocarbon data from *Petit-Maire* [1994] showing evidence of more humid conditions during the Middle Holocene: ◯ = soil; * = charcoal; ★ = human bones and pottery; △ = large animals (e.g. elephants, ostrich); ◇ = molluscs, fish, shells; □ = plant remains.

38

1.4 Literature Review on Previous Studies

Several studies using atmospheric general circulation models (AGCMs) have found significantly wetter conditions over West Africa during the Middle Holocene (Table 1.2). However, the extent of the monsoon penetration has been consistently underestimated [*Kutzbach and Guetter*, 1986; *Yu and Harrison*, 1996; *Hall and Valdes*, 1997; *Masson and Joussaume*, 1997]. As an example, a series of simulations, using eighteen climate models (AGCMs), based on current and 6K yrs BP forcings have been performed as part of the Palaeoclimate Modeling Intercomparison Project (PMIP) [*Harrison et al.*, 1998; *Joussaume et al.*, 1999]. In these models, the biosphere-atmosphere interaction has been limited by prescribing vegetation characteristics, such as local albedo and surface roughness, to their current values. The output of these simulations has been subsequently used to force the BIOME model [*Prentice et al.*, 1992] giving the vegetation distribution in equilibrium with these forcings. Although the PMIP simulations show a northward shift of the rainfall belt, and correspondingly of steppe and xerophytic biomes at the expense of desert in the Sahel/Sahara region, none of these models produced steppic vegetation north of 19° N. These results imply that orbital changes alone are not sufficient to produce the wetter than today conditions suggested by palaeodata. Some positive feedback mechanisms are then needed to explain the full magnitude of the observed expansion.

Although the vegetation, soil, lake, wetland, and ocean feedbacks on climate have been omitted in these studies, these have been identified as the possible mechanisms through which orbital forcings could have been enhanced to produce the recorded significant rainfall increase. As an example, *Phillips and Held* [1994] studied the response of a climate model to changes in orbital forcings and found that changes in insolation were primarily responsible for the intensification of the Northern Hemisphere monsoons. However, they also found that soil moisture had a significant effect on the African monsoon by increasing precipitation by a factor of two.

Several attempts to at least partially include these effects have resulted in mixed conclusions due to the difficulty in separating robust climate features and those which

39

Model	Type	Resolution [a]	Vegetation	Ocean	Surf. waters	Max. southern [b] desert limit	References
ECHAM4 [c]	AGCM	-	VCP6	SP0	-	21.5° N	*Knorr et al.*, 2000
GENESIS1.02	OAGCM	R15*12	VCP0	SC to a MLOM	-	23° N	*Foley*, 1994
GENESIS2+IBIS	VOAGCM	R15*16	SC to IBIS	SC to a MLOM	-	20° N	*Doherty et al.*, 2000
GENESIS2+MOM1	OAGCM	3.75°*3.75°*-	-	AC to MOM1	-	23° N	*Kutzbach and Liu*, 1997
IPSL	OAGCM	64*50*11 (92*76*31)	AC to BIOME1	SC (OAGCM)	-	21° N	*Braconnot et al.*, 1999
LMD4.3 and LMD5.3	AGCM	48*36*11 and 64*50*11	VCP0	SP0	-	21° N	*Masson and Joussaume*, 1997
LMD5.3+Océan Parallélisé model	OAGCM	64*50*11 (92*76*31)	VCP0	SC (OAGCM)	-	21.5° N	*Braconnot et al.*, 2000
LMD5.3	AGCM	64*50*11	AC to BIOME1	SP0	-	18° N	*Texier et al.*, 1997
NCAR CCM3	AGCM	T42*18	VCP0	SP0	SW6	20° N	*Coe and Bonan*, 1997
NCAR CCM3	AGCM	-	VCP6	SP0	SW6	20° N	*Bröstrom et al.*, 1998
18 AGCMs (PMIP)	AGCM	Several	VCP0	SP0	-	19° N	*Joussaume et al.*, 1999
Several	AGCM	Several	VCP0	SP0	-	20° N	*Yu and Harrison*, 1996 *Harrison et al.*, 1998

[a] Spectral horizontal resolution*vertical levels, or number of grid points in longitude*latitude*vertical, or ° longitude*° latitude*vertical levels. Values in parenthesis indicate resolution of oceanic model.

[b] Directly stated on reference or approximately determined as location of 200 mm/yr of precipitation.

[c] All simulations, except this one, use 6K yrs BP solar insolation. For this simulation, modern solar insolation was used (see text).

AGCM = atmospheric general circulation model; OAGCM = oceanic and atmospheric general circulation model; VOAGCM = vegetation, oceanic and atmospheric general circulation model; AC = asynchronously coupled; SC = synchronously coupled; VCP0 = vegetation conditions prescribed as present; VCP6 = vegetation conditions prescribed as for 6K yrs BP; MLOM = mixed layer ocean model; SP0 = SSTs prescribed as present; SW6 = surface water prescribed as for 6K yrs BP; PMIP = Palaeoclimate Modeling Intercomparison Project; - = not specified.

Table 1.2: Summary of simulations of the Middle Holocene (6K yrs BP) and results for West Africa.

are model dependent. For example, *Broström et al.* [1998] found a reduction in the discrepancy between the simulated and recorded steppe/desert limit from a range of $5 - 9°$ to a range of $2 - 5°$ in latitude when prescribing land-surface conditions based on *Hoelzmann et al.*'s [1998] map of palaeovegetation and soils, instead of the current distribution. However, incorporating prescribed changes to the lake and wetland areas did not produce a further northward migration of the monsoon front. This is contrary to *Coe and Bonan*'s study [1997], in which they found a slight northward shift of the monsoon frontal boundary in July and increased precipitation along ˜18° N as a result of an increased moisture availability and circulation changes due to a prescribed higher water level for Lake Mega Chad. Nevertheless, the increased precipitation found by *Coe and Bonan* [1997] was not enough to fully reproduce the surface waters used in their study.

Other studies have gone beyond by asynchronously coupling ocean and/or static-vegetation models to AGCMs [*Texier et al.*, 1997; *Braconnot et al.*, 1999; *de Noblet-Ducoudré et al.*, 2000]. Using a global coupled ocean-atmosphere GCM iteratively coupled to a biome model, *Braconnot et al.* [1999] found that synergistic feedbacks between the ocean and vegetation are needed to fully reproduce the observed 5° northward shift in the desert/steppe boundary. The role of the ocean has been found to be in enhancing the moisture advection inland, while the main contribution of vegetation was found to be in increasing local recycling. Although these models do not allow for simulating the transient response of the climate system, these have served as tools to better understand and isolate the mechanisms through which feedbacks can take place, especially when studying long-term climate change [*Liu et al.*, 1999].

The importance of using models in which the components of the climate system are synchronously coupled has been stressed by several studies as the key to more accurately reproduce the palaeoclimate [*Broström et al.*, 1998; *Hoelzmann et al.*, 1998; *Braconnot et al.*, 1999; *Foley et al.*, 2000]. The main reason behind this is that, contrary to asynchronous coupling, synchronous coupling guarantees the use of one common parameterization for the surface processes and its interactions resulting in more consistent simulations [*Foley et al.*, 1998]. Additionally, synchronous coupling,

avoids the introduction of excessive interannual variability through the buffering action of the biosphere, includes different timescales of interaction between the atmosphere and the biosphere, and allows for the inclusion of not only physical feedbacks but also exchanges of water and carbon between both components [*Foley et al.*, 2000]. Consequently, synchronous coupling allows for a more detailed analysis of transient and long-term climate change, and results in a better understanding of the interaction between those processes that are being simulated. However, efforts in this direction have been limited both by computational constraints and the lack of a quantitative set of boundary/initial conditions for the period.

After a thorough literature search, we have only found one study, for both current and 6K yrs BP forcings, in which the ocean, atmosphere, and vegetation have been synchronously coupled [*Ganopolski et al.*, 1998]. In this study it has been found that vegetation dynamics account for the major precipitation changes in the region, while the role of the ocean remained ambiguous. This is contrary to the significant positive ocean contribution found by *Kutzbach et al.* [1997], *Braconnot et al.* [1999], and *Liu et al.* [1999]. Although these results agree well with the palaeoclimate, the coarse model resolution (10° in latitude by 51° in longitude) does not allow for a detailed analysis of regional dynamics. The most recent effort in this direction has been done by *Doherty et al.* [2000] with the synchronous coupling of a climate and vegetation model with a higher resolution (4.5° in latitude by 7.5° in longitude). However, as with other models, the expected greening of the Sahara has not been fully reproduced.

More recently, *Knorr et al.* [2000] have been able to almost fully reproduce the Middle Holocene greening of the Sahara by simply prescribing changes to the surface albedo in the region, thereby affecting the amount of solar radiation reflected back into the atmosphere. For the current climate, the surface albedo was derived based on measurements by the Meteosat satellite [*Pinty et al.*, 2000a,b], while for the Middle Holocene it was prescribed based on *Hoelzmann et al.*'s [1998] map of palaeovegetation. In their study, insolation changes resulting from changes in the Earth's orbital configuration were not taken into account. Therefore, it is suggested that it is the partitioning of solar radiation, rather than the absolute amounts reaching the top of

the atmosphere, which predominantly determined the radiation balance in the region, and consequently, the strength of the monsoon circulation. Although this could be an artifact resulting from the specific parameterizations in the ECHAM-4 climate model, this issue deserves further study in order to assess whether these results are model dependent.

Another issue deserving further analysis is the different zonal distribution of the simulated northward grassland expansion between models. Data for the Middle Holocene show grassland to at least 23° N in the western and eastern Sahara, and up to 26° N in the region north of Lake Chad. In *Kutzbach et al.*'s [1996] simulations, the largest expansion simulated was to the east of Lake Chad and into the Sudan when orbital, vegetation, and soil changes were prescribed to Middle Holocene values. On the contrary, in *Claussen and Gayler*'s [1997] study, grassland expanded northward much more significantly in the west than in the east, similar to *de Noblet-Ducoudrè et al.*'s [2000] simulations with the ECHAM model. Other models [*Texier et al.*, 1997; *Doherty et al.*, 2000] have simulated a larger response to orbital forcings in the east, but a larger response to vegetation feedbacks in the west.

It is evident that there exist many issues regarding the simulation of conditions in the West African region during the Middle Holocene. Even though there exists a relatively high amount of palaeodata available for the period, the spatial coverage is still sparse and the reconstruction of atmospheric, biospheric, and oceanic conditions remains qualitative, an issue that will prove important in our research. In addition, due to the different parameterizations of processes in climate models, it is important to determine which features of the simulated climate are robust and which are model dependent. Several efforts in this direction include the PMIP AGCM simulations, in which 18 research groups have come together to explore this issue under a common set of boundary and initial conditions. However, their analysis has been limited by prescribing both vegetation characteristics and SSTs to their current values. Ideally, global climate models with high temporal and spatial resolution in which the atmosphere, biosphere, and ocean are synchronously coupled, would be required to bring palaeoclimate simulations closer to observations. This will in turn increase our de-

43

gree of confidence in the model for simulating future climate change. However, until computational constraints, uncertainties in model parameterizations, and the lack of a quantitative set of boundary and initial conditions for the period can be overcome, we will still be dealing with simplification and uncertainty.

1.5 Research Objectives

The research presented in this thesis is based on a series of model simulations using a zonally symmetric, synchronously coupled biosphere-atmosphere model (ZonalBAM), which has been used as a tool to study the main features of the response of the West African climate to varying insolation forcings and the relative contributions of vegetation and ocean dynamics. For this purpose, the Middle Holocene has been selected as a basis for comparison with current forcings. The reasoning behind lies in that the Middle Holocene presents a unique opportunity to isolate the effects of insolation on climate resulting from well-known changes in the Earth's orbit since the ice sheets had already retreated to their current extent, the atmospheric CO_2 concentrations were close to their preindustrial levels, and evidence indicates that SST anomalies were not significant. In addition, there exists a relatively-high amount of palaeodata for comparison against model simulations, which has motivated its study by several research groups.

The basic motivations behind this research are:

1. To validate the use of a zonally symmetric biosphere-atmosphere model in simulating climate change over the region of West Africa. In other words, forcing the model with boundary and initial conditions different from the current in order to assess its performance. Understanding how the biosphere-atmosphere-ocean feedbacks take place when subject to various forcings represents a significant step in predicting the full impact of future climate change.

2. To understand the mechanisms responsible for a greener Sahara during the Middle Holocene, including well-known changes in top-of-the-atmosphere insolation

44

resulting in modified atmospheric circulation, and the relative contributions of vegetation and ocean feedbacks.

3. To analyze the model's sensitivity to qualitatively-known boundary and initial conditions, especially during the Middle Holocene.

4. To determine the equilibrium states that could potentially exist under Mid-Holocene forcings.

1.6   Thesis Structure

This thesis is composed of five chapters. Chapter 1 is an introduction to the research presented in this thesis. Evidence on the expansion of grassland into the region currently occupied by the Sahara, as well as the main reasons behind this expansion are explained. In addition, a literature review of previous studies on the topic is presented. Finally, the objectives of our research are discussed. In Chapter 2, our zonally symmetric biosphere-atmosphere model (ZonalBAM) is described and its validation is explained. In addition, a section is devoted to the modification of ZonalBAM by the addition of a mixed layer ocean model. Finally, the advantages and disadvantages of using ZonalBAM for simulating the climate of West Africa during the Middle Holocene are presented.

Chapter 3 presents the simulations that were performed using the original version of ZonalBAM, which includes atmospheric and biospheric components. The mechanisms underlying the expansion of grassland into the Sahara during the Middle Holocene are addressed. Sections are devoted to the effects of well-known changes in top-of-the-atmosphere insolation, the impact of vegetation dynamics, and the sensitivity of the biosphere-atmosphere system to initial vegetation conditions. Several issues regarding the validity of ZonalBAM in simulating Mid-Holocene conditions, as well as its sensitivity to boundary and initial conditions, are discussed in these sections. Finally, a mechanism for the enhancement of the West African summer monsoon during the Middle Holocene is presented based on a comparison of the most

realistic pair of simulations.

Chapter 4 presents the simulations performed with ZonalBAM coupled to a mixed layer ocean model (MLOM). First, a section discusses the validation of MLOM based on current forcings. Then, the MLOM is applied to a simulation based on Middle Holocene forcings and the effect of ocean dynamics is discussed. The main results and conclusions of this research, are finally summarized in Chapter 5.

Chapter 2

Model Description

2.1 Introduction

In Chapter 1, it was shown that conditions over the region that is currently occupied by the Sahara Desert were significantly wetter/greener during the Middle Holocene (6K yrs BP). Data for the Middle Holocene show grassland expanding to at least ~23° N in the western and eastern Sahara, and up to ~26° N in the region north of Lake Chad. However, here we focus our interest on the region to the west of 15° E. The basis for the selection of this particular region is explained hereafter.

The region of West Africa, hereafter defined as the region from 5° N-35° N, and 15° W-15° E (Figure 2-1), is currently under the influence of both the meridional overturning known as the Hadley circulation, and the monsoon circulation (Figure 2-2). The first results from latitudinal temperature gradients and has its descending branch at ~30° N where it produces desert conditions. The latter results from the differential boundary-layer moist static energy distribution of land and ocean surfaces [*Emanuel*, 1995; *Eltahir and Gong*, 1996]. In summer, the Hadley circulation over the region becomes weaker while the monsoon circulation becomes the dominant circulation. Since air rises where it is warm, and the land is usually warmer than the ocean during summer (in terms of moist static energy), the monsoon circulation brings moisture from the ocean into the land where its rising branch produces rainfall. Since the Atlantic coast is basically parallel to the Equator and due to the

physiographic simplicity of the region (i.e. most land lies below 400 m), the monsoon circulation is mainly a meridional phenomenon. These two circulations together result in a close to zonally symmetric climate, which justifies the use of zonally symmetric climate models. The validity of this assumption, has been tested by *Zheng and Eltahir* [1998], where they showed that the meridional components of both the net water vapor flux and moist static energy in the region are significantly larger than their zonal counterparts. Similarly, *Eltahir and Gong* [1996], and *Gong and Eltahir* [1996] concluded that the meridional gradient of boundary-layer moist static energy drives the monsoon circulation, and that the primary source of moisture for the West African monsoon is evaporation over the Tropical Atlantic.
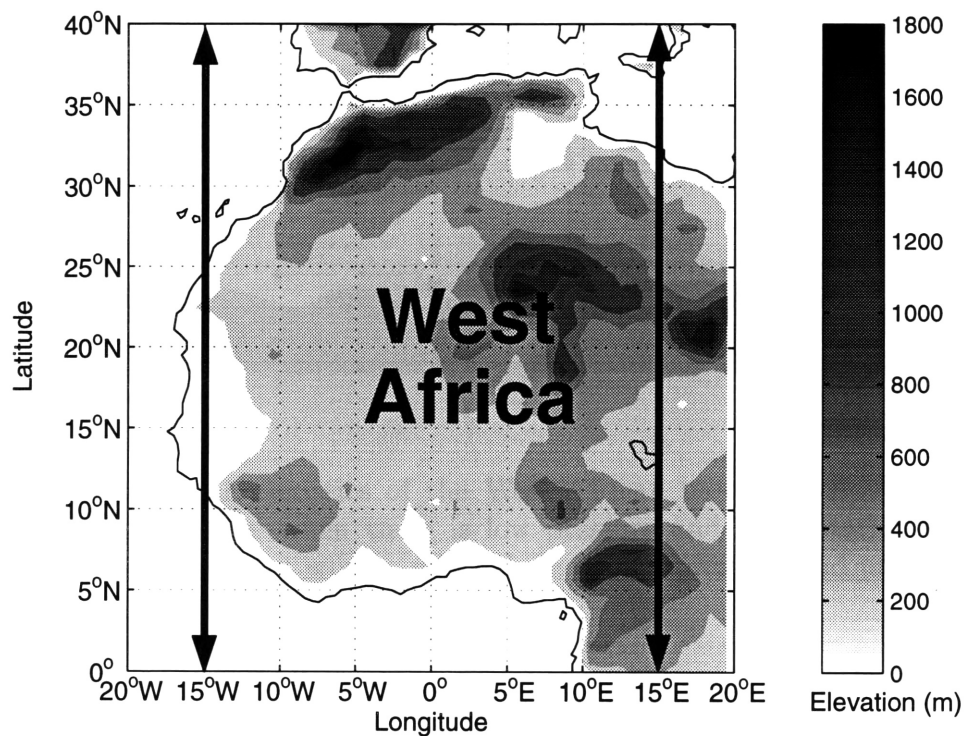
Figure 2-1: Region under study. The average conditions between 15° W and 15° E are simulated in the model. In the original model, the West African coastline is set at 5° N with ocean southward and land northward of this location. However, here we also include a representation of the Mediterranean from 35° N to 40° N.

In previous studies, a zonally symmetric, synchronously coupled biosphere-atmosphere model (ZonalBAM), which includes explicit representation of ecosystem dynamics, has been developed [*Wang*, 2000] and validated based on current forcings [*Wang and Eltahir*, 2000a] over the region of West Africa. It combines a zonally symmetric atmospheric model and a fully dynamic biospheric model through which feedbacks in the system can take place. Here, we assess the ability of ZonalBAM in simulating climate change over the region of West Africa by using the Middle Holocene as a basis for comparison with current conditions.

(a)   (b)
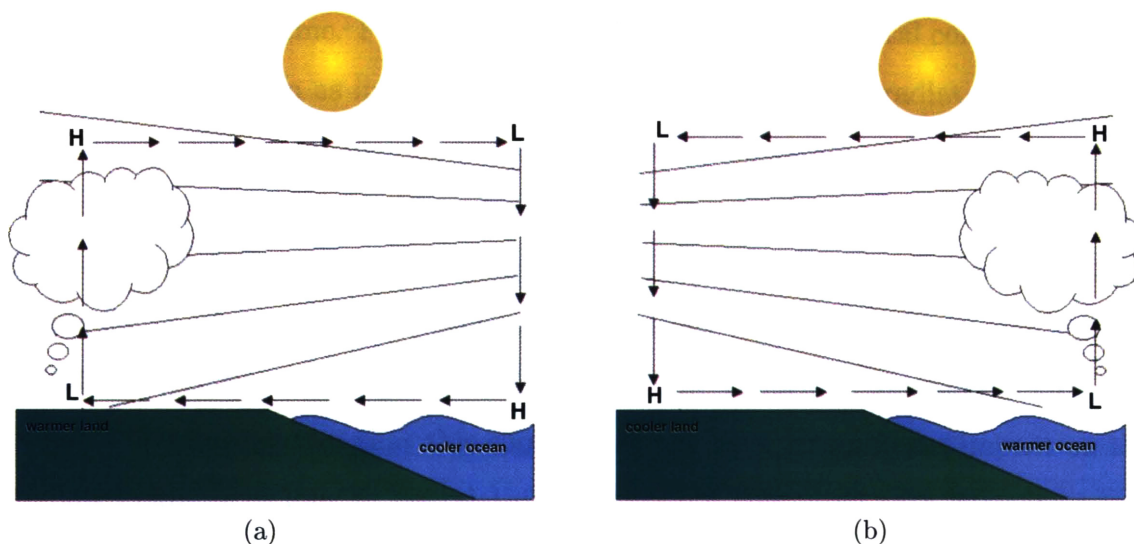
Figure 2-2: Main characteristics of the West African monsoon circulation during (a) summer, when there is low pressure and precipitation over land, and during (b) winter, when there is high pressure and precipitation is suppressed over land.

2.2   Model Components and Validation

The zonally symmetric biosphere-atmosphere model (ZonalBAM) has been developed and validated by *Wang* [2000]. The model domain covers the whole globe with a uniform resolution in sine of latitude (46 grid points, ~2.5° near the tropics) representing the zonal average between 15° W and 15° E, and 21 non-uniformly spaced vertical

levels (Figure 2-1). In the original model, the West African coastline is set at 5° N with ocean southward and land northward of this location. However, here we also include a representation of the Mediterranean from 35° N to 40° N. The timestep is 20 minutes. During the model development, several schemes representing physical and biogeochemical processes were coupled together and are described hereafter (Figure 2-3).

The atmospheric model is based on the *Zheng* [1997] model, which includes a representation of atmospheric dynamics, a radiation scheme, and a convection scheme. Additional to the processes simulated by the Zheng model, ZonalBAM includes representation for key processes such as a boundary layer scheme, and a simple cloud parameterization scheme. Parameters describing the Earth's orbital configuration for a given time are given as inputs from which the incoming solar radiation at the top of the atmosphere is calculated. For the radiation calculation, the solar constant is kept fixed, seasons are defined based on the modern calendar with the vernal equinox fixed at March 21, and months are kept as for the present-day orbital configuration. Consequently, changes in the length of the seasons due to changes in the Earth's orbital configuration are neglected. For the Middle Holocene, *Joussaume and Braconnot* [1997] have shown that this choice does not have a significant impact on the simulated climate as long as lag relationships are not compared with current.

Due to the model's regional configuration, it does not take into account large-scale forcings such as those imposed by global SST conditions. Therefore, it can only be forced with time series of Atlantic SSTs or with its climatology. Forcing the model with the climatology of regional SSTs (from NCEP optimum interpolation SST analysis [*Smith and Reynolds*, 1998]), averaged over 15° W to 15° E, has been found to accurately reproduce the current climate [*Wang and Eltahir*, 2000a]. For the Middle Holocene, the Tropical Atlantic SSTs have been found to assert a dominant influence in Sahel rainfall when compared to ENSO anomalies [*Otto-Bliesner*, 1999]. Additionally, faunal evidence on the Peruvian coast of stable and warm tropical water seems to be indicative of the absence of ENSO for some millenia before 5K yrs BP [*Sandweiss et al.*, 1996]. This is encouraging when using ZonalBAM for simulating

The Zonally Symmetric Model for the Biosphere-Atmosphere System

Cloud Scheme   (developed based on Kvamsto, 1991)

Radiation Scheme

(Chou *et al*, 1991)

Dynamics Scheme

(Plumb & Hou, 1992;

new numerical scheme)

Convection Scheme

(Emanuel, 1991)

Atmospheric Boundary Layer Scheme

(developed based on Holtslag and Boville, 1993)

Dynamic Biospheric Model IBIS

(Foley *et al,* 1996)

Interception Scheme

(developed based on Shuttleworth, 1988; Eltahir and Bras, 1993)
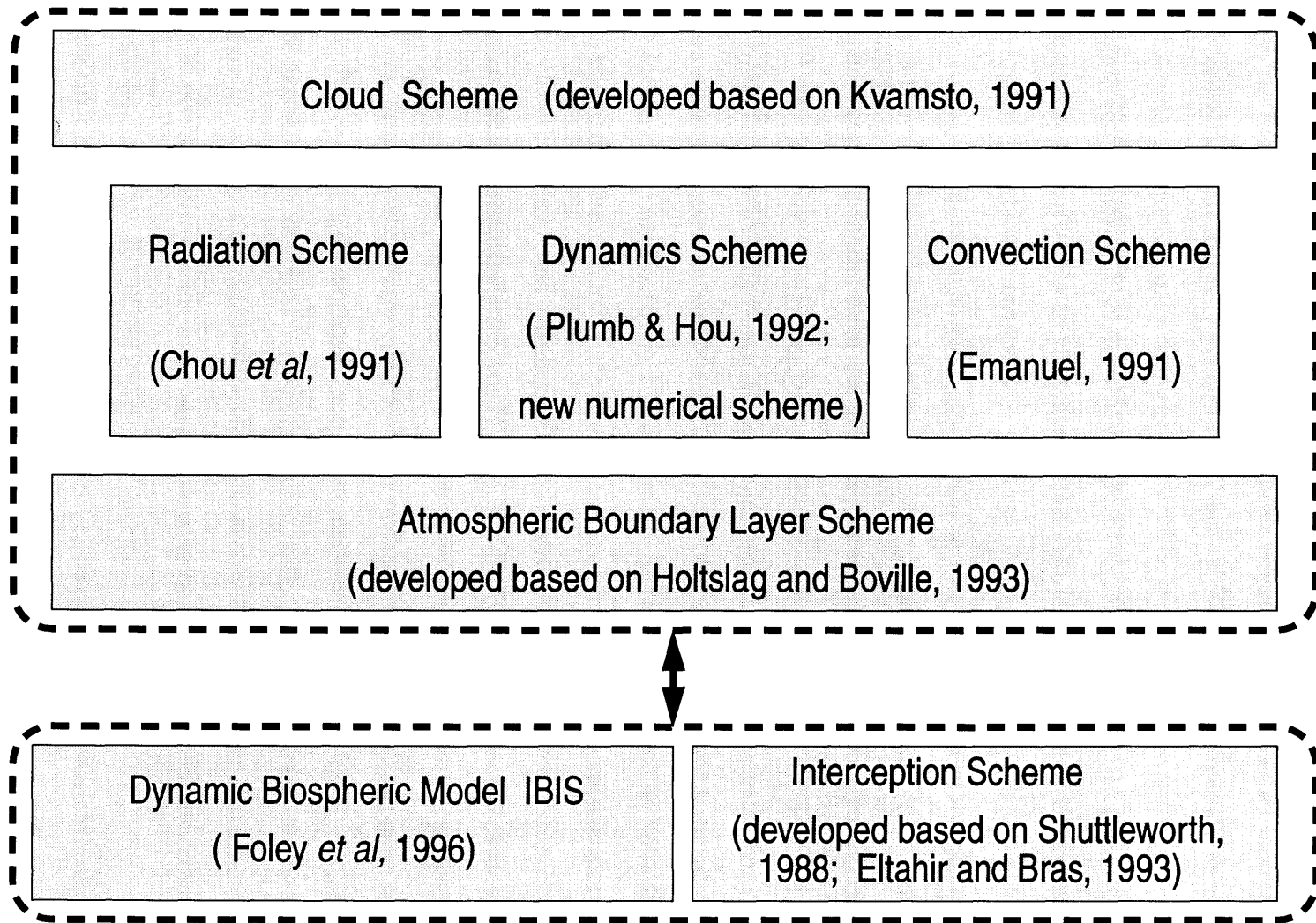
Figure 2-3: Components of the coupled biosphere-atmosphere model [*Wang*, 2000].

51

the West African climate during the period. Here, we also include a representation of the Mediterranean from 35° N to 40° N for which we fix the SSTs to their current climatology. As part of this research, a mixed layer ocean model (MLOM) has been coupled to ZonalBAM in order to account for ocean feedbacks. However, due to ZonalBAM's zonal symmetry, only changes in the SSTs in the South-Eastern Tropical Atlantic region (SETA: 25° S-5° N and 15° W-15° E) can be simulated. The inclusion of ocean feedbacks will allow us to simulate a more complete response of the climate system to changes in orbital forcings.

Being a zonally symmetric model, ZonalBAM is computationally more efficient than other 3-D models, but on the other side its applicability is limited. Due to its zonal symmetry, the model does not provide for the simulation of asymmetrical features such as the eddies resulting from baroclinic instability, which represent an important transport mechanism in middle latitudes, especially during winter. For this reason, in an effort to reduce model biases, the climatology of fluxes and temperatures beyond the tropics (averaged between 15° W and 15° E) can be specified as boundary conditions, and fixed throughout a simulation, as has been done in simulations of the current climate [*Wang and Eltahir*, 2000a; *Wang*, 2000]. However, since these conditions are not quantitatively known for the Middle Holocene, here we choose to let the model interactively calculate these fluxes assuming that a zonally symmetric circulation can describe the mean circulation in mid-latitudes. *Petit-Maire and Guo* [1997] have determined that northwestern polar depressions and Atlantic cyclones were a more important contributor to winter rainfall in the northern Sahara during the Middle Holocene than today. Therefore, the lack of simulation of these disturbances in ZonalBAM could result in some mismatch with palaeoprecipitation reconstructions over the region.

The biospheric component of ZonalBAM uses the Integrated BIosphere Simulator (IBIS), developed by *Foley et al.* [1996]. IBIS can represent 18 vegetation types, each composed of a particular combination of 12 possible plant functional types (pfts). IBIS takes the meteorological forcings provided by the atmospheric model as inputs, returns to the atmospheric model outputs that describe surface properties and fluxes,

and updates the biospheric state including the vegetation structure based on the carbon budget for each pft. ZonalBAM additionally incorporates a canopy interception scheme to IBIS, which accounts for the impact of rainfall sub-grid variability [*Wang*, 2000]. Since ZonalBAM is a zonally symmetric model, it basically takes the whole globe as land north of the Coast of Guinea (5° N) and ocean southward (Figure 2-1), except for a representation of the Mediterranean. Initial vegetation conditions are specified for the land region, and can be fixed in a certain region or could be let to dynamically interact with the atmosphere until an equilibrium is established.

In previous studies by *Wang and Eltahir* [2000a], ZonalBAM has been validated by the successful simulation of current climate (biosphere-atmosphere) conditions in the region of West Africa. Based on experiments starting from different initial vegetation conditions, it has been found that extremely different equilibrium states –dry and green regimes– can coexist under current forcings. It has also been found that vegetation dynamics act as a significant mechanism for both climate persistence at one state and climate transition between different states, therefore, serving as a modulator of large-scale forcings (SSTs) and producing the observed low-frequency climate variability over the region. Furthermore, it has been demonstrated that vegetation dynamics play an important role in the development and persistence of the current Sahel drought.

Changes in the global and regional SST distribution, as well as regional changes in land cover, have been identified as the most probable mechanism in triggering the current Sahel drought. The reason behind this lies in that the strength of the monsoon circulation, bringing moisture from the ocean inland during summer, is controlled by the gradient of boundary-layer moist static energy between the land and the ocean [*Eltahir and Gong*, 1996]. Consequently, changes in any of the two components will result in changes in the surface fluxes which feed the boundary layer with moist static energy, and will, therefore, affect its gradient (Figure 2-4).

However, regardless of which of the two mechanisms plays a larger role in the onset of the recent regional drought, it has been found that it is the response of the vegetation to initial forcings what is critical in the amplification and persistence of

drought conditions. *Charney*'s hypothesis regarding the relationship between deserts and droughts in the Sahel [1975: *the cooling effect due to albedo increase produced by desertification enhances local subsidence, which reduces precipitation, limits vegetation growth and makes the drought self sustaining*], has been demonstrated by simulating several scenarios of both desertification and deforestation. Results confirm that desertification within the Sahel accounts for the observed drought in the region and the currently observed expansion of the Sahara Desert. Therefore, the possibility of anthropogenic effects inducing or perpetuating climate change in the region has been confirmed.
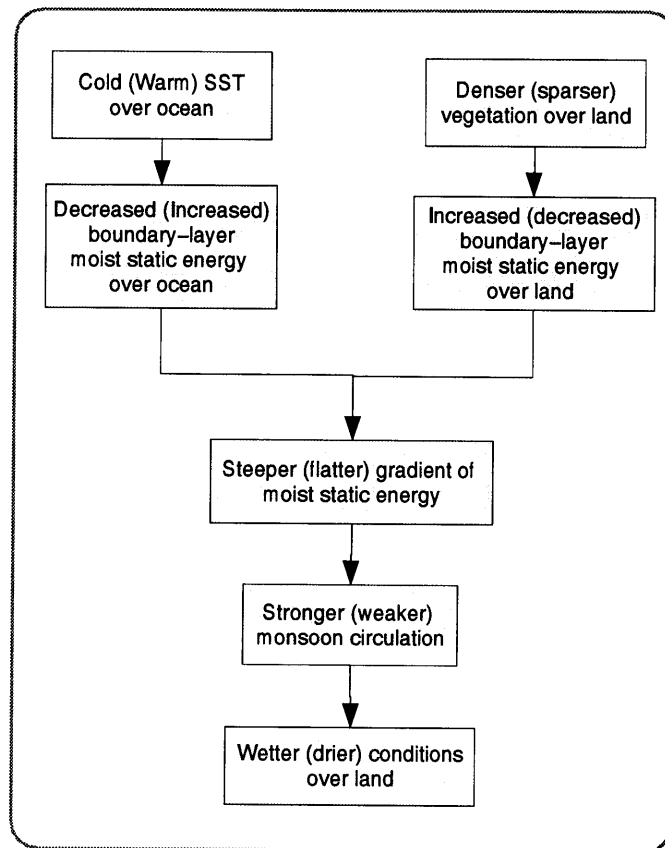
Figure 2-4: Summary of the mechanisms affecting the strength of the monsoon circulation over West Africa [*Eltahir and Gong*, 1996].

2.3 Model Development: Addition of a Mixed Layer Ocean Model

Previous studies have stressed the need for the inclusion of every component of the climate system (i.e. atmosphere, biosphere, ocean, surface waters) in climate models in order to bring simulations closer to observations. As an example, the inclusion of vegetation dynamics [*Broström et al.*, 1998; *Ganopolski et al.*, 1998; *Braconnot et al.*, 1999; *Doherty et al.*, 2000], ocean dynamics [*Kutzbach et al.*, 1997; *Ganopolski et al.*, 1998; *Braconnot et al.*, 1999; *Liu et al.*, 1999; *Doherty et al.*, 2000], and surface waters [*Coe and Bonan*, 1997] has proven important in bringing simulations of West Africa's palaeoclimate closer to observations.

Our model, the zonally symmetric biosphere-atmosphere model (ZonalBAM), has been successful in simulating the current climate of West Africa when forced with prescribed SST climatology and with the time series of SSTs for the past few decades. The climatology of SSTs over the South-Eastern Atlantic has been used to simulate the equilibrium climate in the region. However, it is the inclusion of interannual variability in the SSTs which allowed for the successful simulation of the generation and persistence of the current Sahel drought [*Wang and Eltahir*, 2000c]. Changes in the global and regional SST distribution have been identified by *Wang* [2000] as a probable mechanism in triggering the current Sahel drought.

As demonstrated by *Zheng et al.* [1999], anomalies in the South-Eastern Tropical Atlantic (SETA: 25° S-5° N and 15° W-15° E) spring (AMJ) SSTs are correlated to West African summer (JAS) rainfall. They showed that a positive spring SST anomaly warms the ocean's atmosphere resulting in a weakened monsoon during spring. Consequently, there is less spring precipitation over land. However, as the anomalous moisture is advected inland, and a positive cloud-radiation feedback takes place, summer precipitation increases over land. Also, *Eltahir and Gong* [1996] showed that the strength of the monsoon circulation, bringing moisture from the ocean inland during summer, is controlled by the summer gradient of boundary-layer moist static energy between the land [*Zheng and Eltahir*, 1998] and the SETA [*Eltahir and Gong*,

1996; *Gong and Eltahir*, 1996]. Consequently, changes in any of the two components result in changes in the surface energy fluxes, which feed the boundary layer with moist static energy, and, thereby, affect the monsoon circulation. Additionally, *Eltahir and Gong* [1996], and *Gong and Eltahir* [1996] have demonstrated that the primary source of moisture for the West African monsoon is evaporation over the Tropical Atlantic. Therefore, any perturbation to the ocean heat budget has repercussions on the amount of moisture transported into West Africa by affecting any of the two mechanisms. *Druyan and Koster* [1989] have concluded that some droughts in the Sahel region are due to deficiencies in the moisture supply while others are the consequence of too few rain-generating wave disturbances even when moisture is ample. Additionally, *Saravanan and Chang* [1999] demonstrated that thermodynamic ocean feedbacks can enhance the persistence of atmospheric flow anomalies through a reduction in the surface heat flux, specially in the shallow tropical mixed layer regions. *Brenner* [1996] has demonstrated that the inclusion of ocean feedbacks results in a better forecasting skill for the tropics.

Several studies indicate that the West African monsoon circulation is also highly sensitive to changes in the SSTs over the Tropical North Atlantic sector (TNA: 10° N-25° N). For example, in *Eltahir and Gong*'s [1996] study on the dynamics of wet and dry years in West Africa, a dipole is observed between the SSTs in the SETA and TNA sectors. A similar distinctive pattern between the SST anomalies and West African precipitation has been observed by *Lamb* [1978], *Maley* [1997], *Otto-Bliesner* [1999], and *Sutton et al.* [2000] for the current climate, and simulated by *Maley* [1997] and *Braconnot et al.* [1999] for the Middle Holocene. In summers characterized by wet (dry) conditions, negative (positive) SST anomalies were observed over SETA, while positive (negative) SST anomalies were observed over TNA. For the Middle Holocene, *Kutzbach and Liu* [1997], simulated slightly warmer SSTs over the Tropical North Atlantic. These changes resulted in increased precipitation over West Africa, comparable in magnitude to those obtained by prescribing denser (Mid-Holocene) vegetation over the region.

The relationship between West African precipitation and global SST anomalies has

56

been the object of significant debate. For example, *Palmer* [1986], and *Otto-Bliesner* [1999] have found a strong correlation between ENSO anomalies and interannual-decadal variability in the western Sahel precipitation. However, *Druyan and Koster* [1989], and *Maley* [1997] found that the influence of ENSO anomalies on July precipitation over the western Sahel is of secondary importance. Moreover, *Sutton et al.*'s [2000] results support the view that the cross-equatorial flow during summer is most strongly influenced by the variability in the Equatorial Atlantic SST as well as in the Atlantic dipole pattern. They have also found that the NE trade winds during winter are most strongly influenced by ENSO variability in the Tropical Pacific.

It becomes evident that the inclusion of changes to the ocean is critical when simulating climate change over the region. Changes in the Mid-Holocene SSTs have been reported for the Tropical Atlantic region [*Morley and Dworetzky*, 1993; *Ruddiman and Mix*, 1993], but because opposite changes are recorded for relatively small areas, their interpretation has been difficult. Simulations of the Middle Holocene with global SSTs prescribed to their current values [*Yu and Harrison*, 1996; *Coe and Bonan*, 1997; *Masson and Joussaume*, 1997; *Texier et al.*, 1997; *Broström et al.*, 1998; *Harrison et al.*, 1998; *Joussaume et al.*, 1999] have significantly underestimated the expected monsoon expansion by limiting the response of the climate system to prescribed orbital changes. However, simulations of the Middle Holocene in which summer SSTs over the SETA region have been decreased by $1 - 3°$ K as compared to current conditions [*Texier et al.*, 2000], resulted in a significant rainfall increase, specially in the eastern Sahara. Therefore, in order to allow for a more complete response of the climate system to changes in external forcings (i.e. changes in SSTs), the inclusion of an ocean component into ZonalBAM is required. This would add another mechanism through which interactions in the climate system could take place shaping its variability.

For the Middle Holocene, Tropical Atlantic SSTs have been found to assert a dominant influence in Sahel rainfall when compared to ENSO anomalies based on the results of GCM simulations [*Otto-Bliesner*, 1999], and on faunal evidence from the Peruvian coast [*Sandweiss et al.*, 1996]. This is encouraging when using ZonalBAM

for simulating the climate during the period. Being a zonally symmetric model, ZonalBAM can only simulate the zonally averaged (15° W-15° E) conditions in the region of West Africa, while asymmetrical climate features (e.g. upwelling/sinking, synoptic disturbances) and global dynamics (e.g. teleconnections to ENSO, NAO), which can influence the local climate, cannot be simulated. Due to ZonalBAM's configuration, ocean feedbacks, which could affect the monsoon circulation [*Zheng et al.*, 1999], are limited to the region south of the Guinea coast (SETA region). Using a coupled ocean-atmosphere model, *Braconnot et al.* [2000] found cooler SSTs in the SETA region during the Middle Holocene. As a result, the West African summer monsoon started one month earlier and retreated more slowly in autumn. However, in *Kutzbach and Liu*'s [1997] study, only small changes in the SSTs were simulated south of the Atlantic coastline. Nevertheless, the complicated patterns in the observed SSTs for the period makes it hard to determine whether this is a model-dependent or a robust climate feature.

The influence of the Mediterranean in winter rainfall over the northern Sahara is believed to have been larger during the Middle Holocene than today [*Petit-Maire and Guo*, 1997]. Therefore, here we also include a representation of the Mediterranean from 35° N to 40° N for which we always fix the SSTs to their current climatology. The reason behind fixing the Mediterranean SSTs is due to its location in middle latitudes, where it is influenced by eddies, asymmetrical features that cannot be simulated by ZonalBAM.

Due to ZonalBAM's simplicity, we include ocean dynamics by adding a mixed layer ocean model (MLOM) in which SSTs in the SETA region are computed based on energy balance considerations. Several theoretical studies have demonstrated that the finite heat capacity of the oceanic mixed layer affects the atmospheric variability through thermodynamic feedbacks [*Saravanan and McWilliams*, 1998]. Since air-sea interactions take place mostly in the top ocean layer, and wind mixing produces uniform conditions in the top ~100 m, a mixed layer ocean model (MLOM) can be a first-order approximation to these interactions, and their effects on the ocean heat budget. The energy balance in this top layer consists of incoming net radiation, latent

and sensible heat fluxes, and an advection term representing the ocean heat fluxes (Figure 2-5). These terms together contribute to changes in the SSTs according to the following relation:

$$C_p h \frac{\partial T}{\partial t} = R_{net} - E_t - H + O \qquad (2.1)$$

where C_p is the ocean's heat capacity (= 4,218 J/kg/K), h is the mixed layer depth from the World Ocean Atlas [*Levitus*, 1994], T is the SST, t is time, R_{net} is the net radiation, E_t is latent heat flux, H is sensible heat flux, and O is the ocean heat flux. As has been demonstrated by *Saravanan and Chang* [1999], the inclusion of spatial and temporal variability in the mixed layer ocean depth is important in order to accurately simulate the SST variability. Therefore, here we include the latitudinal and seasonal variability of the mixed layer ocean depth (Figure 2-6).
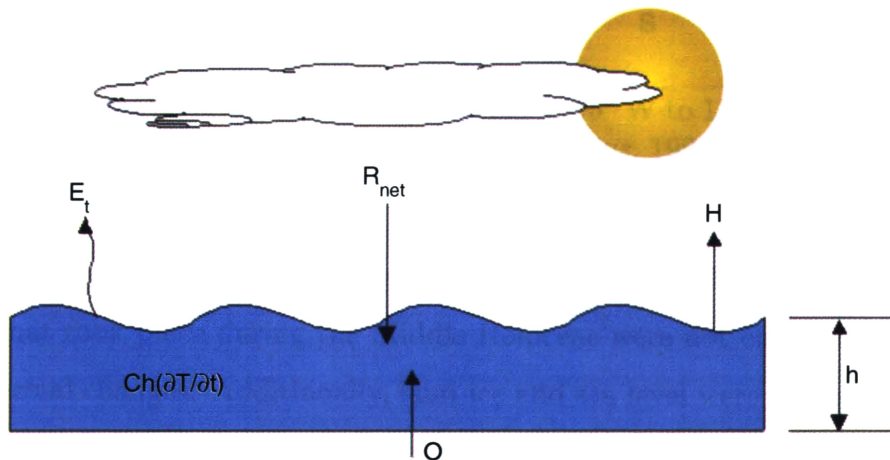
Figure 2-5: Representation of the mixed layer ocean model (MLOM). C_p is the ocean's heat capacity, h is the mixed layer depth from the World Ocean Atlas [*Levitus*, 1994], T is the SST, t is time, R_{net} is the net radiation, E_t is latent heat flux, H is sensible heat flux, and O is the ocean heat flux.

In our studies, the MLOM is only applied to the region between 25° S and 5° N (average over 15° W-15° E), which interacts directly with the zonally-symmetric monsoon circulation. The basis for this is that mid-latitude winds, which influence the sensible and latent heat fluxes from the ocean, are affected by eddies resulting from baroclinic instability, and these cannot be described by ZonalBAM. In addition, this simple ocean model cannot simulate changes in ice cover. Therefore, we chose to prescribe the SSTs south of 25° S to their current climatology.
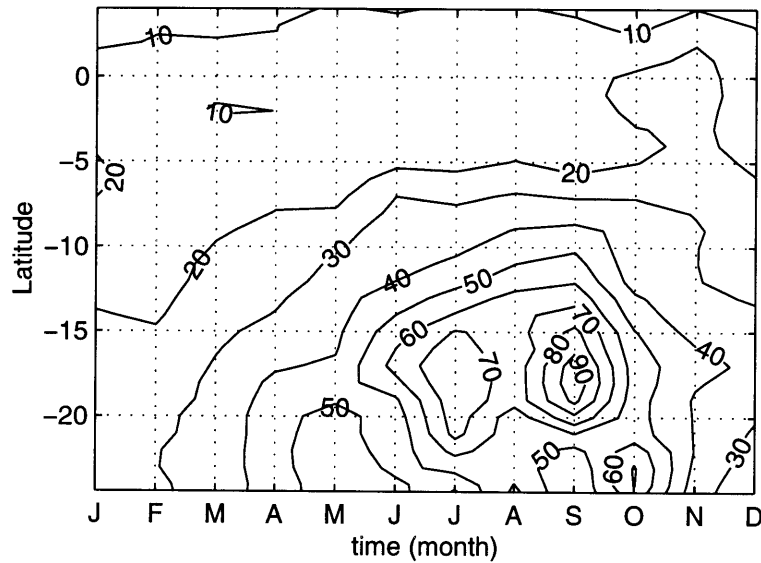
Figure 2-6: Climatology of the zonally-averaged (15° W to 15° E) mixed layer depth (m) from the World Ocean Atlas [*Levitus*, 1994].

It is believed that due to the large thermal capacity of the ocean, the insolation changes that took place during the Middle Holocene were not enough to cause large direct thermal changes. Additionally, land ice and sea level were the same as current since the Laurentide and Scandinavian ice sheets had already retreated [*Kutzbach and Guetter*, 1986; *COHMAP Members*, 1988; *Peltier*, 1993; *Ruddiman and Mix*, 1993; *Felzer et al.*, 1998]. Atmospheric CO_2 concentrations were also close to their preindustrial levels. For all these reasons, SST anomalies are expected to be small as shown in reconstructions. However, it is believed that an orbitally-induced increased low-level flow into West Africa could have resulted in weaker trade winds and equa-

60

torial upwelling during the Middle Holocene producing a small warming of the TNA [*Kutzbach*, 1981; *Ruddiman and Mix*, 1993]. An interplay between a small orbitally-induced direct cooling of the SETA region, and an indirect warming of the TNA due to the weaker trade winds, could at least partially explain the complicated patterns found in the SST anomalies during the Mid-Holocene. Since these ocean heat fluxes are not quantitatively known for the Middle Holocene, we have chosen to fix them to their current values. Therefore, the latter of these effects will not be taken into account in our MLOM. Details on the calculation of this ocean heat fluxes term will be discussed in more detail in Chapter 4, where the validation of the MLOM based on current forcings is explained. In addition, this MLOM is used in simulations of the Middle Holocene climate of West Africa in order to determine whether the inclusion of ocean dynamics can bring simulations closer to palaeoclimate reconstructions.

2.4 Validity of Using ZonalBAM to Simulate West African Conditions During the Middle Holocene

Before attempting to use a climate model for simulating future climates, it should be able to appropriately reproduce conditions existing under current forcings. Our zonally symmetric climate model, ZonalBAM, has been able to successfully reproduce current conditions over the region of West Africa. However, in order to increase our confidence in the model's ability in simulating climate change, it must successfully reproduce the main features of past climates for regions where there is enough proxy data available to allow for comparison. Here, we have chosen the Middle Holocene as a case study since evidence that the ice sheets had already retreated to their current extent and the SSTs were similar to the current allows for isolating the effects of insolation on climate. Additionally, the vast amount of proxies available for climate reconstruction over the region of West Africa presents a unique opportunity to test model results against observations. Here, we present the reasoning behind the use

of ZonalBAM to simulate the West African climate during the Middle Holocene. Additionally, limitations arising from ZonalBAM's simplifications are discussed.

Reasoning behind the use of ZonalBAM to simulate the West African climate during the Middle Holocene:

1. Our climate model, being a zonally symmetric model, is limited to the simulation of regional dynamics in tropical West Africa since the region is characterized by the meridional monsoon circulation which results in a close to zonally symmetric climate and vegetation distribution as has been quantitatively proven by *Zheng and Eltahir* [1998]. During the Middle Holocene, the main cause of climate change was due to variations in the Earth's orbital parameters resulting in a higher insolation at the top of the atmosphere during the Northern Hemisphere summer. Due to the different thermal capacities of the land and the ocean, these insolation changes had a larger heating effect over the land surfaces, increasing the energy gradient between the two and resulting in an enhanced monsoon circulation. Synergistic feedbacks between the vegetation and ocean are believed to have produced a further enhancement of the monsoon resulting in significantly wetter conditions over the region as compared to current [*Braconnot et al.*, 1999]. It is also believed that an orbitally-induced increased low-level flow into West Africa during the period, resulted in weaker trade winds. Additionally, due to the relatively short timescale of climate change considered here, the main topographic features over the region were basically the same as today, so that topographically-induced changes to the atmospheric circulation were again secondary. Therefore, *Zheng et al.*'s [1999] argument that the circulation in the region is dominated by zonal symmetry is again valid for the Middle Holocene. It then becomes reasonable to use ZonalBAM to simulate the main features of the Mid-Holocene conditions over West Africa.

2. Due to ZonalBAM's zonal symmetry, it is computationally more efficient than other 3-D models. Therefore, savings in computer time can then be used for the synchronous coupling of a biospheric component, for which a small time step

62

of 20 minutes is required in order to simulate the different possible timescales of interaction. Additionally, these savings allow for the coupling of an ocean component.

3. During the Middle Holocene, the Tropical Atlantic SSTs have been found to assert a dominant influence in Sahel rainfall when compared to ENSO anomalies [*Sandweiss et al.*, 1996; *Otto-Bliesner*, 1999], which is encouraging when using ZonalBAM in simulating the West African climate during the period.

Limitations in using ZonalBAM to simulate the climate of West Africa during the Middle Holocene:

1. Being a zonally symmetric model, ZonalBAM can only simulate the zonally averaged (15° W-15° E) conditions in the region of West Africa, while asymmetrical climate features and global dynamics, which can influence the local climate, cannot be simulated:

   (a) Eddies, low and high pressure systems generated as a result of baroclinic instability in middle latitudes, cannot be simulated. In order to reduce biases associated with the lack of simulation of these features in ZonalBAM, fluxes, temperatures and vegetation conditions in middle and high latitudes need to be prescribed. These data are readily available for the current climate from a variety of sources. However, these are not quantitatively known for the Middle Holocene. Therefore, we have chosen not to fix conditions in mid-latitudes. Instead, we let ZonalBAM to interactively calculate them. In doing so, we are assuming that the main transport mechanism over mid-latitudes is a zonally symmetric simulation, while we neglect the existence of eddies as a transfer mechanism. *Petit-Maire and Guo* [1997] have determined that northwestern polar depressions and Atlantic cyclones were a more important contributor to winter rainfall in the northern Sahara during the Middle Holocene as compared to today. Therefore, sensitivity experiments regarding these northern influences are required.

(b) Due to ZonalBAM's configuration, only changes to the SSTs over the SETA region (25° S-5° N and 15° W-15° E) can be taken into account. Although of secondary importance, changes in the conditions over the TNA (10° N-25° N) could influence conditions over West Africa, specially in the coastal margins during summer when the current wind climatology shows an eastward component. Although, the relationship between West African precipitation and ENSO anomalies has been the object of significant debate, ENSO-related changes to the global atmospheric circulation could also influence conditions over West Africa.

2. Although no evidence has been found for significantly different SSTs [*Morley and Dworetzky*, 1993; *Ruddiman and Mix*, 1993] during the Middle Holocene in terms of global and annual scales, there is a common belief that local and seasonal variations might have contributed to enhancing the monsoon circulation over West Africa. Several limitations to the inclusion of an interactive mixed layer ocean model include:

(a) This simple model requires the inclusion of ocean heat fluxes as an additional term. This term should account for the advection of heat by ocean currents and local upwelling/sinking, processes which cannot be simulated by ZonalBAM and are not quantitatively known for the Middle Holocene. This forces us to prescribe these fluxes in the Middle Holocene to their current value.

(b) The fact that the atmospheric circulation over the region between 25° S and 5° N is zonally-symmetric does not imply that the ocean circulation has to be. In fact, the SETA region is currently characterized by strong coastal upwelling in the Benguela system off the western coast of South Africa.

(c) In Chapter 4, it will be shown that the validation of our MLOM based on current forcings yielded a cold bias in the simulated current SSTs, which can have implications for the simulation of Mid-Holocene ocean conditions.

Chapter 3

Simulations Using the Coupled Biosphere-Atmosphere Model

3.1 Introduction

The successful simulation of past climate change is a critical component in the process of validating a climate model. It would give us more confidence when attempting to use the model to simulate future climate change. Additionally, it would give us some insight into the way in which interactions between the components of the climate system (i.e. atmosphere, biosphere, ocean, surface waters) take place. The gained understanding would ultimately allow for model improvements. For this purpose, we attempt to validate the utility of our climate model, ZonalBAM, in reproducing climate change over the region of West Africa by using the Middle Holocene as a basis for comparison with current forcings. Our objective here is to understand the mechanisms responsible for a greener Sahara during the Middle Holocene.

According to *Eltahir and Gong* [1996], the gradient of moist static energy between the land and the ocean affects the strength of the monsoon circulation. Therefore, changes in any of the two components will ultimately result in precipitation changes over land. Here, our objective is to understand how changes to the energy balance over land could have resulted in wetter conditions during the Middle Holocene. The reasoning behind this lies in the fact that the land surface exerts a strong influence in

the amount of net radiation reaching the surface and the way in which it is partitioned, thereby affecting the amount of moist static energy (latent and sensible heat fluxes) fed into the land boundary layer and the strength of the monsoon [*Eltahir and Gong*, 1996; *Eltahir*, 1998; *Zheng and Eltahir*, 1998].

With the objective of assessing the relative contributions of orbitally-induced changes in radiation, vegetation dynamics, and the sensitivity to initial vegetation conditions, four pairs of experiments based on current and 6K yrs BP orbital forcings were designed and are summarized in Table 3.1. Results of these simulations are tabulated in Table 3.2 in terms of the simulated location of the southern desert margin, hereafter defined as the location of 200 mm/yr annual precipitation. The sets of simulations O𝒜-VS0-SS0-1 and O𝒜-VS6-SS0-1, in which static vegetation is fixed to either the current or Mid-Holocene distribution (Tables 3.3 and 3.4), were performed with the intention of isolating the response of the climate system to orbitally-induced changes in top-of-the-atmosphere insolation. In the sets of simulations O𝒜-VD0-SS0-1 and O𝒜-VD6-SS0-1, vegetation in the region from ˜5° N-27° N is initialized to either the current or Mid-Holocene distribution, and allowed to dynamically interact with climate until an equilibrium is established. The reasoning behind these two last sets of simulations is to assess whether these initial vegetation conditions can in fact be sustained under different orbital forcings. The particular objective is to assess whether the Mid-Holocene climate system can evolve into a wetter equilibrium through vegetation dynamics enhancing the orbital signal alone (simulation O6-VD0-SS0-1), or if the initial vegetation conditions (simulation O6-VD6-SS0-1) play a significant role in determining the equilibrium attained by the system.

These simulations are described in more detail in the following sections and the main forcings used are tabulated in Table 3.5. In all simulations, we chose to let the fluxes and temperatures in the north to be model-calculated and any vegetation north of ˜27° N (except for the Mediterranean Sea) was fixed as grassy-savannah.

Name of simulation[a]	Orbital forcing	Vegetation	Ocean	Fluxes and temperatures north of 27° N	Vegetation north of 27° N fixed to
O0-VS0-SS0-1	0K yrs BP	Fixed to current[b]	Fixed to current	Model-calculated	Grassy-savannah
O6-VS0-SS0-1	6K yrs BP	Fixed to current	Fixed to current	Model-calculated	Grassy-savannah
O0-VD0-SS0-1	0K yrs BP	Dynamic from current[c]	Fixed to current	Model-calculated	Grassy-savannah
O6-VD0-SS0-1	6K yrs BP	Dynamic from current	Fixed to current	Model-calculated	Grassy-savannah
O0-VS6-SS0-1	0K yrs BP	Fixed to Mid-Hol.[d]	Fixed to current	Model-calculated	Grassy-savannah
O6-VS6-SS0-1	6K yrs BP	Fixed to Mid-Hol.	Fixed to current	Model-calculated	Grassy-savannah
O0-VD6-SS0-1	0K yrs BP	Dynamic from Mid-Hol.[e]	Fixed to current	Model-calculated	Grassy-savannah
O6-VD6-SS0-1	6K yrs BP	Dynamic from Mid-Hol.	Fixed to current	Model-calculated	Grassy-savannah

[a] Name of simulation has the form: O$\mathcal{A}$-V$\mathcal{B}$-S$\mathcal{C}$-$\mathcal{D}$, where; O = orbital forcing; $\mathcal{A}$ = 0 or 6 corresponding to 0 or 6K yrs BP orbital forcings respectively; V = vegetation conditions; $\mathcal{B}$ = S0 or S6 corresponding to static vegetation fixed to current or Mid-Holocene conditions, D0 or D6 corresponding to dynamic vegetation initialized to current or Mid-Holocene conditions; S = ocean conditions; $\mathcal{C}$ = S0 or S6 corresponding to static ocean fixed to current or Mid-Holocene conditions; $\mathcal{D}$ = simulation number.

[b] Derived from *USGS Global Land Cover Characterization Data, Gornitz and NASA* [1995], and *Foley et al.* [1996].

[c] Dynamic vegetation initialized from current distribution.

[d] Derived from *Hoelzmann et al.*'s [1998] map of palaeovegetation.

[e] Dynamic vegetation initialized based on *Hoelzmann et al.*'s [1998] map of palaeovegetation.

Table 3.1: Summary of simulations for 0 and 6K yrs BP using the zonally symmetric biosphere-atmosphere model (ZonalBAM).

Name of simulation set[a]	Vegetation[b]	Location of the southern desert margin for 0K yrs BP	Location of the southern desert margin for 6K yrs BP	Difference in the southern desert margin (6K-0K yrs BP)
OA-VS0-SS0-1	Static from current	16.3° N	17.4° N	1.1°
OA-VD0-SS0-1	Dynamic from current	15.7° N	18.1° N	2.4°
OA-VS6-SS0-1	Static from Mid-Hol.	20.4° N	21.4° N	1.0°
OA-VD6-SS0-1	Dynamic from Mid-Hol.	15.4° N	20.5° N	5.1°

[a] See Table 3.1 for a description.

[b] This refers to the vegetation conditions between ~5° N and ~25° N. In all simulations, vegetation north of ~27° N has been fixed to grassy-savannah.

Table 3.2: Summary of results based on the simulated location of the southern desert margin.

Latitudes (°)	Vegetation type [a]	
	Current (0K yrs BP)[b]	Mid-Holocene (6K yrs BP)[c]
5.0 - 7.5	1	1
7.5 - 10.0	2	2
10.0 - 12.6	4	4
12.6 - 15.1	5	4
15.1 - 17.7	6	5
17.7 - 20.4	8	6
20.4 - 23.0	8	7
23.0 - 25.8	8	8
25.8 - 28.6	8	7
28.6 - 31.4	9	9
31.4 - 34.4	9	9

[a] Description of vegetation types: 1-rain forest, 2-dry forest, 4-woody savannah, 5-tall grass, 6-short grass, 7-semidesert, 8-desert, 9-grassy-savannah.

[b] Close-to-observed vegetation distribution derived from *USGS Global Land Cover Characterization Data, Gornitz and NASA* [1995], and *Foley et al.* [1996].

[c] Palaeovegetation distribution derived from *Hoelzmann et al.* [1998].

Table 3.3: Initial vegetation distribution for 0 and 6K yrs BP.

Pft [a]	LAI for vegetation type[b]							
	1	2	4	5	6	7	8	9
Upper canopy:								
Evergreen	4.0	1.0	0.125	0.125	0.025	0.05	0.0005	0.15
Deciduous	2.0	5.0	1.0	0.125	0.025	0.05	0.0005	0.15
Lower canopy	0.5	0.5	4.2	4.2	1.1	0.3	0.026	2.75

[a] Evergreen pfts include tropical broadleaf evergreen tree, temperate conifer evergreen tree, warm-temperate broadleaf evergreen tree, boreal conifer evergreen tree. Deciduous pfts include tropical broadleaf drought-deciduous tree, temperate broadleaf cold-deciduous tree, boreal broadleaf cold-deciduous tree, boreal conifer cold-deciduous tree. Lower canopy pfts include evergreen shrub, cold-deciduous shrub, warm (c4) grass, cool (c3) grass.

[b] See Table 3.3 for a description.

Table 3.4: Total leaf area index for evergreen, deciduous and lower canopy plant functional types (pfts) comprising each vegetation type in ZonalBAM.

Parameter	0K yrs BP	6K yrs BP
Orbital parameters: [a]		
Eccentricity	0.0167	0.0187
Obliquity (°)	23.45	24.10
Precession (°)	102.04	0.87
South Eastern Atlantic SSTs	Current	Current
Mediterranean SSTs	Current	Current
Vegetation north of ~27° N	Fixed to grassy-savannah	Fixed to grassy-savannah

[a] Derived from *Berger* [1978a,b].

Table 3.5: Parameters used in simulations.

3.2 Orbitally-Induced Climate Change

During the Middle Holocene (6K yrs BP), the insolation anomaly was about 6% (~25 W/m^2) greater in the Northern Hemisphere summer and 6 % lower in the Northern Hemisphere winter, mainly due to the fact that perihelion occurred near the autumnal equinox (rather than close to winter solstice as today) and the Earth's axial tilt was larger than at present. It is our interest to understand the mechanisms through which these insolation changes enhanced the monsoonal climate over West Africa during the period resulting in a significant rainfall increase, as has been widely recorded.

An initial set of simulations (OA-VS0-SS0-1) were performed with the purpose of isolating the effect of the different orbital forcings for 0 and 6K yrs BP. Therefore, in these simulations, we fixed the vegetation to the close-to-observed distribution (Figure 3-1; and Table 3.3, column 2), which consists of rain forest in the Coast of Guinea (~5° N), gradually becoming sparser northward. The specific characteristics associated to each vegetation type, such as the combination of plant functional types (pfts) and their corresponding fractional coverage and leaf area index (LAI), were also kept constant among simulations (Table 3.4).
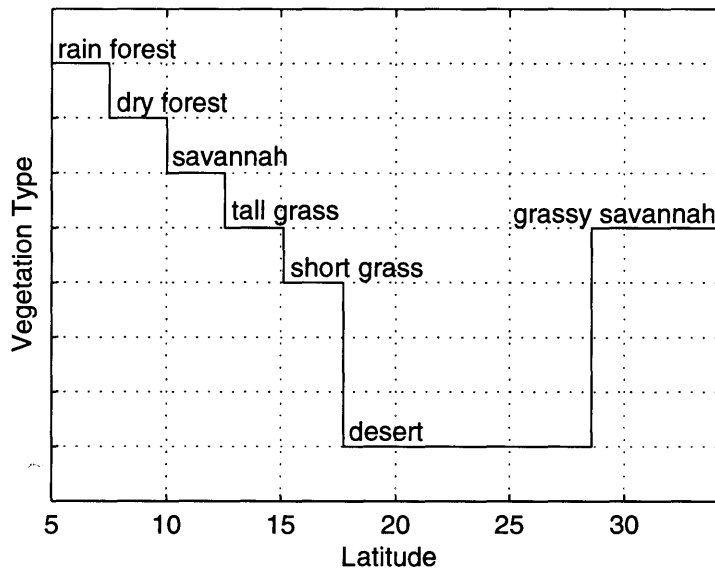
Figure 3-1: Close-to-observed vegetation distribution.

70

Results show that the 6K yrs BP forcing produces a slight rainfall increase (Figure 3-2, solid-circled and dashed-circled lines) over the region from ~9° N to ~19° N due to a simulated local strengthening of the monsoon during summer (Figure 3-3c). However, in these simulations, vegetation is not allowed to respond to this rainfall increase, and its distribution is inconsistent with the Middle Holocene. Consequently, the static vegetation basically serves to anchor the system to the current climate so that the expected monsoon expansion during the Middle Holocene is not well simulated.

The most dramatic difference in land cover between 6K yrs BP and present is recorded for the region between ~16.5° N and ~23.5° N, with the current land surface being desert and the 6K yrs BP land being covered by grass/savannah. Therefore, the most significant changes during the Middle Holocene are expected to occur during summer in the regions of the Sahel-Sahara between ~16.5° N and ~23.5° N. Results for this critical region (Table 3.6) show that the orbitally-induced increase in top-of-the-atmosphere radiation for the Middle Holocene summer is capable of increasing the net radiation received at the land surface by only ~11 W/m^2. This limited response in the net radiation results from the fixed surface albedo over the region, which is inconsistent with conditions during the Middle Holocene, and acts by reflecting a significant amount of radiation back to space. This small increase in the net surface radiation results in a warmer surface temperature, and acts to increase the latent and sensible heat fluxes over land. However, due to the higher soil moisture content associated to wetter conditions for the 6K yrs BP simulation, the Bowen ratio is reduced (from 2.2 for current forcings to 1.5 for Mid-Holocene forcings) so that most of the increase in net radiation goes to evapotranspiration. With conditions over the ocean being anchored by the specified fixed SST climatology, the increased fluxes of latent and sensible heat fed into the land boundary layer produce a slightly steeper gradient of moist static energy (Figure 3-4). As a consequence, the summer monsoon slightly strengthens producing a northward migration of the southern desert margin (defined as the location of 200 mm/yr precipitation) by ~1.1° (from 16.3° N to 17.4° N, Table 3.2).
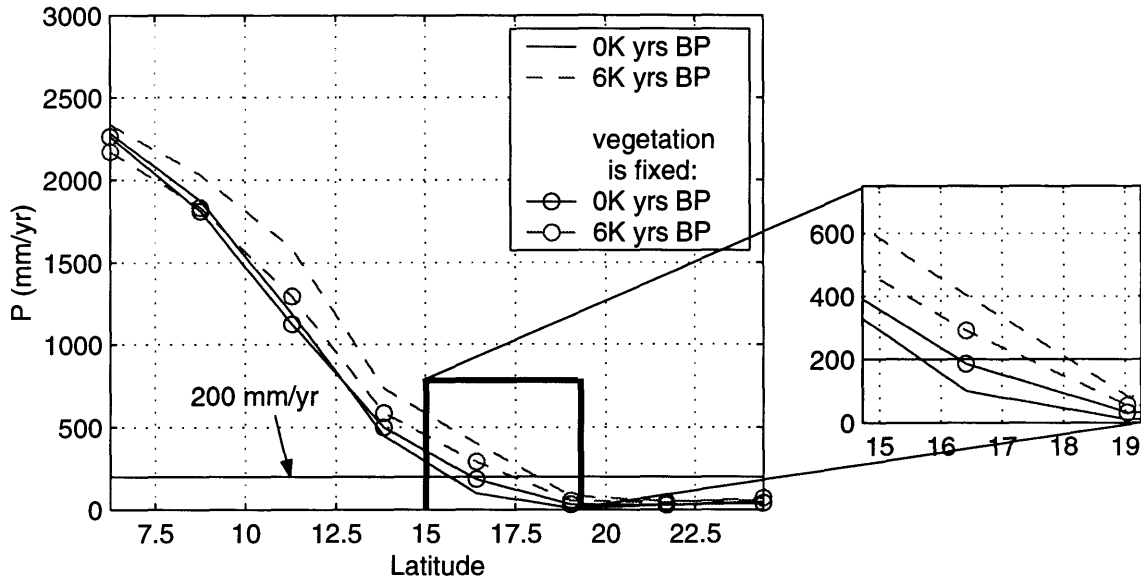
Figure 3-2: Distribution of total annual precipitation (mm/yr) for simulations with dynamic vegetation initialized to the current distribution (simulations 0$\mathcal{A}$-VD0-SS0-1; solid and dashed lines). Lines with circles represent simulations in which static vegetation conditions were fixed to the current distribution (simulations 0$\mathcal{A}$-VS0-SS0-1).

Variable	0K yrs BP (O0-VS0-SS0-1)	6K yrs BP (O6-VS0-SS0-1)
B_o	2.2	1.5
$W_{soil,veg.}$	0.05	0.06
SHF (W/^{2})	37.2	39.1
LHF (W/m^2)	16.8	25.6
E_t (mm/day)	0.6	0.9
R_{net} (W/m^2)	163.1	174.3
P (mm/day)	0.5	0.7

B_o = Bowen ratio, $W_{soil,veg.}$ = soil moisture content available to vegetation = f(soil moisture, rooting profile), SHF = sensible heat flux, LHF = latent heat flux, E_t = evapotranspiration, R_{net} = net radiation, P = precipitation.

Table 3.6: Average value of key variables for current (simulation O0-VS0-SS0-1) and Mid-Holocene (simulation O6-VS0-SS0-1) summer (JAS) conditions in the region between 16.5° N and 23.5° N for simulations on the orbitally-induced climate change.
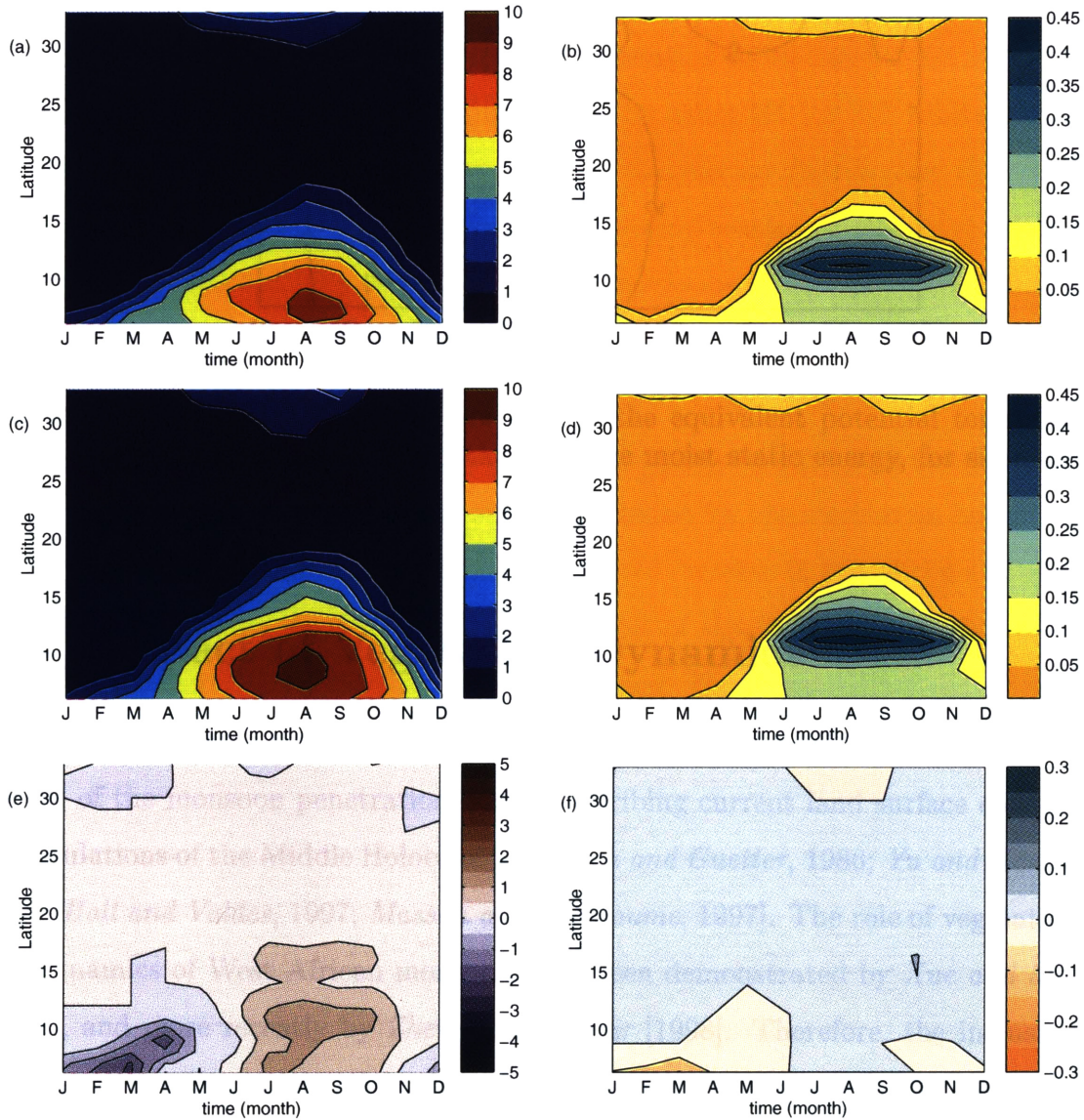
Figure 3-3: Results for simulations with static vegetation fixed to the current distribution (simulations O$\mathcal{A}$-VS0-SS0-1): (a) Seasonal cycle of rainfall (mm/day) and (b) net primary productivity (kgC/m^2/mo) for 0K yrs BP; (c) Seasonal cycle of rainfall and (d) net primary productivity for 6K yrs BP; (e) = (c) - (a); (f) = (d) - (b).
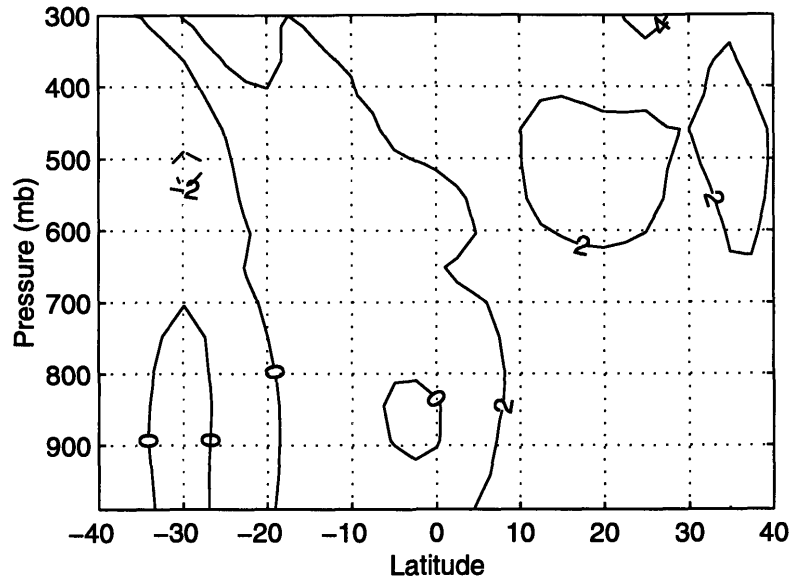
Figure 3-4: Difference (6K - 0K yrs BP) in the equivalent potential temperature (° K), which is proportional to the moist static energy, for simulations O.4-VS0-SS0-1.

3.3 Impact of Vegetation Dynamics

Several studies using general circulation models have consistently underestimated the extent of the monsoon penetration when prescribing current land surface conditions in simulations of the Middle Holocene [*Kutzbach and Guetter*, 1986; *Yu and Harrison*, 1996; *Hall and Valdes*, 1997; *Masson and Joussaume*, 1997]. The role of vegetation in the dynamics of West African monsoons has been demonstrated by *Xue and Shukla* [1993], and more recently by *Zheng and Eltahir* [1998]. Therefore, the inclusion of vegetation dynamics into simulations of climate change [*Foley et al.*, 2000] such as for the Middle Holocene becomes critical.

In order to allow for a more complete response of the climate system to the different orbital forcings, vegetation in the region from ˜5° N to ˜27° N, was initialized to the close-to-observed distribution, and allowed to dynamically interact with the climate until an equilibrium is established (simulations O.4-VD0-SS0-1). It is found that the 6K yrs BP forcing produces a higher rainfall over the whole domain (Figure 3-2, solid and dashed lines), specially during summer (Figure 3-5c). Consequently, water

demanding vegetation expands slightly northward. However, the rainfall increase near the desert margin is not enough to allow for a significant northward expansion of vegetation, contrary to what is expected from palaeoclimatic reconstructions.

In simulations O$\mathcal{A}$-VS0-SS0-1, where we isolated the response of the West African climate to insolation changes by prescribing vegetation to its current distribution, we found a slight rainfall increase for the simulation using 6K yrs BP orbital forcings. However, since vegetation was fixed to the close-to-observed distribution, the response of the climate system was limited in that the expected northward shift of the southern desert margin was not fully simulated. When vegetation is allowed to be dynamic, it responds to this increase in rainfall by becoming greener (Figure 3-5f), which again feeds back and adds to the strength of the monsoon circulation.

Since a lower surface albedo is associated with a greener vegetation distribution, we find a significant increase in the net surface radiation for the simulation based on 6K yrs BP forcings (Table 3.7). The orbitally-induced increase in top-of-the-atmosphere radiation for the Middle Holocene is now capable of significantly increasing (by ~46 W/m^2) the net radiation reaching the land surface. The increased net radiation generally produces increased surface temperature, except for the the region between ~15° N- 20° N during summer, where evapotranspiration from the expanded vegetation cools the surface. Additionally, the increased net radiation reaching the surface allows for a significant increase in the total latent and sensible heat fluxes, compared to conditions simulated for the current climate. However, again, the largest increase is in the latent heat flux as drawn from the significant decrease in the Bowen ratio (from 3.5 for current forcings to 1.2 for Mid-Holocene forcings). This is due to a higher soil moisture content and greener conditions which favor evapotranspiration over sensible heating. The increase in the energy fluxes fed into the land boundary layer results in an even steeper gradient of moist static energy with respect to the ocean (Figure 3-6), and hence a healthier monsoon. As a result, the southern margin of the desert border migrates northward by ~2.4° (from 15.7° N to 18.1° N, Table 3.2) as compared to ~1.1° when vegetation dynamics were not allowed.
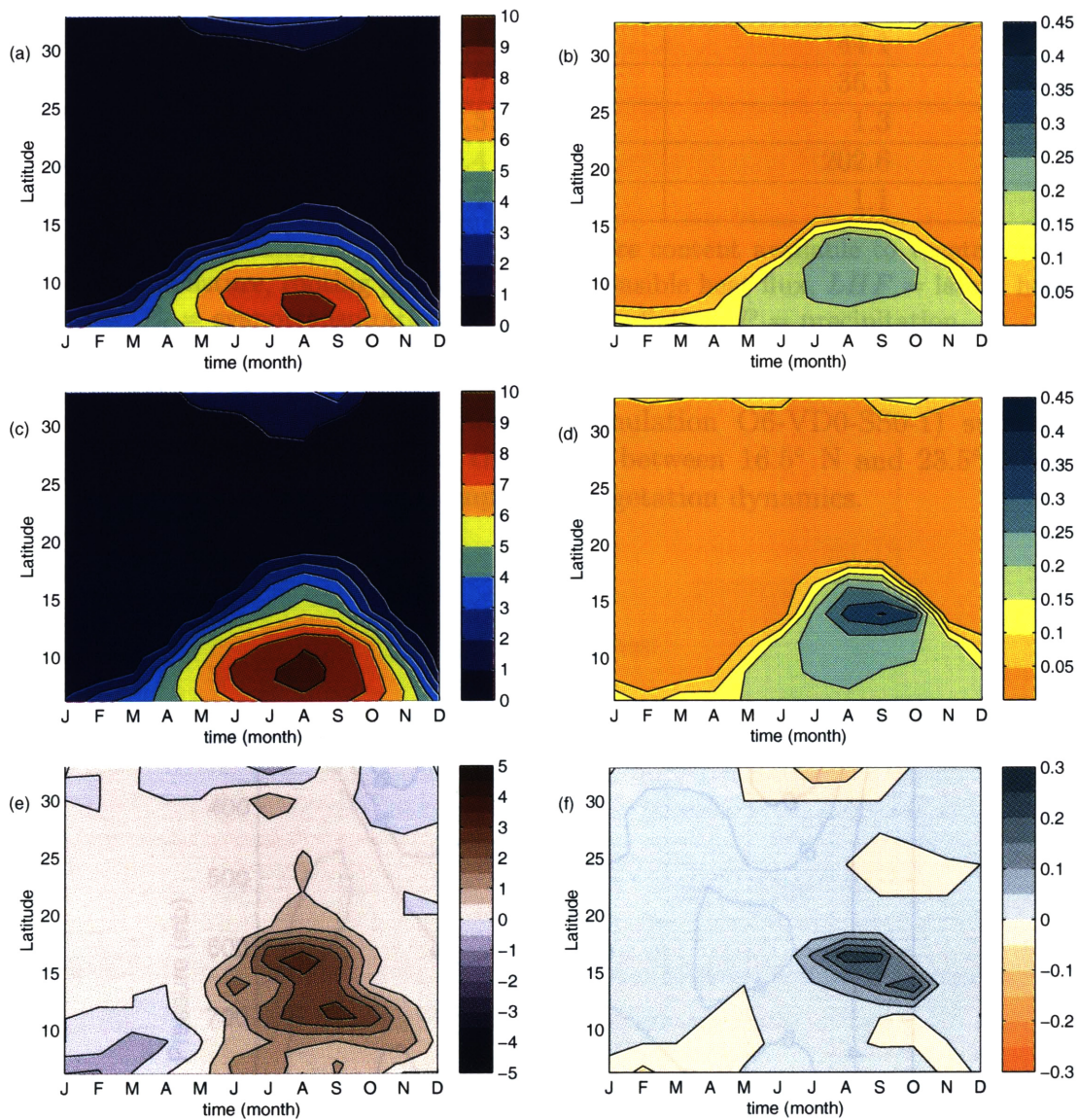
Figure 3-5: Results for simulations with dynamic vegetation initialized to the current distribution (simulations O$\mathcal{A}$-VD0-SS0-1): (a) Seasonal cycle of rainfall (mm/day) and (b) net primary productivity (kgC/m^2/mo) for 0K yrs BP; (c) Seasonal cycle of rainfall and (d) net primary productivity for 6K yrs BP; (e) = (c) - (a); (f) = (d) - (b).

Variable	0K yrs BP (O0-VD0-SS0-1)	6K yrs BP (O6-VD0-SS0-1)
B_o	3.5	1.2
$W_{soil,veg.}$	0.02	0.06
SHF (W/m^2)	34.3	44.1
LHF (W/m^2)	9.9	36.3
E_t (mm/day)	0.3	1.3
R_{net} (W/m^2)	156.4	202.6
P (mm/day)	0.2	1.1

B_o = Bowen ratio, $W_{soil,veg.}$ = soil moisture content available to vegetation = f(soil moisture, rooting profile), SHF = sensible heat flux, LHF = latent heat flux, E_t = evapotranspiration, R_{net} = net radiation, P = precipitation.

Table 3.7: Average value of key variables for current (simulation O0-VD0-SS0-1) and Mid-Holocene (simulation O6-VD0-SS0-1) summer (JAS) conditions in the region between 16.5° N and 23.5° N for simulations on the impact of vegetation dynamics.
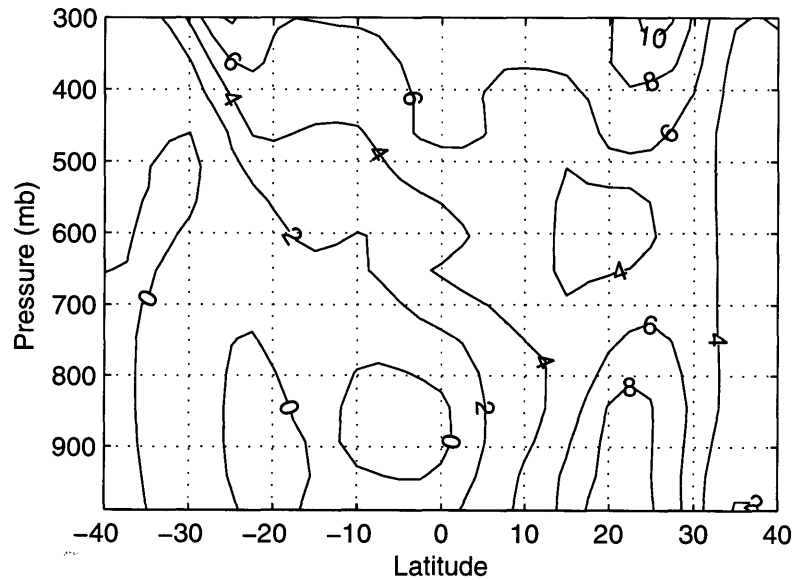
Figure 3-6: Difference (6K - 0K yrs BP) in the equivalent potential temperature (° K), which is proportional to the moist static energy, for simulations OA-VD0-SS0-1.

77

3.4 Impact of Changes in Initial Vegetation Conditions

Previous studies [*Kutzbach et al.*, 1996; *Broström et al.*, 1998] have demonstrated the importance of incorporating Mid-Holocene vegetation conditions in order to bring simulations closer to palaeoclimatic reconstructions. The need for a detailed database of vegetation distribution and characteristics for the Middle Holocene is critical. Reconstructions of the Middle Holocene vegetation have been done by several groups [*Adams et al.*, 1997; *Hoelzmann et al.*, 1998].
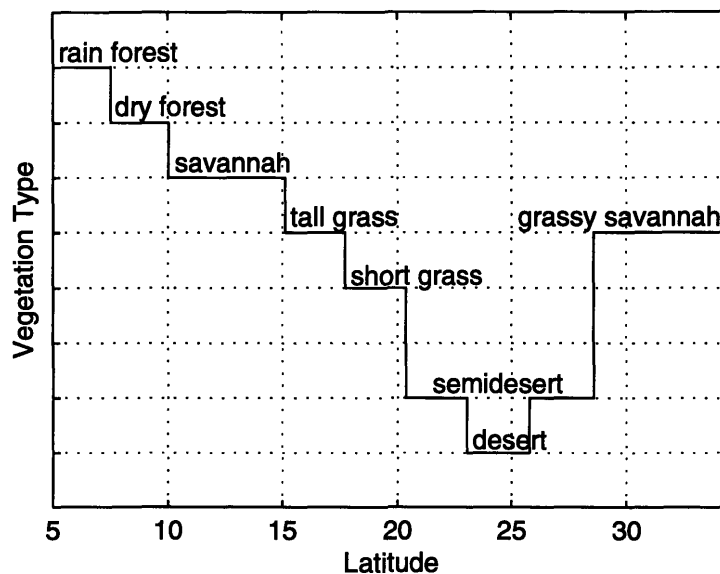
Figure 3-7: Initial vegetation distribution for the Middle Holocene reconstructed by *Hoelzmann et al.* [1998].

Based on the information derived from *Hoelzmann et al.*'s [1998] map of palaeovegetation, we determined the extent of the vegetation belts during the Middle Holocene. Prescribing these vegetation conditions (Table 3.3, column 3; Table 3.4; Figure 3-7) to the region from ~5° N to ~27° N in a simulation based on current orbital forcings (simulations O0-VS6-SS0-1), we find significantly wetter conditions than currently observed (Figures 3-8 and 3-9a,b). However, when vegetation in this region is allowed to dynamically respond to climate (simulations O0-VD6-SS0-1), we find that these

78

cannot be sustained under current forcings (Figures 3-8 and 3-9a,b and 3-11a,b). The model reaches an equilibrium very similar to the currently observed climate, the same as when it was forced with the close-to-observed vegetation distribution (Figures 3-8 and 3-13a).
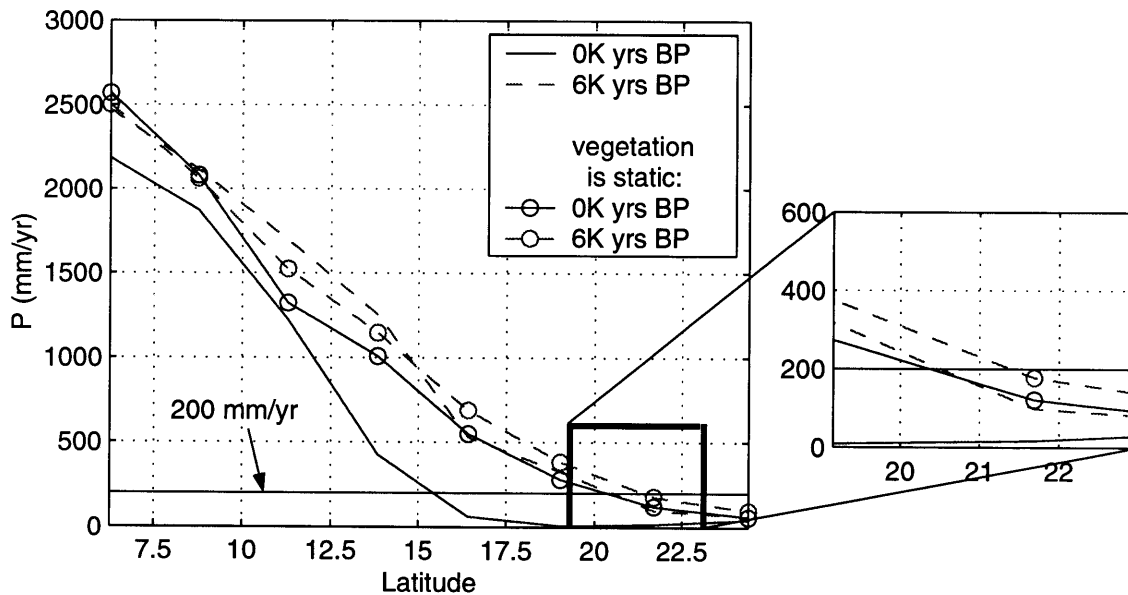
Figure 3-8: Distribution of total annual precipitation (mm/yr) for simulations on the impact of changes in vegetation conditions. Simulations with dynamic vegetation initialized to the Mid-Holocene distribution (simulations O4-VD6-SS0-1) are the solid and dashed lines, while lines with circles represent simulations in which static vegetation conditions were fixed to the Mid-Holocene distribution (simulations O4-VS6-SS0-1).

Prescribing this more realistic vegetation distribution for the Middle Holocene (simulation O6-VS6-SS0-1), we find a wetter equilibrium for the period as compared to the currently observed conditions (Figure 3-8 and 3-9c,d). When vegetation dynamics are allowed (simulation O6-VD6-SS0-1), the equilibrium climate (Figure 3-8 and 3-11c,d) does not depart much from that of the simulation with fixed vegetation (simulation O6-VS6-SS0-1). This suggests that these vegetation conditions can indeed survive under Mid-Holocene forcings.
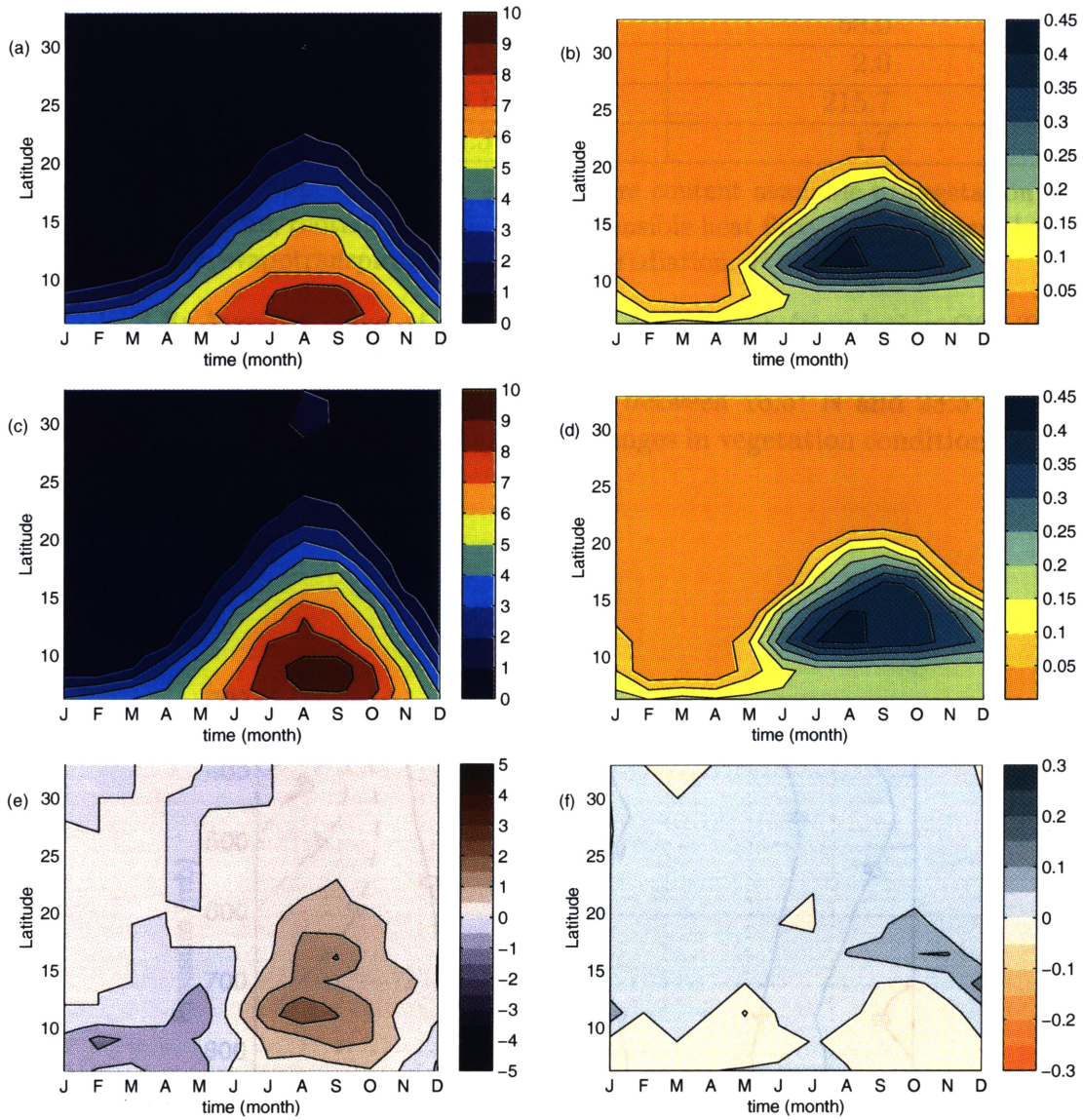
Figure 3-9: Results for simulations with static vegetation fixed to the Mid-Holocene distribution (simulations OA-VS6-SS0-1): (a) Seasonal cycle of rainfall (mm/day) and (b) net primary productivity (kgC/m²/mo) for 0K yrs BP; (c) Seasonal cycle of rainfall and (d) net primary productivity for 6K yrs BP; (e) = (c) - (a); (f) = (d) - (b).

Variable	0K yrs BP (O0-VS6-SS0-1)	6K yrs BP (O6-VS6-SS0-1)
B_o	1.1	0.9
$W_{soil,veg.}$	0.15	0.17
SHF (W/m²)	48.1	50.0
LHF (W/m²)	43.2	58.0
E_t (mm/day)	1.5	2.0
R_{net} (W/m²)	196.1	215.7
P (mm/day)	1.3	1.7

B_o = Bowen ratio, $W_{soil,veg.}$ = soil moisture content available to vegetation = f(soil moisture, rooting profile), SHF = sensible heat flux, LHF = latent heat flux, E_t = evapotranspiration, R_{net} = net radiation, P = precipitation.

Table 3.8: Average value of key variables for current (simulation O0-VS6-SS0-1) and Mid-Holocene (simulation O6-VS6-SS0-1) summer (JAS) conditions in the region between 16.5° N and 23.5° N for simulations on the impact of changes in vegetation conditions with fixed vegetation.
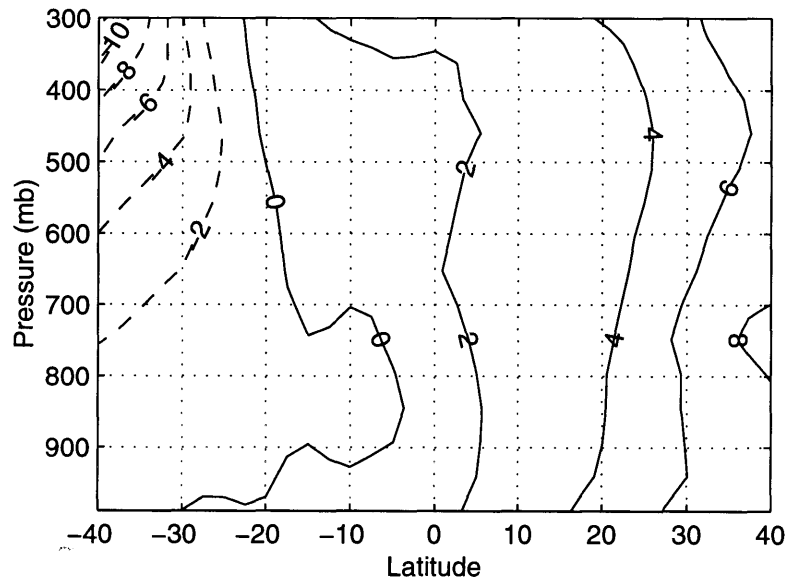
Figure 3-10: Difference (6K - 0K yrs BP) in the equivalent potential temperature (° K), which is proportional to the moist static energy, for simulations O$\mathcal{A}$-VS6-SS0-1.
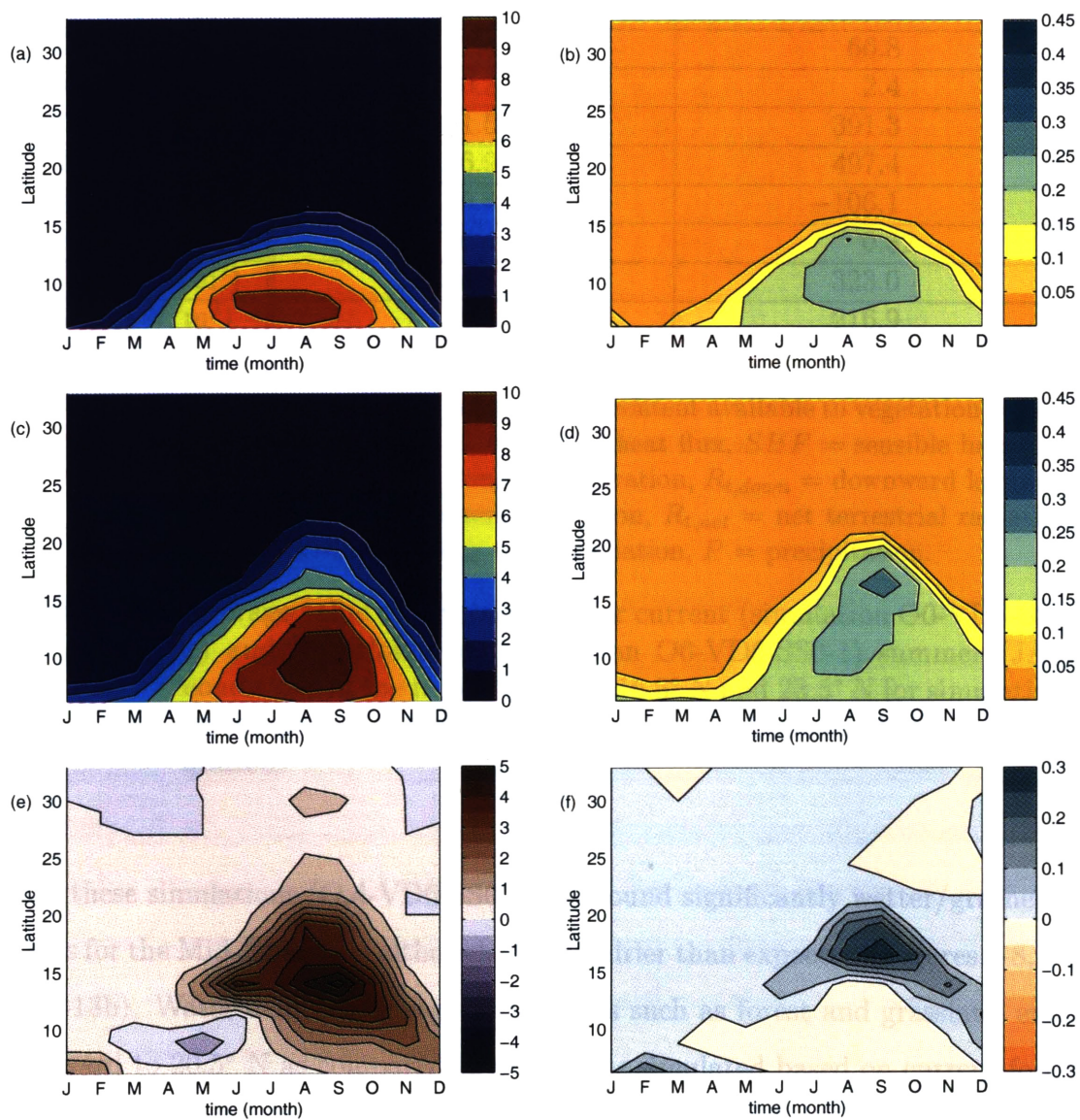
Figure 3-11: Results for simulations with dynamic vegetation initialized to the Mid-Holocene distribution (simulations O$\mathcal{A}$-VD6-SS0-1): (a) Seasonal cycle of rainfall (mm/day) and (b) net primary productivity (kgC/m^2/mo) for 0K yrs BP; (c) Seasonal cycle of rainfall and (d) net primary productivity for 6K yrs BP; (e) = (c) - (a); (f) = (d) - (b).

Variable	0K yrs BP (O0-VD6-SS0-1)	6K yrs BP (O6-VD6-SS0-1)
B_o	4.9	0.8
$W_{soil,veg.}$	0.01	0.16
G (W/m^2)	118.7	106.6
SHF (W/m^2)	36.1	49.8
LHF (W/m^2)	7.4	66.8
E_t (mm/day)	0.3	2.4
$R_{t,down}$ (W/m^2)	361.5	391.3
$R_{t,up}$ (W/m^2)	486.9	497.4
$R_{t,net}$ (W/m^2)	-125.4	-106.1
surface albedo	0.40	0.32
$R_{s,net}$ (W/m^2)	284.7	323.0
R_{net} (W/m^2)	159.3	216.9
P (mm/day)	0.2	2.2

B_o = Bowen ratio, $W_{soil,veg.}$ = soil moisture content available to vegetation = f(soil moisture and rooting profile), G = ground heat flux, SHF = sensible heat flux, LHF = latent heat flux, E_t = evapotranspiration, $R_{t,down}$ = downward longwave radiation, $R_{t,up}$ = upward longwave radiation, $R_{t,net}$ = net terrestrial radiation, $R_{s,net}$ = net solar radiation, R_{net} = net radiation, P = precipitation.

Table 3.9: Average value of key variables for current (simulation O0-VD6-SS0-1) and Mid-Holocene (simulation O6-VD6-SS0-1) summer (JAS) conditions in the region between 16.5° N and 23.5° N for simulations on the impact of changes in vegetation conditions with dynamic vegetation.

In these simulations (O$\mathcal{A}$-VD6-SS0-1), we found significantly wetter/greener conditions for the Mid-Holocene, although slightly drier than expected (Figures 3-8, 3-11c and 3-13b). Water demanding vegetation types such as forest and grassland expand northward to 20.5° N as compared to conditions simulated based on current forcings (~15.4° N, defined as location of 200 mm/yr precipitation). The equilibrium vegetation classes for the simulation based on 6K yrs BP orbital forcings differ from the initial distribution in that savannah was replaced by dry forest. The same behavior was observed when simulating the current climate starting from the close-to-observed vegetation distribution. This can be attributed to the fact that the model does not represent the external disturbances (e.g. grazing, fires) which are believed necessary for the maintenance of savannah vegetation in this model [*Wang*, 2000]. Although
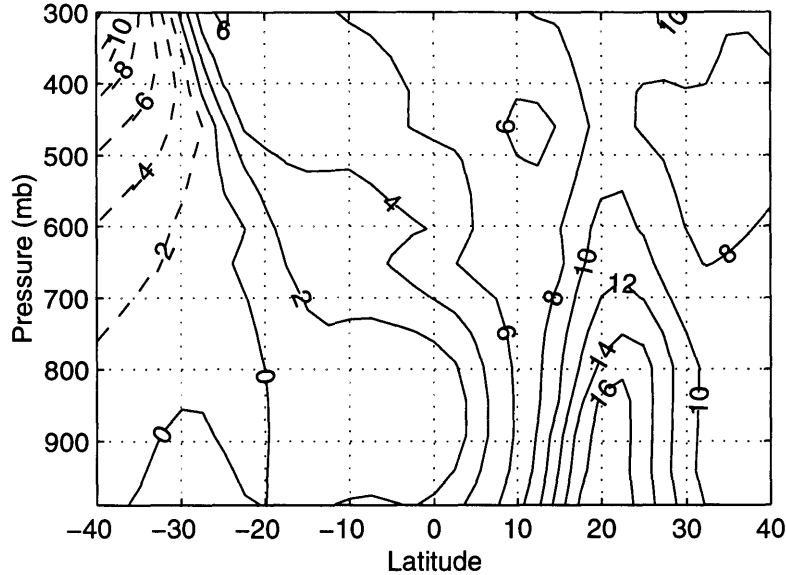
Figure 3-12: Difference (6K - 0K yrs BP) in the equivalent potential temperature
(° K), which is proportional to the moist static energy, for simulations
O$\mathcal{A}$-VD6-SS0-1.

we were successful in simulating a northward expansion of ~500 km in vegetation,
our model was not able to sustain the initially specified sparse vegetation at ~23° N
consistent with observations. Other simulations with 3-D general circulation models
have similarly failed to fully capture the full grassland expansion [*Texier et al.*, 1997;
Joussaume et al., 1999]. This mismatch with reconstructions of palaeoprecipitation
is probably due to the lack of other significant feedbacks in the system, such as soil
texture, surface waters, and changes in the ocean conditions. Despite of this, it is
remarkable that a simple zonally symmetric model was able to capture the retreated
Sahara during the Middle Holocene.

Contrary to previous studies [*Claussen and Gayler*, 1997; *Brovkin et al.*, 1998;
Claussen et al., 1999], which have identified only a single green equilibrium for the
West African region during the Middle Holocene, we find multiple equilibria for the
period as drawn from the different results obtained when using different initial vege-
tation conditions corresponding to the current (simulation O6-VD0-SS0-1) and Mid-
Holocene distributions (simulation O6-VD6-SS0-1). For the Holocene, *Brovkin et al.*
[1998], using a simple conceptual model, found only a stable green equilibrium from

about 10 to 6K yrs BP. They also found a dry stable equilibrium, and an intermediate, but unstable equilibrium appearing since the Middle Holocene (6K yrs BP). This multiple equilibria state starting at 6K yrs BP is probably what is being reflected in our results. For the current climate, *Wang and Eltahir* [2000b,d], found the existence of multiple climate equilibria, and demonstrated how climate transitions between different equilibria shape the currently observed low-frequency rainfall variability over the region. Based on this, here, we hypothesize that similar transitions could have taken place during the Middle Holocene causing the southern desert margin to migrate between 18.1° N (simulation O6-VD0-SS0-1) and 21.4° N (simulation O6-VD6-SS0-1).

Several studies suggest that conditions during the Middle Holocene were more complex than previously thought with smaller-scale fluctuations reflecting possible different causes than the broad trends attributable to orbital forcings [*Street-Perrott and Perrott*, 1993]. As an example, *Gasse and Van Campo* [1994] found several dry spells on the reconstructed lake levels of the Termite (16°05' N, 11°15' E) and Bougdouma (13°19' N, 11°40'E) sites. In their study the possible mechanisms reflecting these fluctuations have been identified as a competition between the vegetation-related decrease in the surface albedo and the increased evapotranspiration from the expanded lakes and vegetation. We hypothesize that West African conditions during the Middle Holocene were in general wetter than today with possible higher frequency fluctuations superimposed on these mean conditions. Small perturbations either in the land surface conditions or in the external forcings (e.g. SSTs) could have driven the system from the wetter equilibrium to the drier one for relatively short intervals of time (decade to century).

In the following section, a more detailed comparison of the simulated climate for 0 and 6K yrs BP is presented based on the simulations (O*A*-VD6-SS0-1) initialized with a vegetation distribution derived from *Hoelzmann et al.*'s [1998] map of palaeovegetation.
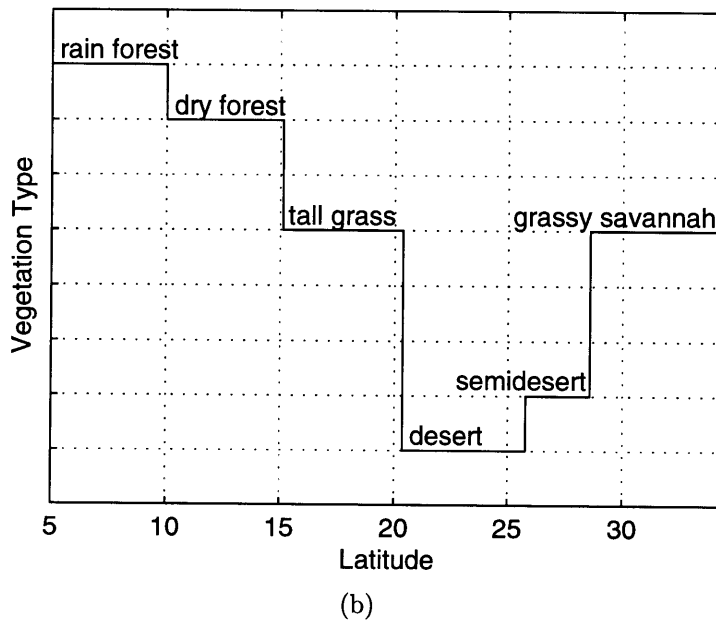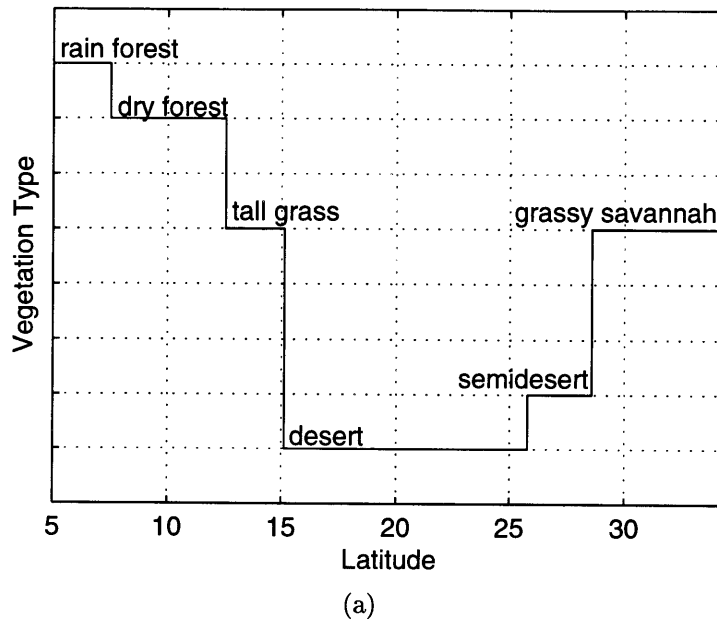
Figure 3-13: Equilibrium vegetation distribution for simulations (a) O0-VD6-SS0-1, and (b) O6-VD6-SS0-1, on the impact of changes in vegetation conditions with dynamic vegetation.

3.5 A Mechanism for Monsoon Enhancement During the Middle Holocene

In this section, we present a more detailed comparison of the simulated climate for 0 and 6K yrs BP for the set of simulations in which vegetation is initialized based on *Hoelzmann et al.*'s [1998] map of palaeovegetation and vegetation dynamics are subsequently allowed (simulations O$\mathcal{A}$-VD6-SS0-1). Significantly wetter/greener conditions were simulated in the case based on 6K yrs BP forcings as a result of a significant enhancement of the West African summer monsoon, although these were slightly drier than expected from palaeoclimatic reconstructions (Figures 3-8, 3-11c, and 3-13b). Here, our intention is to present in a coherent manner, the mechanisms responsible for the enhancement of the West African summer monsoon during the Middle Holocene. A comparison of the main changes between current and Mid-Holocene summer (JAS) conditions simulated for the region between 16.5° N and 23.5° N (currently part of the Sahara Desert) is shown in Table 3.9.

The mechanisms through which the monsoon circulation was enhanced during the Middle Holocene can be explained starting from radiative considerations and are summarized in Figure 3-14. During the Middle Holocene, perihelion –the time when the Earth is located closest to the Sun– occurred closer to the northern summer, and the tilt of the Earth's rotational axis was larger than at present. These changes resulted in an insolation anomaly of about +6 % (~25 W/m^2) at the top of the atmosphere during the Northern Hemisphere summer. Conversely, they resulted in decreased insolation during the Northern Hemisphere winter. As a consequence of the increased summer insolation over West Africa, the monsoon circulation was enhanced during the season. Moreover, the increased summer insolation alone has proven insufficient to fully reproduce the wetter conditions expected over West Africa during the Middle Holocene, suggesting the need for the inclusion of feedbacks into the system.
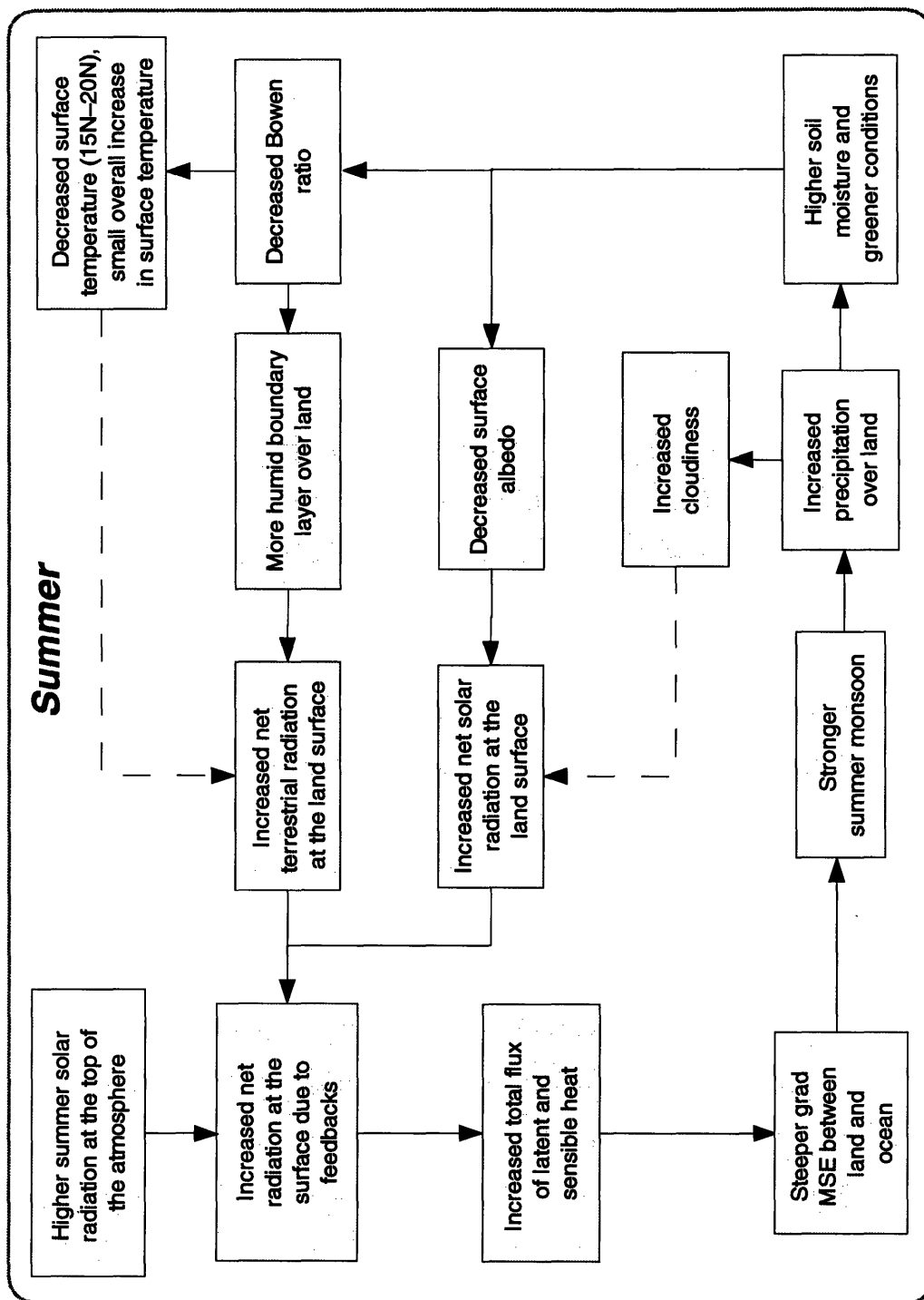
Figure 3-14: Summary of positive (solid lines) and negative (dashed lines) feedback mechanisms resulting in an enhanced summer monsoon circulation and wetter/greener conditions in the region between ˜15° N-˜20° N during the Middle Holocene for simulations O𝒜-VD6-SS0-1.

The simulated seasonal cycle of net radiation shows significantly higher values during the Middle Holocene than at present (Figure 3-15) and Table 3.9. However, the difference is much larger than the 25 W/m^2 expected for the top of the atmosphere during summer, suggesting an enhancement of the insolation anomaly due to feedbacks operating in the system. Our modeling results provide some insight into the way in which the biosphere-atmosphere feedback contributes to this enhancement and, consequently, to the wetter conditions during the period. For this purpose, we recall the hypothesis developed by *Emanuel et al.* [1994], *Eltahir* [1996, 1998], and *Eltahir and Gong* [1996] on the role of the gradient of moist static energy between the land and the ocean in regulating the dynamics of large-scale atmospheric tropical circulations (i.e. monsoons). In addition, we base our discussion on the hypothesis developed by *Eltahir* [1996, 1998] for relating land surface conditions and subsequent rainfall processes.

With else being equal, the increased solar radiation at the top of the Earth's atmosphere during the Mid-Holocene summer, results in a slight increase of the net radiation received at the land surface. Based on energy balance considerations, increases in the net radiation at the land surface have to be balanced roughly by corresponding increases in the total energy fluxes (latent and sensible heat fluxes, Figures 3-16 and 3-17) into the land's boundary layer. With conditions over the ocean being fixed by the specified current SST climatology, the resulting increase in energy fed into the land's boundary layer steepens the gradient of moist static energy between land and the ocean (Figure 3-12). It has been shown by *Eltahir and Gong* [1996] that a steeper gradient of moist static energy results in a stronger monsoon circulation (Figure 3-18). Consequently, the initial increase in the summer net radiation over land that resulted from changes in the Earth's orbital configuration during the Middle Holocene, provides an initial mechanism for the enhancement of the summer monsoon circulation over West Africa. As shown in Figure 3-19, the healthier monsoon circulation simulated for the Middle Holocene results in significant moisture convergence $(P - E_t)$ as compared to current conditions. As a result, a positive precipitation anomaly is generated over land (Figure 3-11e) producing moister soil conditions (Figure 3-20)

and a greener vegetation distribution (Figures 3-7 and 3-13).

The equilibrium vegetation types simulated for the Middle Holocene are significantly greener than for the present. Water demanding vegetation types such as forest and grassland show a significant northward expansion to ~20.5° N. This expansion results from a higher water availability, especially during summer/early fall, as compared to present conditions. The greener vegetation distribution and moister soil conditions simulated for the Middle Holocene, result in a significant difference in the way in which the biosphere-atmosphere interactions take place. As shown in Figure 3-14, the expanded vegetation and moister soil conditions exert a strong influence in the energy balance at the land surface through two mechanisms: (1) decreased Bowen ratio, and (2) decreased surface albedo (Figure 3-21). It will be shown that both mechanisms result in increased net surface radiation during the Middle Holocene, consistent with *Eltahir*'s [1998] theory.

Due to the positive precipitation anomaly simulated for the Middle Holocene summer, soil conditions are significantly moister (Figure 3-20). Since the plant's stomatal resistance to transpiration is inversely proportional to the available soil moisture content, the moister conditions simulated for the Middle Holocene result in decreased Bowen ratio [(1) above]. Therefore, in the competition between latent and sensible heating for the available energy at the surface, the fraction contributing to evapotranspiration (Figures 3-16, 3-17, and 3-19) is significantly larger for the Middle Holocene, which results in: (a) a significantly more humid boundary layer (Figure 3-22), and (b) cooler surface temperature in the region with expanded vegetative cover (15° N-20° N, Figure 3-23). Since water vapor is the most important greenhouse gas, the more humid boundary layer simulated for the Middle Holocene [(a) above] favors a significantly increased downward longwave radiation. Although, a region of localized cooling is simulated between 15° N-20° N as a result of increased evapotranspiration from the expanded vegetation [(b) above], we find an overall small warming of our region of interest (16.5° N and 23.5° N, currently part of the Sahara Desert). Consistent with this overall small warming of the surface, the upward longwave radiation increases slightly. The net effect of changes in both longwave components is an

increase of the net terrestrial radiation received at the land surface (Table 3.9).

The decreased surface albedo [(2) above] (Figure 3-21) resulting from the simulated greening/wetting of the region currently occupied by the Sahara, results in increased net solar radiation at the land surface. At the same time, the increased reflectivity associated with the increased cloudiness simulated over the region, acts to reduce the amount of net solar radiation reaching the land surface. Our results show that the net solar radiation at the land surface increases significantly, suggesting that the impact of surface albedo out-competes the cloud effect.

As a result of the increased net terrestrial and net solar radiations received at the land surface, there is an increase of the net surface radiation. The increased net radiation at the land surface is again balanced by corresponding increases in the total energy fluxes (mostly in the form of latent heat due to decreased Bowen ratio) fed into the land's boundary layer. With conditions over the ocean being fixed by the specified SST climatology, an even steeper gradient of moist static energy between the land and the ocean (Figure 3-12) is produced. As a consequence, the summer monsoon circulation is further enhanced until an equilibrium is established (Figure 3-14) in which a significantly stronger monsoon (Figure 3-18) can be sustained under 6K yrs BP orbital forcings.
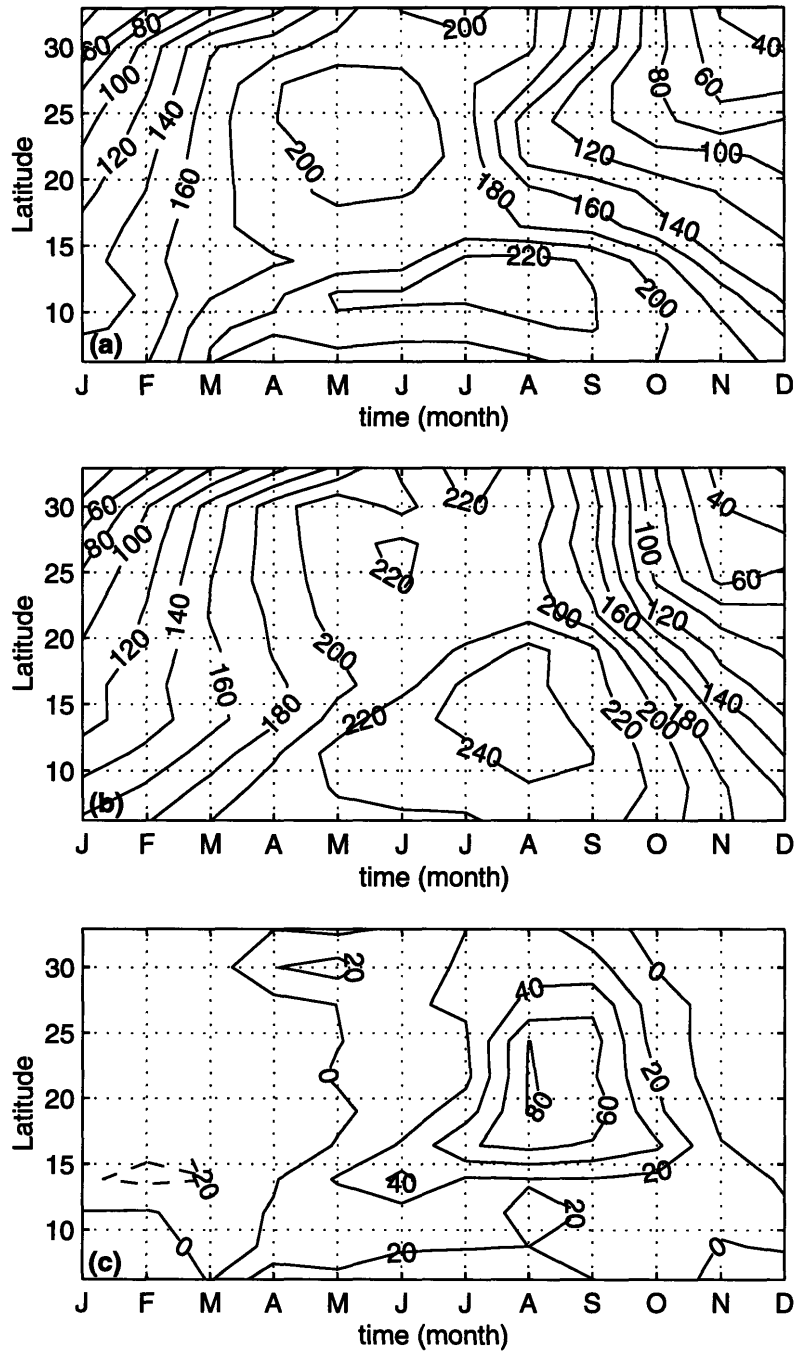
Figure 3-15: Seasonal cycle of net radiation (W/m^2) for simulations on the impact of changes in vegetation conditions with dynamic vegetation: (a) simulation O0-VD6-SS0-1, (b) simulation O6-VD6-SS0-1, and (c) = (b) - (a).
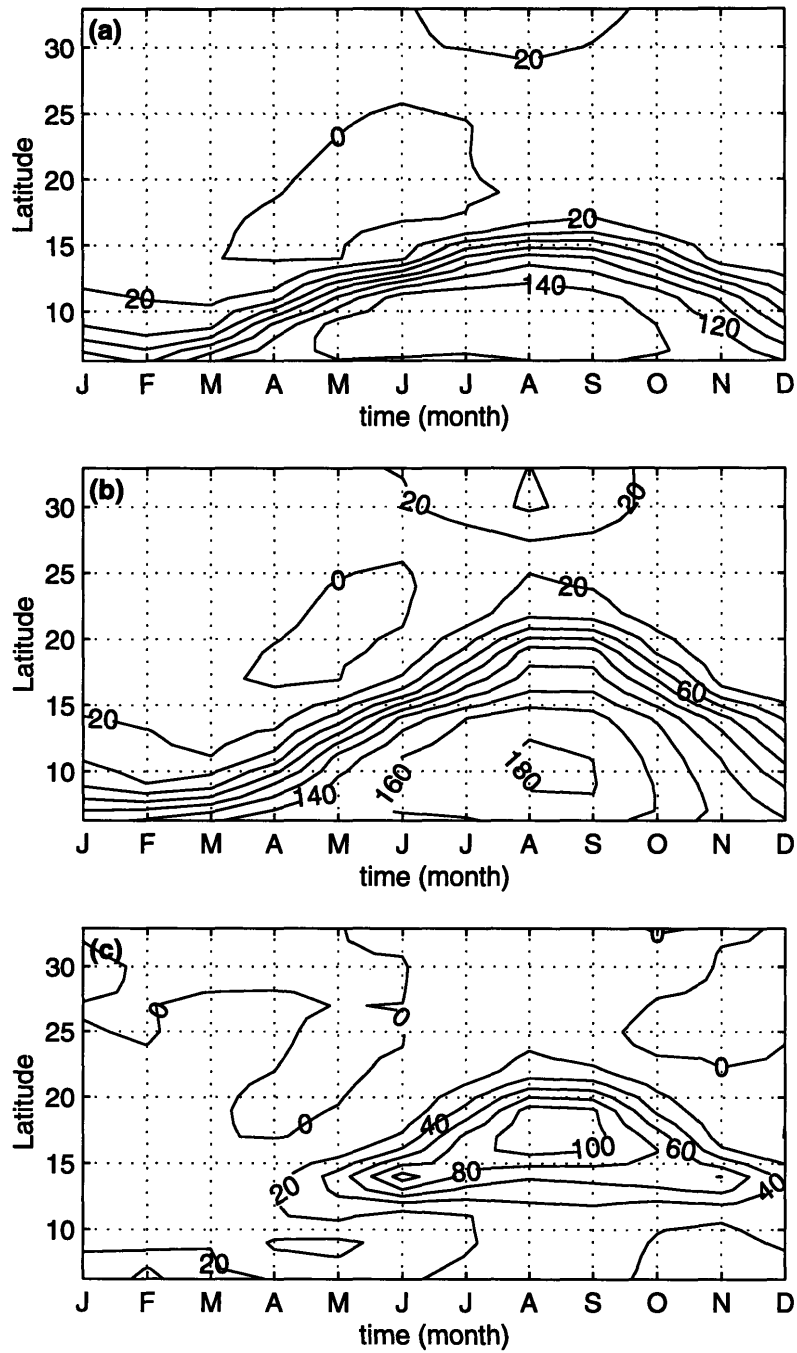
Figure 3-16: Seasonal cycle of latent heat flux (W/m^2) for simulations on the impact of changes in vegetation conditions with dynamic vegetation: (a) simulation O0-VD6-SS0-1, (b) simulation O6-VD6-SS0-1, and (c) = (b) - (a).
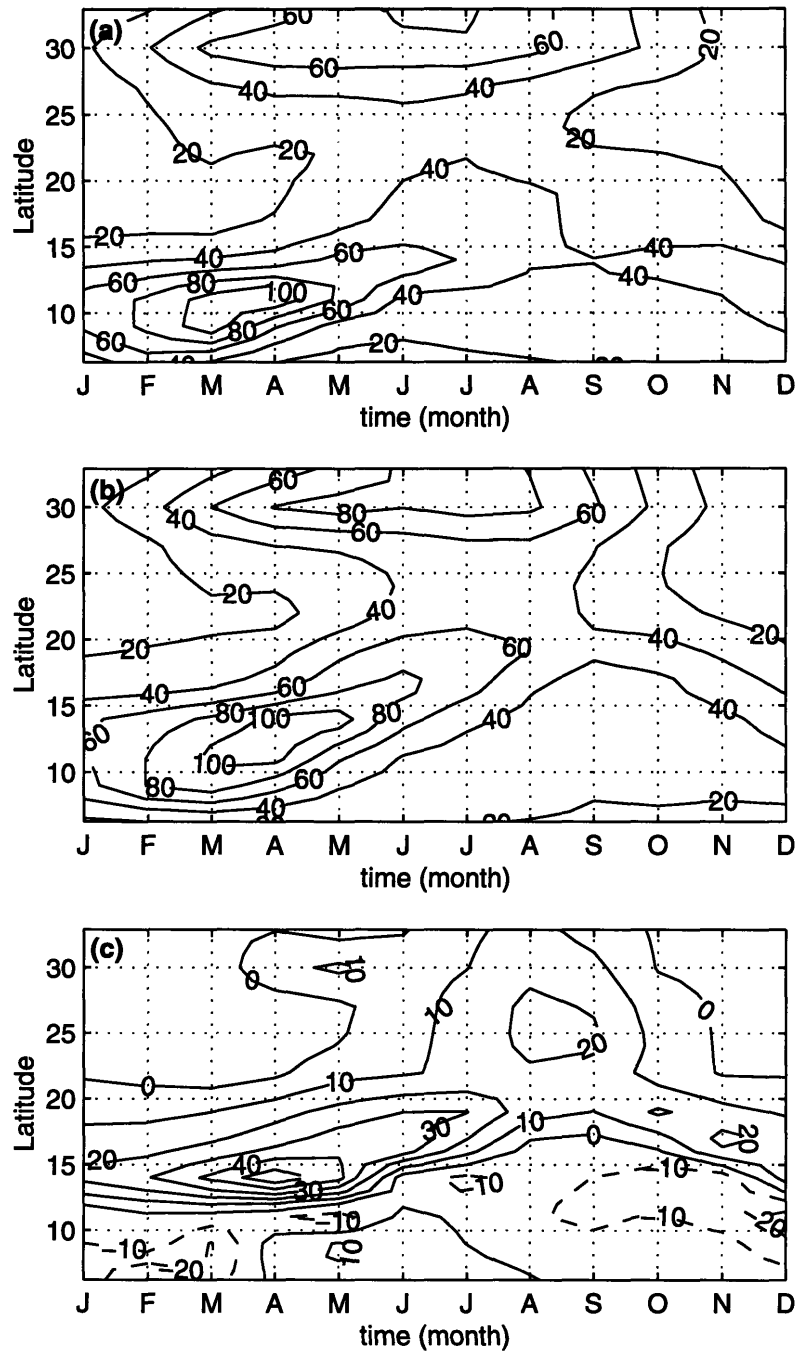
Figure 3-17: Seasonal cycle of sensible heat flux (W/m^2) for simulations on the impact of changes in vegetation conditions with dynamic vegetation: (a) simulation O0-VD6-SS0-1, (b) simulation O6-VD6-SS0-1, and (c) = (b) - (a).
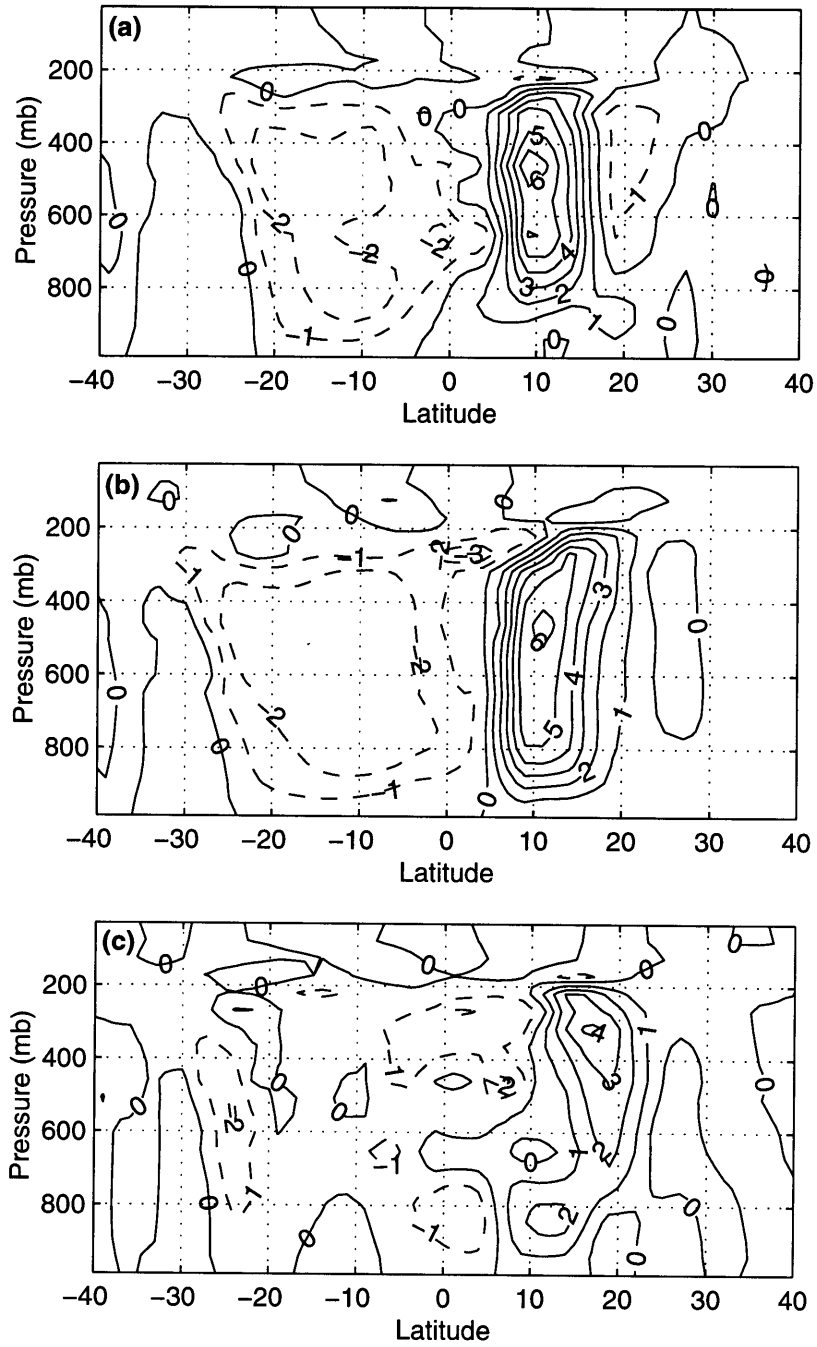
Figure 3-18: Vertical wind (mm/s) during August for simulations on the impact of changes in vegetation conditions with dynamic vegetation: (a) simulation O0-VD6-SS0-1, (b) simulation O6-VD6-SS0-1, and (c) = (b) - (a).
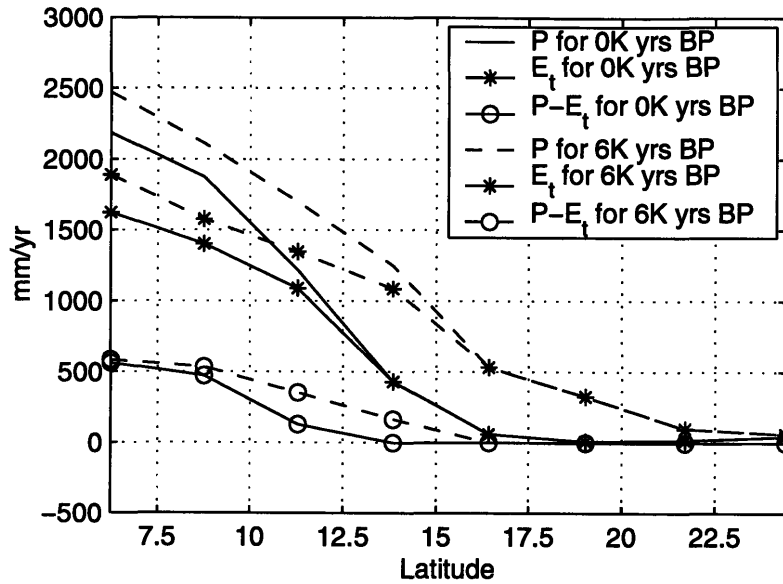
Figure 3-19: Precipitation (P), evapotranspiration (E_t), and moisture convergence $(P - E_t)$ (mm/yr) for simulations on the impact of changes in vegetation conditions with dynamic vegetation: for 0K yrs BP (simulation O0-VD6-SS0-1, solid lines) and 6K yrs BP (simulation O6-VD6-SS0-1, dashed lines).
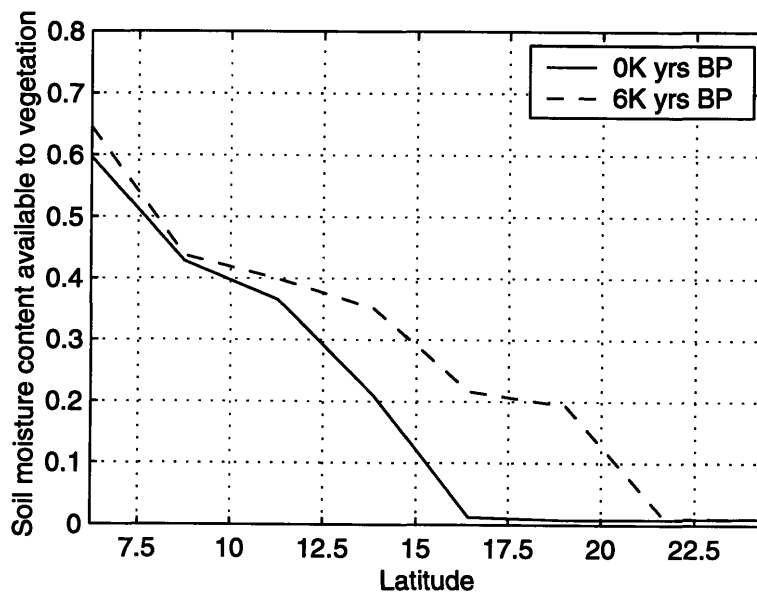
Figure 3-20: Soil moisture content available to vegetation $(W_{soil,veg.}) = f$(soil moisture and rooting profile) for simulations on the impact of changes in vegetation conditions with dynamic vegetation: for 0K yrs BP (simulation O0-VD6-SS0-1, solid line) and 6K yrs BP (simulation O6-VD6-SS0-1, dashed line).
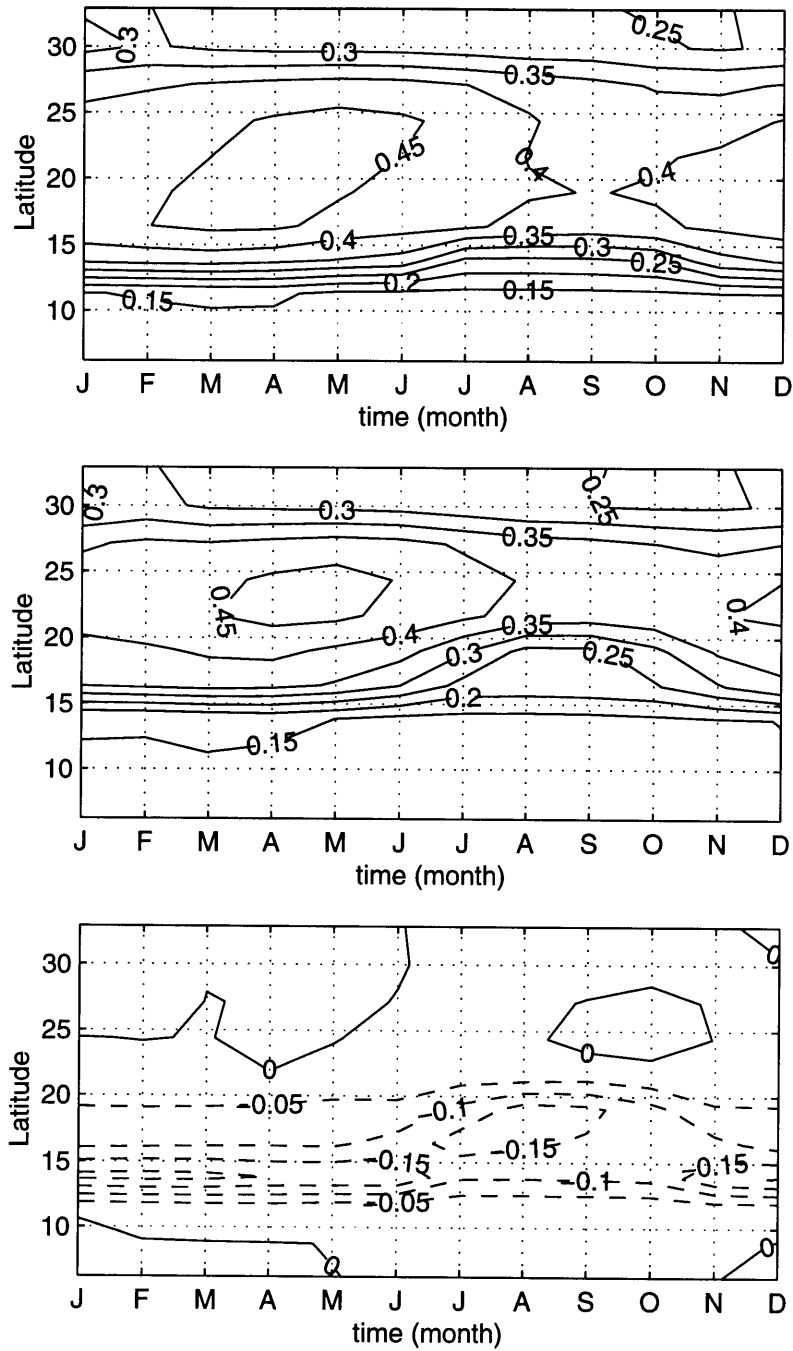
Figure 3-21: Seasonal cycle of surface albedo for simulations on the impact of changes in vegetation conditions with dynamic vegetation: (a) simulation O0-VD6-SS0-1, (b) simulation O6-VD6-SS0-1, and (c) = (b) - (a).
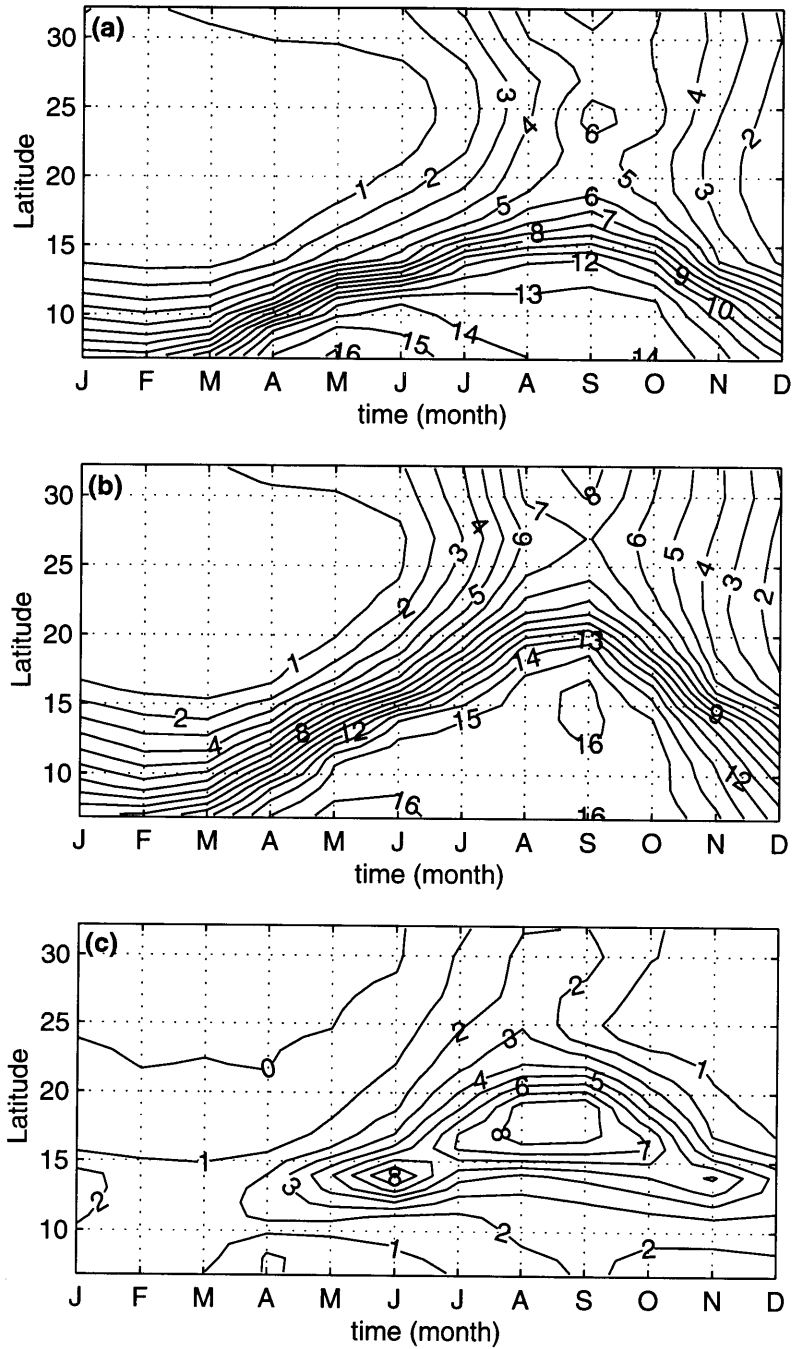
Figure 3-22: Seasonal cycle of specific humidity near the surface (g/kg) for simulations on the impact of changes in vegetation conditions with dynamic vegetation: (a) simulation O0-VD6-SS0-1, (b) simulation O6-VD6-SS0-1, and (c) = (b) - (a).
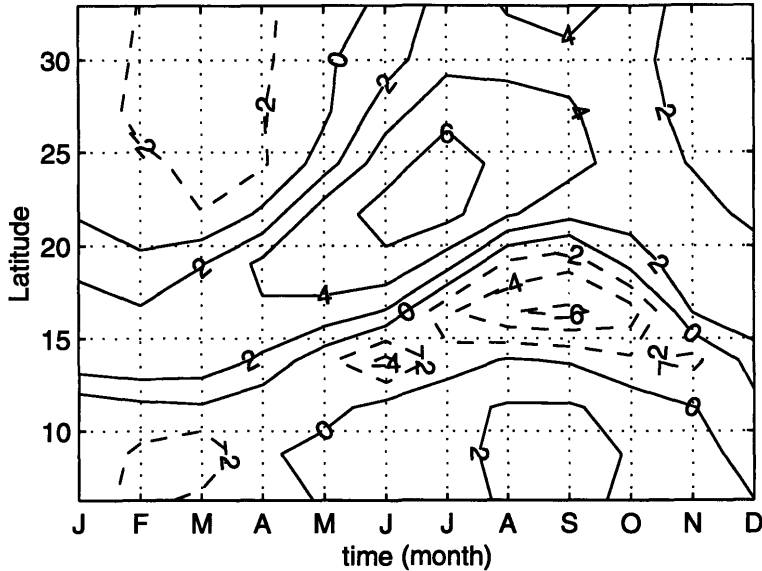
Figure 3-23: Difference (6K - 0K yrs BP) in the seasonal cycle of surface temperature (° K) for simulations on the impact of changes in vegetation conditions with dynamic vegetation (simulations OA-VD6-SS0-1).

3.6 Sensitivity to Conditions in the Northern Boundary

The northern Sahara (north of 27° N) is currently under the influence of the Mediterranean and the Tropical North Atlantic specially during winter when polar depressions and Atlantic cyclones are an important source of precipitation over the region [*Bryson*, 1992]. The region is currently characterized by a vegetation cover consisting of sparse shrubland or grassland, and mediterranean forest, specially in the Atlas mountain range (Figure 2-1). According to *Bryson* [1992], and *Petit-Maire and Guo* [1997], this influence from the north was even more significant during the Middle Holocene than presently, resulting in slightly stronger precipitation and denser vegetation conditions. Since ZonalBAM is a zonally symmetric model, it cannot simulate eddies as an important transfer mechanism in middle latitudes. For this reason, here we constrain our region of interest to the tropics.

The only sources of moisture in ZonalBAM are the South-Eastern Tropical At-

99

lantic in the south, the Mediterranean in the north, and the recycling by vegetation itself. Moisture is basically distributed by a zonally-symmetric meridional circulation, while the existence of eddies as an important transfer mechanism in mid-latitudes is neglected. In dealing with the issue of the northern boundary, we have two options: fixing the vegetation, fluxes and temperature north of the northern tropics (north of 27° N) to their current distribution or allowing the model to interactively calculate them.

For modeling the current climate, these boundary conditions are quantitatively known. Therefore, fixing the fluxes and temperature in the north to their current climatology has allowed for the successful simulation of present conditions. When these boundary conditions are fixed, then specifying any vegetation conditions in the north would not cause any significant difference in results. However, here we show that when these fluxes and temperature are model-calculated, the choice of vegetation conditions specified in the north is critical.

Due to the high degree of uncertainty in these conditions for the Middle Holocene, we believe that letting the model to calculate these fluxes and temperatures while fixing the vegetation conditions is reasonable for several reasons. First, due to the different forcings during the Middle Holocene, conditions in middle latitudes are expected to be somewhat different from the current [*Bryson*, 1992; *Huntley and Prentice*, 1993; *Petit-Maire and Guo*, 1997]. Second, since our intention is to simulate the expansion of the grassland region into the transition zone between low- and mid-latitudes, fixing the fluxes and temperatures north of 27° N could probably limit our model response. Results of several sensitivity analyses show that letting the fluxes in the north to be model-calculated is a good choice as long as the vegetation specified in the north is somewhat realistic and denser than a certain threshold. This choice is specially critical when vegetation dynamics are allowed in the southern portion of the domain (5° N to 27° N).

Name of simulation[a]	Orbital forcing	Vegetation	Ocean	Fluxes and temperatures north of 27° N	Vegetation north of 27° N fixed to
O0-VD0-SS0-1	0K yrs BP	Dynamic from current[b]	Fixed to current	Model-calculated	Grassy-savannah
O6-VD0-SS0-1	6K yrs BP	Dynamic from current	Fixed to current	Model-calculated	Grassy-savannah
O0-VD0-SS0-2	0K yrs BP	Dynamic from current	Fixed to current	Model-calculated	Semidesert
O6-VD0-SS0-2	6K yrs BP	Dynamic from current	Fixed to current	Model-calculated	Semidesert

[a] Name of simulation has the form: O$\mathcal{A}$-V$\mathcal{B}$-S$\mathcal{C}$-$\mathcal{D}$, where; O = orbital forcing; $\mathcal{A}$ = 0 or 6 corresponding to 0 or 6K yrs BP orbital forcings respectively; V = vegetation conditions; $\mathcal{B}$ = S0 or S6 corresponding to static vegetation fixed to current or Mid-Holocene conditions, D0 or D6 corresponding to dynamic vegetation initialized to current or Mid-Holocene conditions; S = ocean conditions; $\mathcal{C}$ = S0 or S6 corresponding to ocean fixed to current or Mid-Holocene conditions; $\mathcal{D}$ = simulation number.

[b] Dynamic vegetation initialized from current distribution.

Table 3.10: Summary of sensitivity simulations for 0 and 6K yrs BP.

We find that if vegetation in the north is prescribed as too sparse (simulations O$\mathcal{A}$-VD0-SS0-2, Table 3.10), and if in top we neglect the existence of eddies as a transfer mechanism by letting the fluxes and temperature in the north to be model-calculated, the domain becomes almost completely deserted. What happens is that by letting fluxes to be model-calculated, we are neglecting the transport of moisture by eddies from the Mediterranean and the Tropical North Atlantic (for ZonalBAM does not account anyways) into the northern Sahara. The only moisture transport mechanism is limited to a zonally symmetric meridional circulation. If in top, we prescribe the vegetation conditions in the region as too sparse, then the moisture recycling by vegetation would be too low. Consequently, the resulting dryness could propagate southward through vegetation dynamics until the equilibrium climate becomes unrealistic. As seen in Figure 3-24, prescribing the vegetation in the north to semidesert (starred lines) (Tables 3.3 and 3.4) produces unrealistically dry conditions when using both current and 6K yrs BP forcings. However, when the vegetation

101

conditions are denser than grassy-savannah (circled lines), we find that the simulated current conditions are realistic.
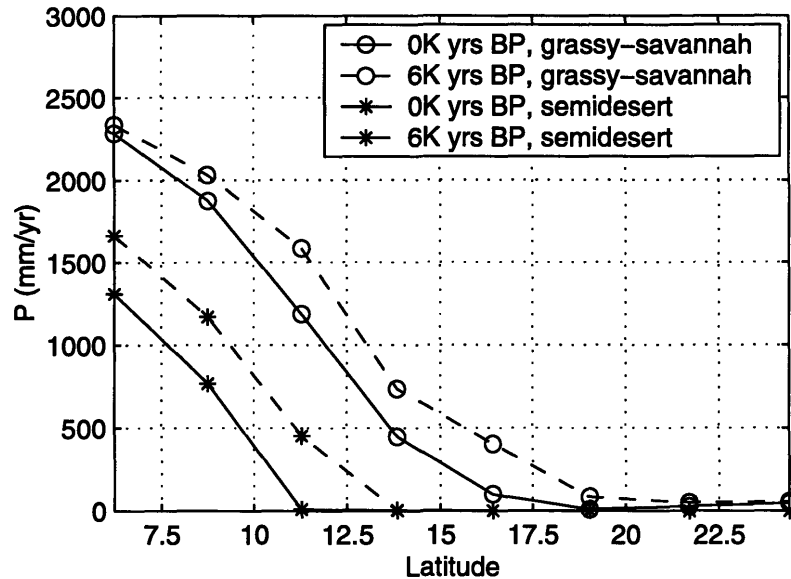
Figure 3-24: Distribution of total annual precipitation (mm/yr) for simulations O0-VD0-SS0-1 (solid-circled line), O6-VD0-SS0-1 (dashed-circled line), and the impact of changing vegetation conditions in the north to semidesert (simulation O0-VD0-SS0-2: solid-starred line, simulation O6-VD0-SS0-2: dashed-starred line).

3.7   Summary

With the purpose of understanding the mechanisms responsible for a greener Sahara during the Middle Holocene, we invoked the theory developed by *Eltahir* [1996], and *Eltahir and Gong* [1996] which suggests that the strength of the monsoon circulation is affected by the gradient of moist static energy between the land and the ocean. In these studies, they have showed that greener conditions enhance the moist static energy over land steepening the gradient of moist static energy and resulting in a stronger monsoon. The relative contribution of orbitally-induced changes in insolation and vegetation dynamics to the energy balance at the land surface, which determines the amount of moist static energy fed into the land boundary layer, were analyzed by

performing four sets of experiments based on current and 6K yrs BP orbital forcings.

Simulations in which vegetation conditions were fixed to the current distribution, show that an orbitally-induced increased seasonality in insolation for the Middle Holocene, by itself, results in a 1.1° northward shift in the location of the southern margin of the Sahara as compared to current forcings. This limited response is due to the fact that the fixed land surface conditions limit the increase in the net radiation at the surface. Therefore, only small increases in the latent and sensible heat fluxes, which feed the land boundary layer with moist static energy, were simulated, producing a limited enhancement of the monsoon. When vegetation is allowed to be dynamic, it responds to the simulated increase in rainfall resulting in greener conditions. As a result of this feedback, more moist static energy is fed into the land boundary layer strengthening the monsoon even further. Consequently, the southern desert margin shifts northward by 2.4° in this case. However, the system by itself was not able to fully reach the greener equilibrium expected based on observations.

Motivated by this limited response, simulations in which vegetation was initialized according to *Hoelzmann et al.*'s [1998] map of palaeovegetation were performed and the question of whether these could be sustained under current and Mid-Holocene orbital forcings was posed. We found that this vegetation distribution cannot not be sustained under current forcings. However, it can be sustained under 6K yrs BP forcings resulting in a 5.1° northward shift in the southern desert margin. Although we were successful in simulating a northward expansion of ~500 km in vegetation, our model was not able to sustain the initially specified sparse vegetation at ~23° N from observations. This mismatch with reconstructions of palaeoprecipitation is probably due to the lack of other significant feedbacks in the system. Despite of this, it is remarkable that a simple zonally symmetric model was able to capture the retreated Sahara during the Middle Holocene. Although, the main mechanisms responsible for the enhancement of the West African summer monsoon during the Middle Holocene have been discussed from the point of view of the biosphere-atmosphere system, we are aware that the incorporation of additional feedbacks could introduce more complication. For example, the incorporation of other feedbacks such as changes

in soil type, surface waters, and ocean dynamics have been identified as possible additional mechanisms resulting in significantly wetter conditions during the Mid-Holocene. In addition, it is important to incorporate into this analysis, a temporal dimension in which seasonal and interannual changes are also taken into account.

Contrary to other studies, our results based on 6K yrs BP forcings suggest that multiple equilibria could have coexisted over the region of West Africa during the Middle Holocene. Furthermore, based on previous similar studies on the current climate over the region [*Wang and Eltahir*, 2000b,d], we hypothesize that transitions between the different equilibria could have taken place during the Middle Holocene causing the southern desert margin to migrate between 18.1° N and 21.4° N. This could act as a mechanism for natural oscillation in the Mid-Holocene climate.

Chapter 4

Simulations Using the Fully-Coupled Biosphere-Atmosphere-Ocean Model

4.1 Introduction

In Chapter 2, it was shown that the addition of an ocean component into ZonalBAM is critical in order to fully simulate climate change over the region of West Africa. It was shown that the strength of the monsoon circulation is strongly dependent on the amount of energy fluxes fed into the oceanic boundary layer and that these fluxes are in turn dependent on the oceanic heat budget. For the Middle Holocene, it is believed that the influence of local SSTs was more important than the effects of global changes in SSTs. For this reason, and due to ZonalBAM's simple configuration, a simple way of including an ocean component into the model is by the addition of a mixed layer ocean model (MLOM). In this MLOM, SSTs are computed based on energy balance considerations in the top (~100 m) ocean layer as discussed in Section 2.3.

Name of simulation[a]	Orbital forcing	Vegetation	Ocean	Fluxes and temperatures north of 27° N	Vegetation north of 27° N fixed to
O0-VD0-SS0-3	0K yrs BP	Dynamic from current[b]	Fixed to current	Fixed to current	Grassy-savannah
O0-VD0-SD0	0K yrs BP	Dynamic from current	Dynamic from current[d]	Fixed to current	Grassy-savannah
O6-VD6-SC0	6K yrs BP	Dynamic from Mid-Hol.[c]	Fixed to corrected current[e]	Model-calculated	Grassy-savannah
O6-VD6-SCD0	6K yrs BP	Dynamic from Mid-Hol.	Dynamic from corrected current[f]	Model-calculated	Grassy-savannah

[a] Name of simulation has the form: O$\mathcal{A}$-V$\mathcal{B}$-S$\mathcal{C}$-$\mathcal{D}$, where; O = orbital forcing; $\mathcal{A}$ = 0 or 6 corresponding to 0 or 6K yrs BP orbital forcings respectively; V = vegetation conditions; $\mathcal{B}$ = S0 or S6 corresponding to static vegetation fixed to current or Mid-Holocene conditions, D0 or D6 corresponding to dynamic vegetation initialized to current or Mid-Holocene conditions; S = ocean conditions; $\mathcal{C}$ = S0 or S6 corresponding to ocean fixed to current or Mid-Holocene conditions, D0 or D6 corresponding to dynamic ocean initialized to current or Mid-Holocene conditions, C0 corresponding to ocean fixed to corrected SST conditions from MLOM validation, CD0 corresponding to dynamic ocean initialized to corrected SST conditions; $\mathcal{D}$ = simulation number.

[b] Dynamic vegetation initialized to the current distribution derived from *USGS Global Land Cover Characterization Data*, *Gornitz and NASA* [1995], and *Foley et al.* [1996].

[c] Dynamic vegetation initialized based on *Hoelzmann et al.*'s [1998] map of palaeovegetation.

[d] SSTs are initialized to NCEP climatology, and the MLOM is subsequently turned on. The ocean heat fluxes are derived from simulation O0-VD0-SS0-3.

[e] SSTs are fixed to the corrected SSTs simulated in O0-VD0-SD0.

[f] SSTs are initialized to the corrected SSTs simulated in O0-VD0-SD0, and the MLOM is subsequently turned on. The ocean heat fluxes are derived from simulation O0-VD0-SS0-3.

* In all simulations the relative humidity threshold over the ocean (RH_0) has been set as 5% larger than over land (See Table 4.2).

Table 4.1: Summary of simulations for 0 and 6K yrs BP to determine the impact of ocean dynamics.

In order to reduce model biases, the seasonal cycle of ocean heat fluxes was derived from a control simulation of the current climate (Figure 4-1) in which vegetation dynamics were allowed and the model was forced with fixed NCEP SST climatology (simulation O0-VD0-SS0-3, Table 4.1). These advective fluxes, which should account for the transport of heat by ocean currents and for oceanic processes such as upwelling/sinking, were then added to the heat budget equation from which the SSTs are calculated. The validation of this MLOM based on current forcings, and the impact of the addition of ocean dynamics into simulations of the Middle Holocene are presented in the next sections. Simulations are summarized in Table 4.1.
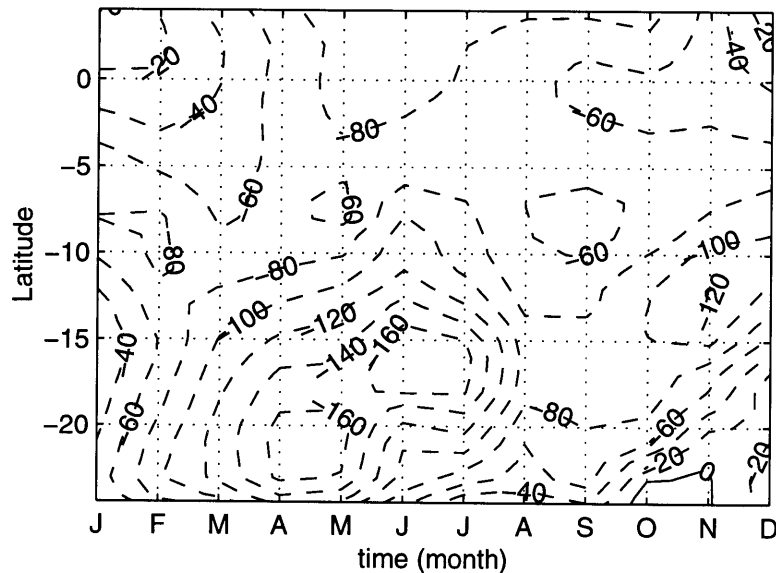
Figure 4-1: Seasonal cycle of ocean heat fluxes (W/m^2), representing the zonal average over 15° W to 15° E, derived from a control simulation of the current climate (simulation O0-VD0-SS0-3, Table 4.1). Negative contours are dashed and represent heat advected away from the location.

4.2   Validation of the Mixed Layer Ocean Model

In this section, the mixed layer ocean model (MLOM) (See Chapter 2) is validated based on current forcings. In our simulations, the MLOM was only applied to the region between 25° S and 5° N (averaged over 15° W-15° E), which directly influences

and is influenced by the zonally-symmetric monsoon circulation. Similar to the coupling process between the atmospheric and biospheric components of ZonalBAM, an initial spinup is required due to the addition of the mixed layer ocean model (MLOM): The model starts with the SSTs fixed to the current climatology from NCEP, and vegetation fixed to the close-to-observed distribution (Figure 3-1). The MLOM is turned on after five years. The ocean heat fluxes, derived from a control simulation of the current climate (Figure 4-1) in which vegetation dynamics were allowed and the model was forced with the current NCEP SST climatology (simulation O0-VD0-SS0-3, Table 4.1), are added in the MLOM heat balance equation. Ten years later (year 15) vegetation dynamics are introduced.

Cloud level	Cloud extent (mb)	Cloud optical depth (τ)	Original RH_0 [a]	RH_0 for MLOM simulations [b]	
				over land	over ocean
High	460-220	2	0.80	0.80	0.85
Middle	640-460	6	0.65	0.65	0.70
Low	940-640	12	0.70	0.70	0.75

[a] Originally used in ZonalBAM over both land and ocean.
[b] Used in simulations with the mixed layer ocean model.

Table 4.2: Summary of the cloud parameterization scheme based on *Kvamstø* [1991].

The validation of the MLOM revealed large cold biases in the simulated SSTs. The cause of mismatch has been identified as an excessively high cloud cover over the ocean immediately after the MLOM is turned on, which results in a significant reduction of the incoming radiation at the ocean surface. ZonalBAM's cloud parameterization scheme is very simple (Table 4.2). Clouds are divided into three groups: high-, middle-, and low-level clouds, whose characteristics are described in terms of fractional cover, vertical expansion, and cloud density [*Wang*, 2000]. Only the fractional cloud cover is predicted by the model based on the relative humidity following the *Kvamstø* [1991] scheme:

$$FC = max(0.0, \frac{RH - RH_0}{1 - RH_0}) \qquad (4.1)$$

where FC is the fractional cover, RH is the relative humidity, and RH_0 is the relative humidity threshold for cloud formation, which is 0.80, 0.65, 0.70 for high-, medium-, and low-level clouds, respectively. These values were appropriate when the SST climatology was fixed, since the cloud-radiation feedback did not have any effect over the ocean. However, when the MLOM is used, this feedback can produce significant biases. In our case, we found a cold SST bias resulting from a higher than observed simulated cloud cover. In order to bring the simulated cloud cover closer to observations, we increased the relative humidity threshold over the ocean by 5 % (to 0.85, 0.70 and 0.75, respectively, Table 4.2). This is a reasonable assumption since the amount of cloud condensation nuclei available over the ocean is smaller than over land, requiring a higher relative humidity threshold for cloud formation. The resulting SSTs still show a cold bias of ~2° K, specially during spring (AMJ) and summer (JAS) (Figure 4-2). However, simulations in which the relative humidity threshold over the ocean was increased even further did not produce any significant improvement in results.

We hypothesize that this small cold bias in the simulated SSTs is due to the simplification of the MLOM into a one dimensional representation (meridional). Since the SETA region is currently characterized by strong coastal upwelling in the Benguela system, we realize that it is important to take into account the zonal variability in the mixed layer. Zonal variations in the mixed layer depth and ocean heat fluxes would result in zonal variations in the sea surface temperature of the region. Since the latent heat flux depends in a non-linear fashion on the sea surface temperature of the mixed layer (following the Clausius-Clapeyron relation), the heat balance on a single grid box with average mixed layer characteristics would be significantly different from the mean heat balance of a number of grid boxes. Also, as has been demonstrated by *Saravanan and Chang* [1999], the inclusion of spatial and temporal variability in

the mixed layer ocean depth is important in order to accurately simulate the SST variability. Therefore, simulations in which the zonal variability of the ocean is taken into account are being carried out.

The effect of the cold bias in the SSTs simulated by the MLOM on the climate of West Africa is detailed in Figure 4-3 and explained hereafter. The value of key variables in the region between 13.0° N and 20.0° N during summer (JAS) (where the largest changes over land are simulated) are given in Table 4.3 for simulations with (simulation O0-VD0-SD0) and without (simulation O0-VD0-SS0-3) the mixed layer ocean model.

Variable	Simulation O0-VD0-SS0-3 (fixed SSTs)	Simulation O0-VD0-SD0 (SSTs from MLOM)
B_o	0.8	0.9
$W_{soil,veg.}$	0.18	0.11
SHF (W/m^2)	46.2	39.8
LHF (W/m^2)	56.5	44.0
E_t (mm/day)	2.0	1.5
$R_{t,down}$ (W/m^2)	367.8	361.5
$R_{t,up}$ (W/m^2)	481.1	482.4
$R_{t,net}$ (W/m^2)	−113.3	−120.9
surface albedo	0.31	0.34
$R_{s,net}$ (W/m^2)	311.4	312.1
R_{net} (W/m^2)	198.1	191.2
P (mm/day)	1.7	1.4

B_o = Bowen ratio, $W_{soil,veg.}$ = soil moisture content available to vegetation = f(soil moisture and rooting profile), SHF = sensible heat flux, LHF = latent heat flux, E_t = evapotranspiration, $R_{t,down}$ = downward longwave radiation, $R_{t,up}$ = upward longwave radiation, $R_{t,net}$ = net terrestrial radiation, $R_{s,net}$ = net solar radiation, R_{net} = net radiation, P = precipitation.

Table 4.3: Average value of key variables for simulations with (simulation O0-VD0-SD0) and without (simulation O0-VD0-SS0-3) the mixed layer ocean model for summer (JAS) conditions in the region between 13.0° N and 20.0° N.
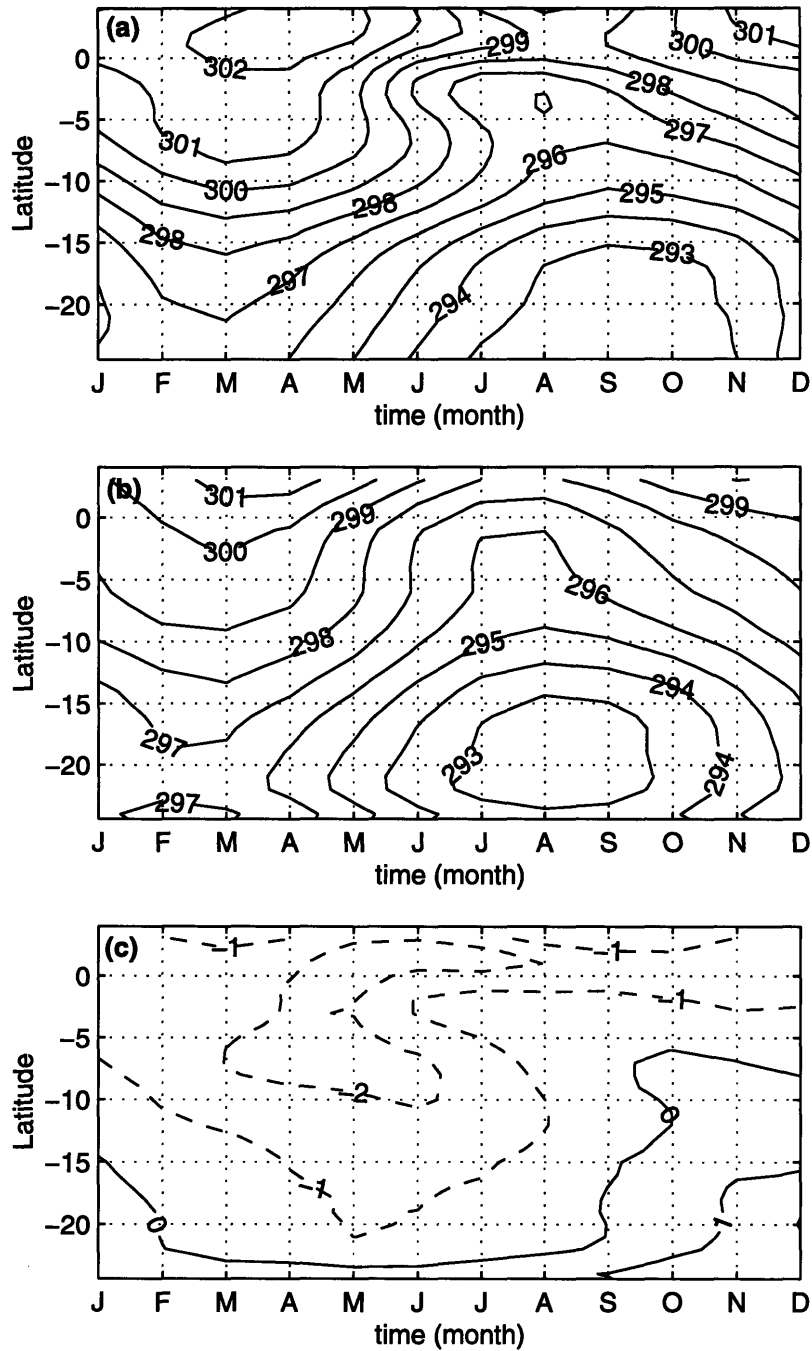
Figure 4-2: (a) SST climatology (° K) from NCEP Reanalysis; (b) Seasonal cycle of SST for the simulation in which the MLOM is validated based on current forcings (simulation O0-VD0-SD0); (c) = (b) - (a).
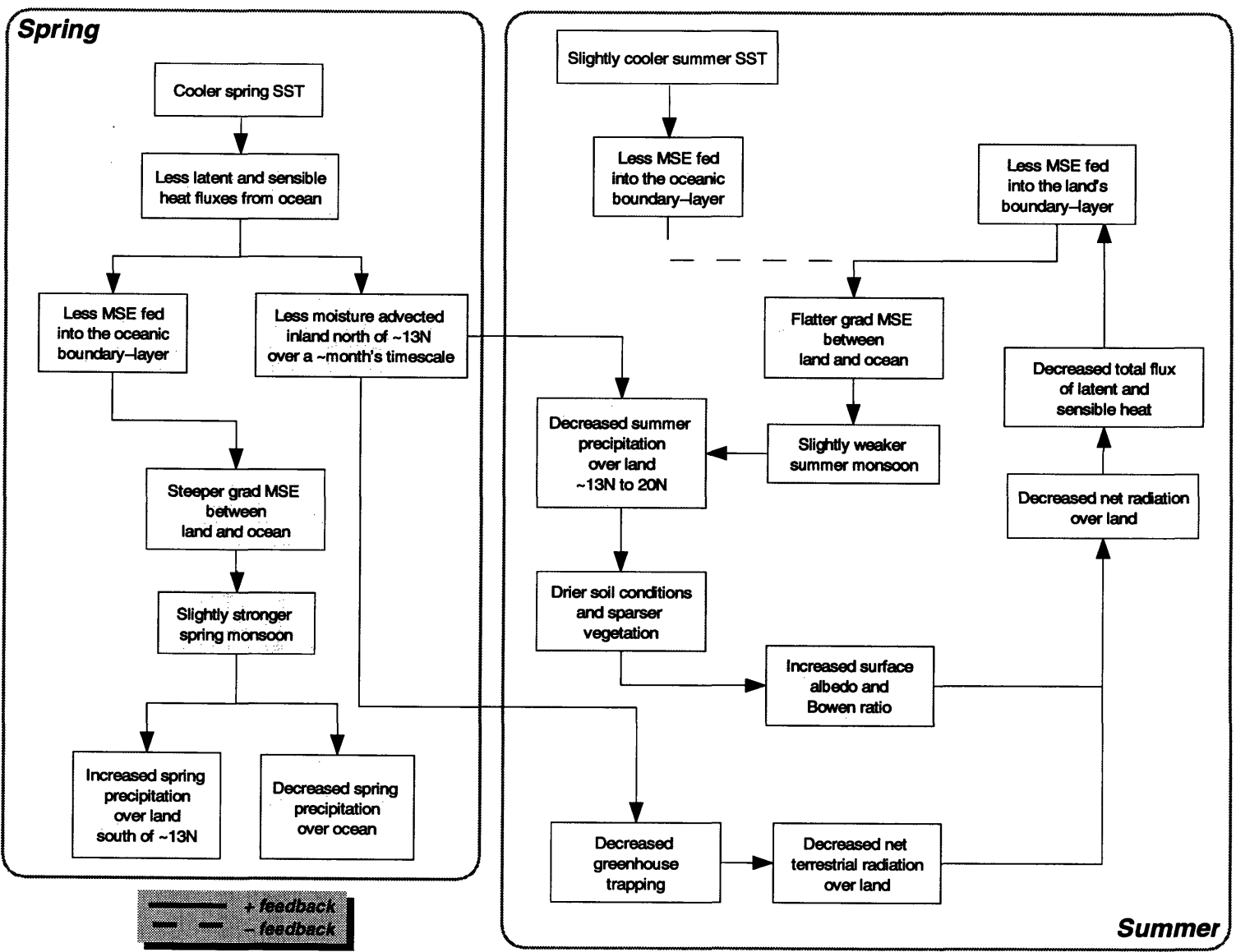
Figure 4-3: Summary of positive (solid lines) and negative (dashed lines) feedback mechanisms resulting in slightly lower precipitation over land, in the region from ~13° N to ~20° N, when validating the MLOM based on current forcings (simulation O0-VD0-SD0).

112

The simulated cold bias in the spring SSTs (Figure 4-2) results in a reduction of the latent and sensible heat fluxes fed into the oceanic boundary layer. As a consequence, the atmosphere directly in contact with the ocean surface is cooled and becomes drier. The decreased energy fluxes fed into the oceanic boundary layer steepen the gradient of moist static energy with respect to the land, and result in a stronger spring monsoon [*Eltahir and Gong*, 1996]. The stronger spring monsoon produces a negative precipitation anomaly over the ocean. At the same time, a positive precipitation anomaly develops over land in the region from ~5° N to ~13° N during the spring season (Figure 4-5). As the monsoon front progresses into land, the negative precipitation anomaly generated over the ocean during spring, propagates northward with it. Since the winds associated with the spring monsoon do not reach farther than ~13° N, and due to the decrease in ocean evaporation, little moisture is advected north of this location. This mechanism of moisture advection, acting with a timescale of about a month, has been identified by *Zheng et al.* [1999] as the initial connection between spring SSTs and summer rainfall over West Africa.

The decreased moisture advected inland during spring results in: (1) a decrease in the precipitable water over land during summer (Figure 4-6), and (2) less greenhouse trapping. The decreased greenhouse trapping [(2) above] acts to reduce the net terrestrial, and consequently, the net radiation (Figure 4-7) at the land surface during summer. Based on energy balance considerations, the decreased net radiation over land during summer has to be balanced roughly by decreases in the total energy fluxes (latent and sensible heat fluxes, Figures 4-8 and 4-9) fed into the land's boundary layer. At the same time, the small negative SST anomaly simulated during summer also results in a small decrease in the moist static energy fed into the oceanic boundary layer. However, the changes that occur over land dominate the gradient of moist static energy between the land and the ocean, which is slightly reduced (Figure 4-10) and results in a slightly weaker summer monsoon (Figure 4-11). This effect, together with the decrease in precipitable water [(1) above] result in less summer (Figure 4-5), and consequently total annual (Figure 4-4) precipitation over land in the region from ~13° N to ~20° N.

The negative precipitation anomaly over land during summer produces drier soil conditions and results in a sparser vegetation distribution (Figure 4-12) during summer. *Zheng et al.* [1999] have found that the resulting soil moisture-rainfall feedback [*Eltahir*, 1998], which acts to decrease the net radiation at the surface (Figure 4-7), is the mechanism responsible for sustaining the initial rainfall anomaly for the whole summer. In this case this mechanism mainly acts through a decrease in the downward longwave radiation as a result of decreased atmospheric humidity, while the upward longwave component and net solar radiation are barely affected (Table 4.3). Figure 4-5 shows that when summer ends and the monsoon reverses, this mechanism of moisture advection acts again to propagate the negative precipitation anomaly into the ocean.
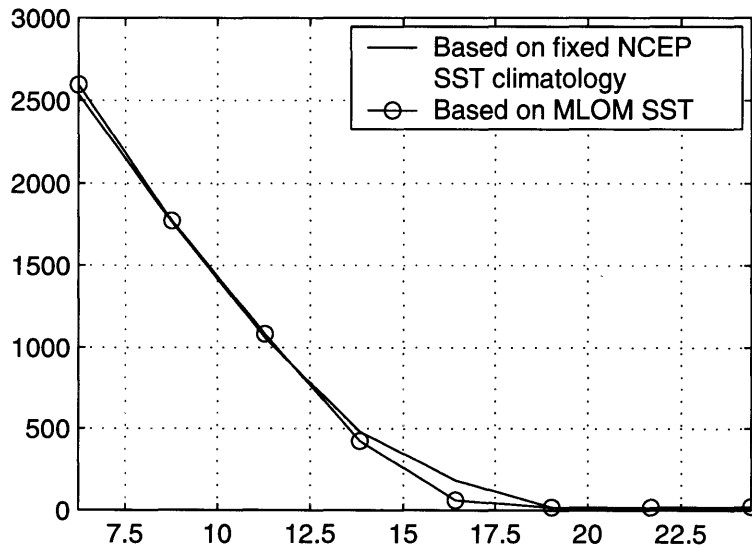
Figure 4-4: Distribution of total annual precipitation (mm/yr) for the simulation with fixed NCEP SST climatology (simulation O0-VD0-SS0-3, solid line), and the simulation in which the MLOM is validated based on current forcings (simulation O0-VD0-SD0, solid-circled line).

114
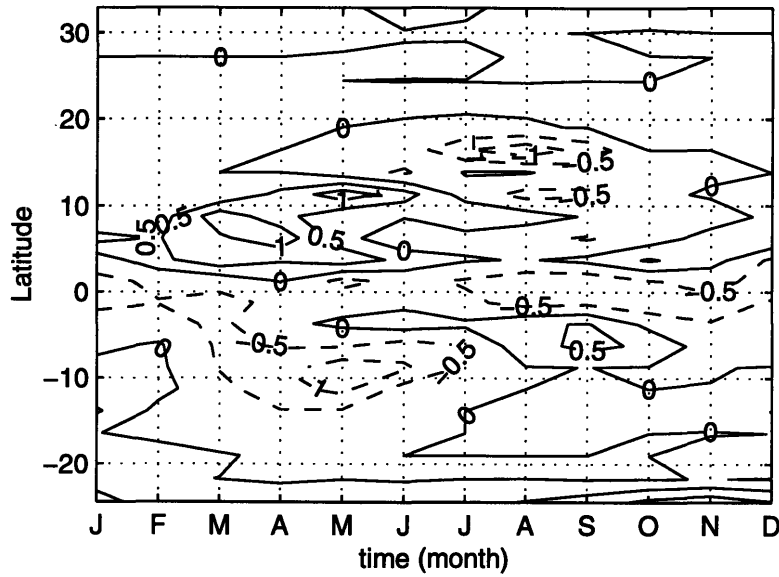
Figure 4-5: Difference in the seasonal cycle of precipitation (mm/day) for the simulation in which the MLOM is validated based on current forcings (simulation O0-VD0-SD0) - the simulation with fixed NCEP SST climatology (simulation O0-VD0-SS0-3).
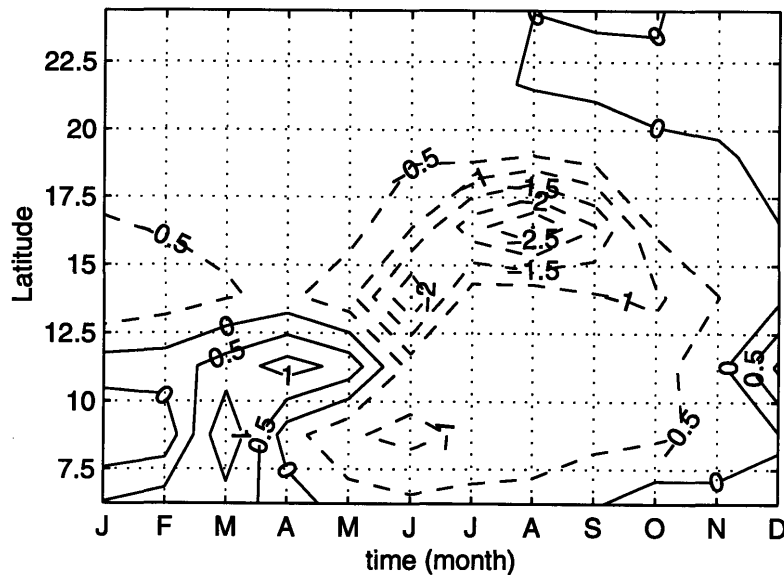
Figure 4-6: Difference in the seasonal cycle of specific humidity near the surface (g/kg) for the simulation in which the MLOM is validated based on current forcings (simulation O0-VD0-SD0) - the simulation with fixed NCEP SST climatology (simulation O0-VD0-SS0-3).

115
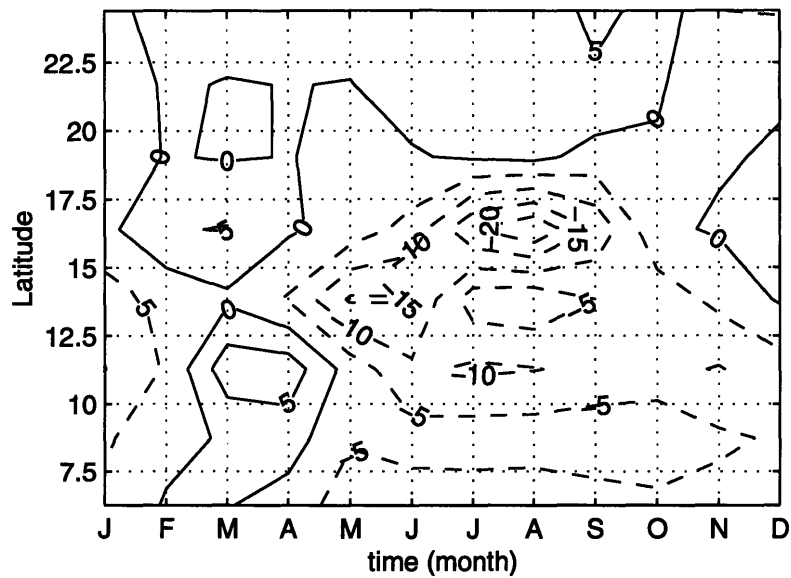
Figure 4-7: Difference in the seasonal cycle of net surface radiation (W/m^2) for the simulation in which the MLOM is validated based on current forcings (simulation O0-VD0-SD0) - the simulation with fixed NCEP SST climatology (simulation O0-VD0-SS0-3).
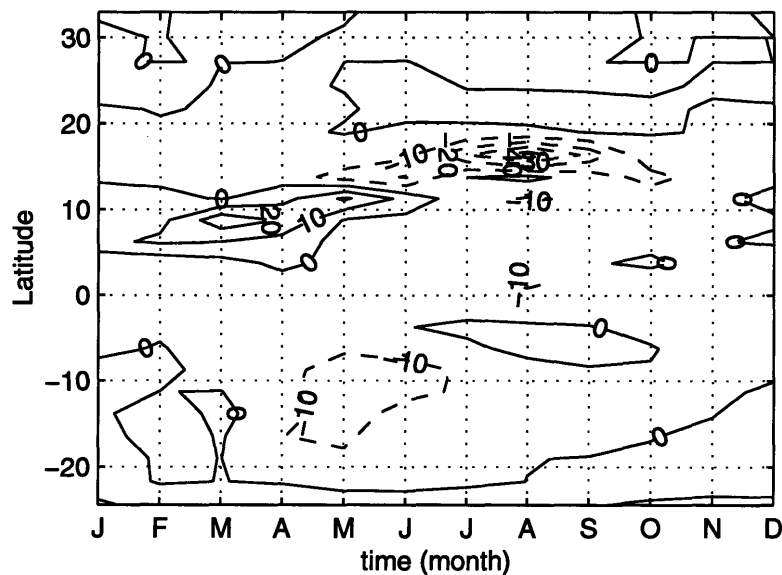
Figure 4-8: Difference in the seasonal cycle of latent heat flux (W/m^2) for the simulation in which the MLOM is validated based on current forcings (simulation O0-VD0-SD0) - the simulation with fixed NCEP SST climatology (simulation O0-VD0-SS0-3).

116
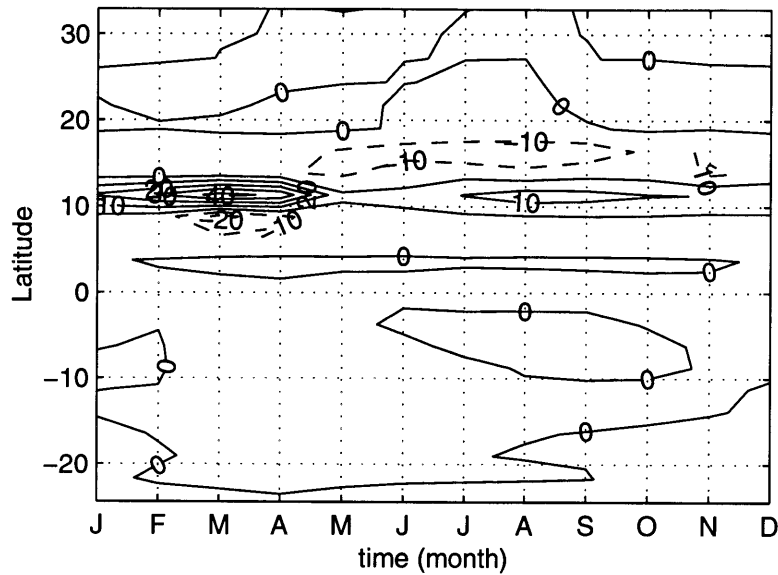
Figure 4-9: Difference in the seasonal cycle of sensible heat flux (W/m²) for the simulation in which the MLOM is validated based on current forcings (simulation O0-VD0-SD0) - the simulation with fixed NCEP SST climatology (simulation O0-VD0-SS0-3).
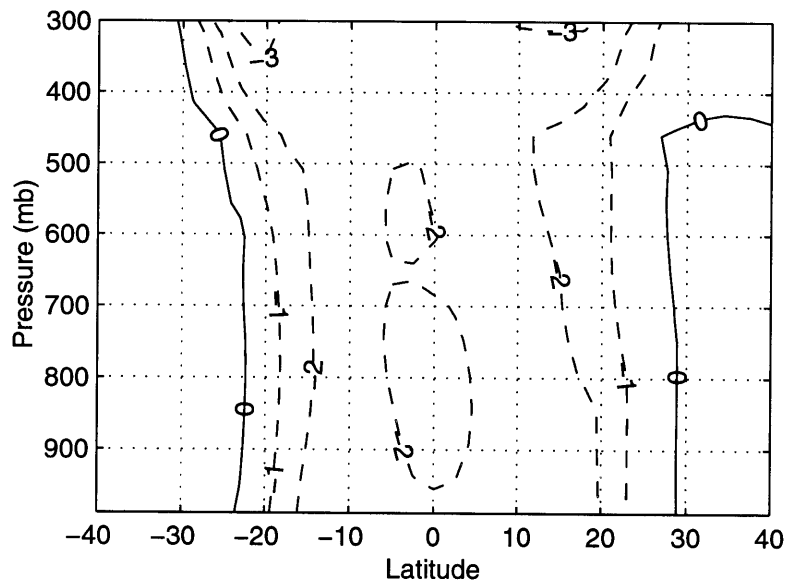
Figure 4-10: Difference in the equivalent potential temperature (° K) during August for the simulation in which the MLOM is validated based on current forcings (simulation O0-VD0-SD0) - the simulation with fixed NCEP SST climatology (simulation O0-VD0-SS0-3).
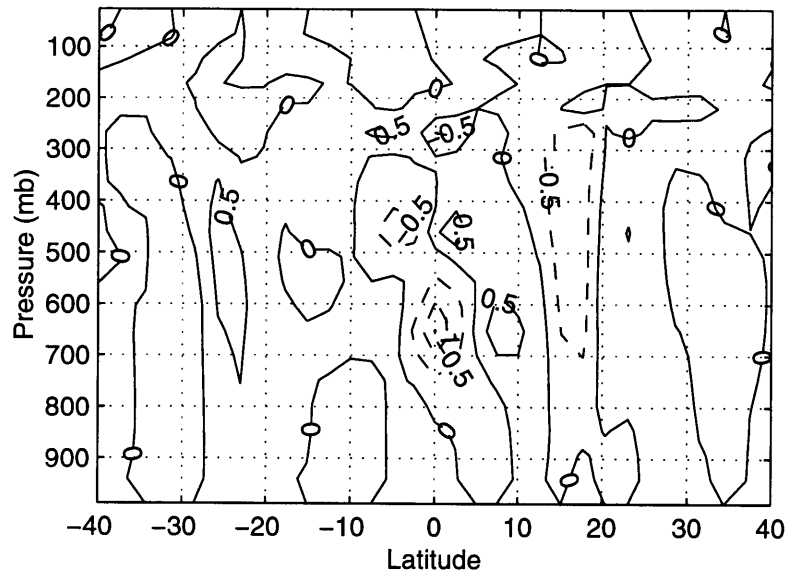
Figure 4-11: Difference in the vertical wind (mm/s) during August for the simulation in which the MLOM is validated based on current forcings (simulation O0-VD0-SD0) - the simulation with fixed NCEP SST climatology (simulation O0-VD0-SS0-3).
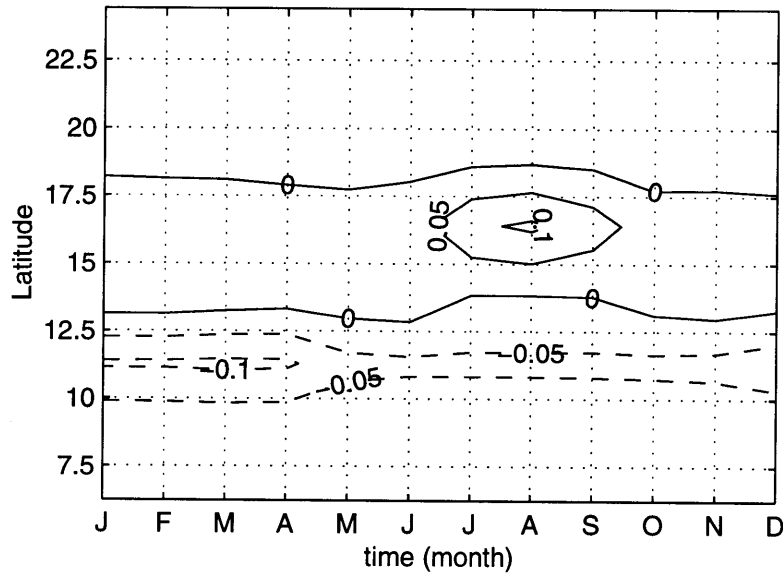
Figure 4-12: Difference in the seasonal cycle of surface albedo for the simulation in which the MLOM is validated based on current forcings (simulation O0-VD0-SD0) - the simulation with fixed NCEP SST climatology (simulation O0-VD0-SS0-3).

118

4.3 Impact of Ocean Dynamics in the Simulation of Mid-Holocene Conditions

Although no evidence has been found for significantly different SSTs in the Tropical Atlantic region during the Middle Holocene [*Ruddiman and Mix*, 1993], there is a common belief that local and seasonal variations might have contributed to enhancing the monsoon circulation over West Africa. Using ZonalBAM with the mixed layer ocean model (MLOM) component, this hypothesis can be tested. However, several limitations exist. First, the MLOM requires the inclusion of an ocean heat fluxes term. This term should account for the advection of heat by ocean currents and for local upwelling/sinking, processes which cannot be simulated by ZonalBAM and that are not quantitatively known for the Middle Holocene. Therefore, our need to prescribe them to their current climatology (from simulation O0-VD0-SS0-3, Table 4.1). Second, the fact that the atmospheric circulation over the SETA region is close to zonally-symmetric does not imply that the ocean circulation has to be and in fact it is not. The region is currently characterized by strong coastal upwelling in the Benguela system off the western coast of South Africa. Third, when attempting to validate the MLOM based on current forcings, a cold bias in the SSTs has been simulated. Therefore, it becomes necessary to take this cold bias into account in some way. However, in spite of these limitations, our MLOM can give us some insight into how seasonal and regional variations in the SSTs could affect the simulated monsoon circulation for the Middle Holocene.

In order to account for the cold bias in the SSTs simulated while validating the MLOM based on current forcings (Figure 4-2c), the corrected SSTs (i.e. by including the bias) are fixed in a simulation using 6K yrs BP forcings, and this is taken as our "control" simulation (simulation O6-VD6-SC0, Table 4.1). Similar to the simulation with current orbital forcings, the fixed corrected SSTs (i.e. by including the bias) result in a reduction of summer, and consequently, total annual precipitation (Figure 4-13, dashed and dashed-stared lines) for the Middle Holocene when compared to the simulation with fixed NCEP SST climatology (simulation O6-VD6-SS0-1, Table 3.1).
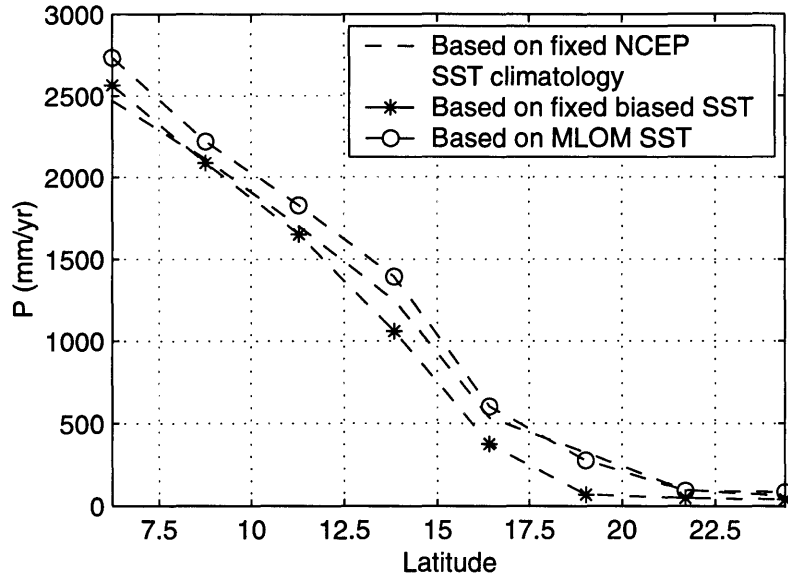
Figure 4-13: Distribution of total annual precipitation (mm/yr) for the simulation with fixed NCEP SST climatology (simulation O6-VD6-SS0-1, dashed line, Table 3.1), the simulation with the fixed corrected SSTs (simulation O6-VD6-SC0, dashed-stared line), and the simulation with the MLOM (simulation O6-VD6-SCD0, dashed-circled line).

With the purpose of assessing the impact of ocean dynamics on the simulated Mid-Holocene conditions over West Africa, the MLOM is applied to the region between 25° S and 5° N (SETA region, representing the average over 15° W-15° E) in a simulation using 6K yrs BP forcings (simulation O6-VD6-SCD0). The ocean heat fluxes were again obtained from a control simulation of the current climate (Figure 4-1) in which vegetation dynamics were allowed, and the model was forced with the current NCEP SST climatology (simulation O0-VD0-SS0-3, Table 4.1). These fluxes were then added to the ocean heat budget equation. Again, the MLOM is turned on after five years in which vegetation is fixed to that of *Hoelzmann et al.*'s [1998] (Figure 3-7) map of palaeovegetation, and the SSTs are fixed to the corrected values. Ten years later (year 15) vegetation dynamics are introduced. In addition, the relative humidity threshold over the ocean is again set as 5 % higher than over land (Table 4.2).

The impact of the addition of an interactive ocean component into simulations of the Middle Holocene is presented hereafter. Average summer (JAS) conditions for

120

the region between 16.5° N and 23.5° N (currently part of the Sahara) are also com-
pared in Table 4.4 for the simulations with (simulation O6-VD6-SCD0) and without
(simulation O6-VD6-SC0) the mixed layer ocean model. Comparing this table with
Table 3.9 (3rd column), it is evident that the effect of the cold bias in the SSTs used
in our "control" simulation is counteracted when the MLOM is let on (Figure 4-13),
so that the values of key variables over the current Sahara are again in accordance
with those of simulation O6-VD6-SS0-1 (See Chapter 3).

Variable	Simulation O6-VD6-SC0 (fixed SSTs)	Simulation O6-VD6-SCD0 (SSTs from MLOM)
B_o	1.3	0.7
$W_{soil,veg.}$	0.06	0.14
SHF (W/m^2)	46.6	49.7
LHF (W/m^2)	35.2	67.2
E_t (mm/day)	1.2	2.4
R_{net} (W/m^2)	204.6	221.2
P (mm/day)	1.1	2.2

B_o = Bowen ratio, $W_{soil,veg.}$ = soil moisture content available to vegetation
= f(soil moisture, rooting profile), SHF = sensible heat flux, LHF = latent
heat flux, E_t = evapotranspiration, R_{net} = net radiation, P = precipitation.

Table 4.4: Average value of key variables for simulations with (simulation
O6-VD6-SCD0) and without (simulation O6-VD6-SC0) the
mixed layer ocean model for summer (JAS) conditions in the
region between 16.5° N and 23.5° N.

The difference between the simulated seasonal cycle of SSTs for the Middle
Holocene (simulation O6-VD6-SCD0) and the corrected SSTs (i.e. by including the
bias) used in our "control" simulation (simulation O6-VD6-SC0) is shown in Figure
4-14. It is noticed that the effect of 6K yrs BP orbital forcings is a further reduction
of the SSTs, specially during the spring (AMJ) and summer (JAS) seasons, consistent
with other studies [*Maley*, 1997; *Braconnot et al.*, 2000; *Texier et al.*, 2000]. How-
ever, some warming is simulated during autumn (OND), and the pattern of the SST
anomalies (Figure 4-14) is quite different from that of the biased SSTs (Figure 4-2c).
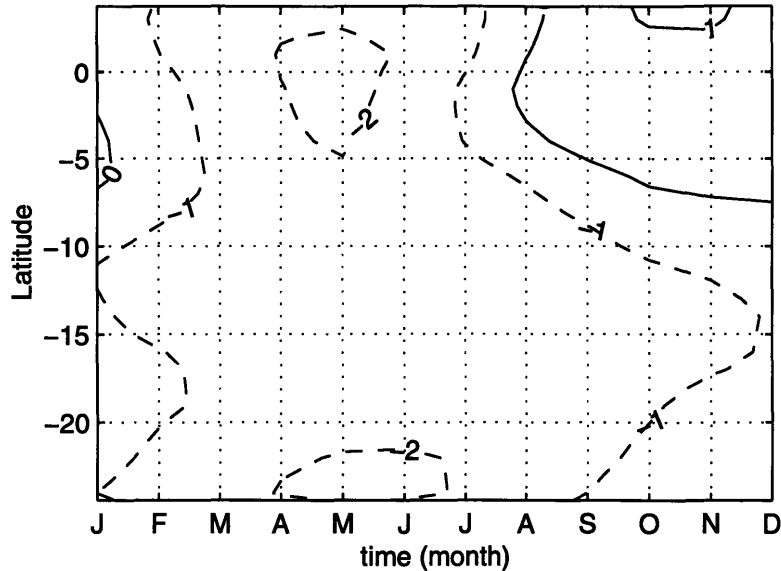
Figure 4-14: Difference in the seasonal cycle of surface temperature (° K) for the simulation with the MLOM (simulation O6-VD6-SCD0) - the simulation with the fixed corrected SSTs (simulation O6-VD6-SC0).

The warm SST anomaly simulated during autumn (OND) results in more moisture fed into the oceanic boundary layer. As a result, a positive precipitation anomaly is generated over the ocean during the season. From Figure 4-15, it is evident how the positive precipitation anomaly generated over the ocean during autumn starts propagating inland during the following season (i.e. winter, JFM). *Zheng et al.* [1999] have identified moisture advection as an important mechanism connecting the SSTs during a season with precipitation over land during the following season, consistent with the migrational pattern observed in our simulated precipitation. Since the West African Coast of Guinea (5° N) is characterized by a northward wind component throughout the year, the anomalous moisture generated over the ocean during autumn is advected to the region by winter.

The increased moisture advected inland during autumn results in: (1) an increase of the precipitable water over land during winter, and (2) more greenhouse trapping. The increased greenhouse trapping [(2) above] acts to increase the net terrestrial, and consequently, the net surface radiation (Figure 4-17) over the Coast of Guinea during winter. This increase in the net radiation is balanced by corresponding increases in

the total energy fluxes (latent and sensible heat fluxes; Figures 4-18 and 4-19) fed into the land's boundary layer. At the same time, a negative anomaly in the SSTs is generated over the ocean, which results in a reduced amount of energy fed into the oceanic boundary layer. Resulting from these two processes, a steeper gradient of moist static energy between the land and the ocean develops and results in a stronger monsoon. This effect, together with the increased precipitable water [(1) above] result in higher winter precipitation over the Coast of Guinea. The stronger winds associated with the simulated stronger monsoon during winter help to bring the positive precipitation anomaly further north.

As the seasons progress and the land area affected by the positive precipitation anomaly increases, the land surface responds by becoming greener (Figure 4-16) and the total energy fluxes fed into the land's boundary layer increase accordingly. At the same time, the negative anomaly in the simulated SSTs grows resulting in reduced energy into the oceanic boundary layer. So, the steeper gradient of moist static energy generated as a result of both mechanisms, act to sustain the precipitation anomaly until summer when it reaches its most northward position (Figures 4-20 and 4-21). As the summer season (JAS) ends and the monsoon starts to naturally weaken, the additive effects of a decreased moisture source from the cooler SSTs simulated through mid-winter/spring/summer also act to decrease the precipitation over land, moving the positive precipitation anomaly again from the land into the ocean. These results are consistent with other studies [Druyan and Koster, 1989], which have identified two mechanisms for dry conditions over the Sahel: one being the deficiencies in the moisture supply, and the other the consequence of too few rain-generating wave disturbances even when moisture is ample.

In summary, the simulated anomaly pattern in the Middle Holocene SSTs, produces a distinct migrational pattern in the precipitation difference field, as well as in other key variables, which is related to a longer-lasting and stronger monsoon. Our results agree with those of other studies. As an example, using a coupled ocean-atmosphere model, Braconnot et al. [2000] simulated cooler SSTs over the SETA region during the Middle Holocene. As a result, the effects of the West African mon-

Figure 4-15: Difference in the seasonal cycle of precipitation (mm/day) for the simulation with the MLOM (simulation O6-VD6-SCD0) - the simulation with the fixed corrected SSTs (simulation O6-VD6-SC0).

soon over land lasted longer resulting in increased precipitation. Similarly, *Texier et al.* [2000] found that by prescribing the SSTs 1-3° K cooler than their current values, a significant increase in rainfall was generated over the Sahara.

In our simulation, when the effects of the corrected (i.e. by including the bias) SSTs and the simulated anomaly pattern in the SSTs for 6K yrs BP are superimposed, the simulated year-round increase in precipitation near the coast dominates resulting in increased coastal precipitation (Figure 4-13). However, near the desert margin, the increase in precipitation resulting from the SST anomalies simulated for the Middle Holocene is counteracted by the precipitation decrease associated with the corrected SSTs. As a consequence, the simulated location of the southern desert margin stays the same as in the simulation with fixed NCEP SST climatology (simulation O6-VD6-SS0-1, See Chapter 3).
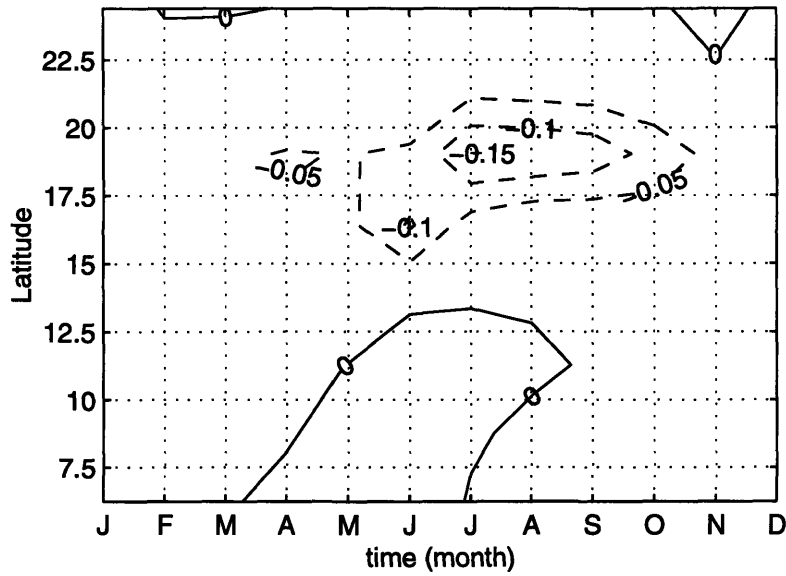
Figure 4-16: Difference in the seasonal cycle of surface albedo for the simulation with the MLOM (simulation O6-VD6-SCD0) - the simulation with the fixed corrected SSTs (simulation O6-VD6-SC0).
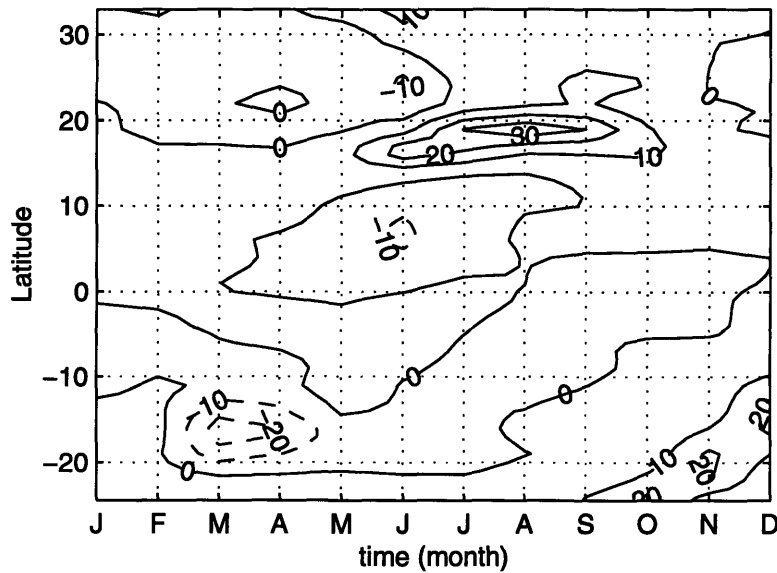
Figure 4-17: Difference in the seasonal cycle of net radiation (W/m^2) for the simulation with the MLOM (simulation O6-VD6-SCD0) - the simulation with the fixed corrected SSTs (simulation O6-VD6-SC0).
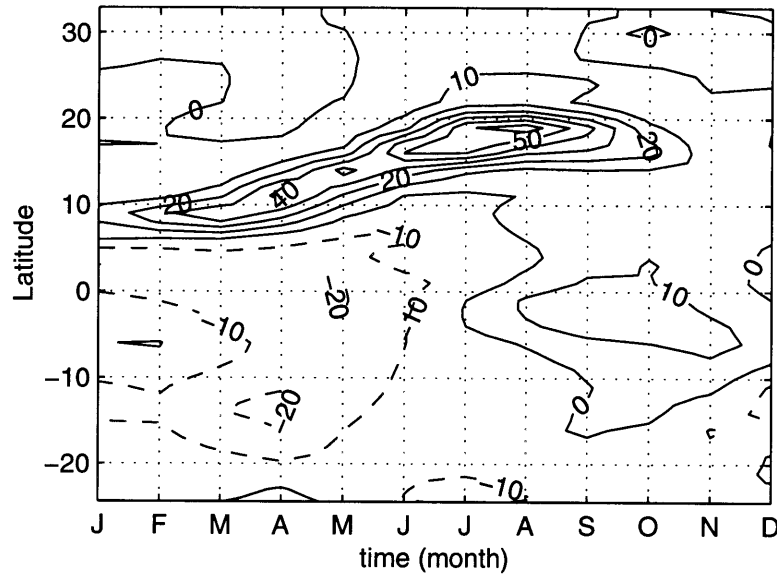
Figure 4-18: Difference in the seasonal cycle of latent heat flux (W/m²) for the simulation with the MLOM (simulation O6-VD6-SCD0) - the simulation with the fixed corrected SSTs (simulation O6-VD6-SC0).
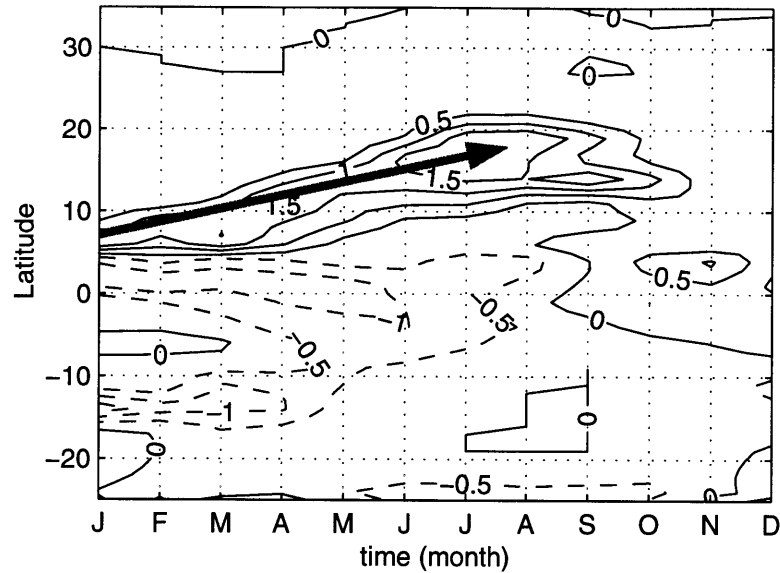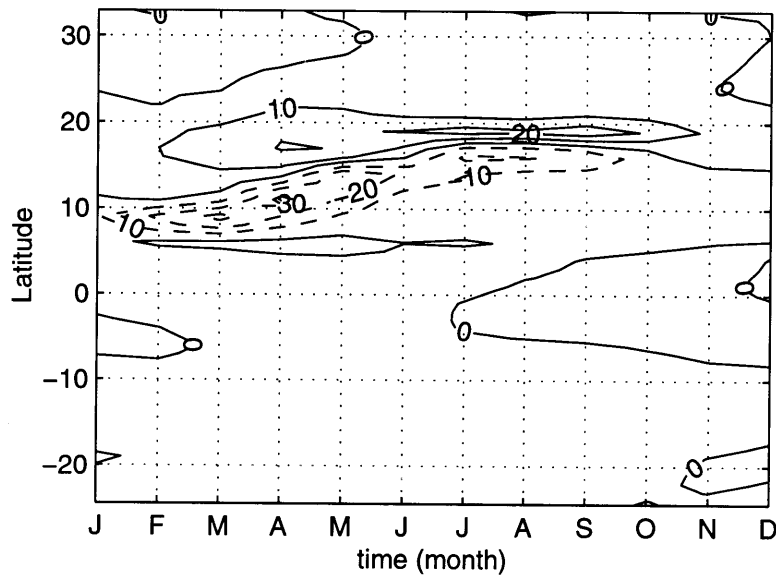

Figure 4-19: Difference in the seasonal cycle of sensible heat flux (W/m²) for the simulation with the MLOM (simulation O6-VD6-SCD0) - the simulation with the fixed corrected SSTs (simulation O6-VD6-SC0).
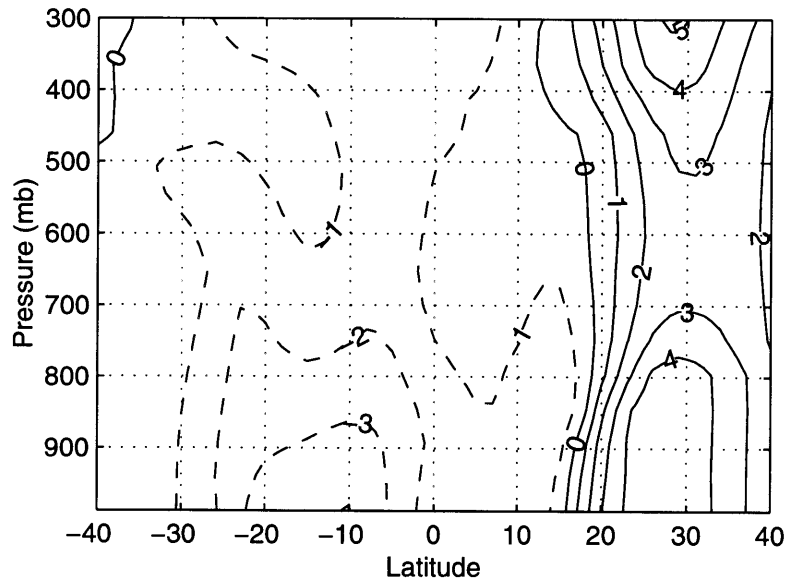
Figure 4-20: Difference in the equivalent potential temperature (° K) during August for the simulation with the MLOM (simulation O6-VD6-SCD0) - the simulation with the fixed corrected SSTs (simulation O6-VD6-SC0).
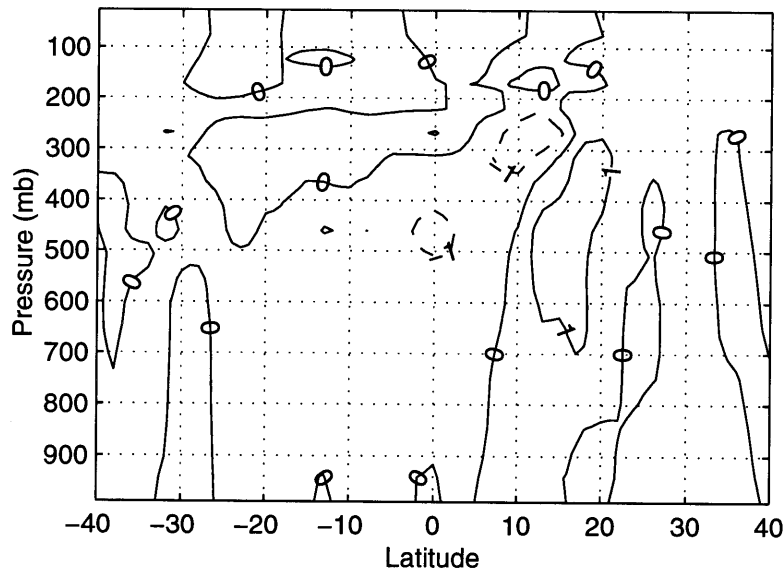
Figure 4-21: Difference in the vertical wind (mm/s) during August for the simulation with the MLOM (simulation O6-VD6-SCD0) - the simulation with the fixed corrected SSTs (simulation O6-VD6-SC0).

127

4.4 Summary

In this section, an interactive mixed layer ocean model (MLOM) has been added to ZonalBAM in order to consider the effects of ocean dynamics in the West African climate. The validation of the MLOM was complicated by the fact that cold biases in the SSTs resulted from a simulated higher than observed cloud cover over the ocean. By increasing the relative humidity threshold over the ocean, the simulated SSTs were in much better agreement with the observed climatology. However, a small cold bias is still observed specially during spring/summer, which results in a lower summer, and consequently, total annual, precipitation over land in the region from ˜13° N to ˜20° N.

In order to account for the cold bias in the simulated current SSTs, results with the interactive MLOM based on 6K yrs BP forcings were compared to results from a "control" simulation with 6K yrs BP forcings in which the corrected (i.e. by including the bias) SSTs were fixed. Results from this "control" simulation using the biased SSTs and 6K yrs BP forcings, show slightly drier conditions than those of the simulation with fixed NCEP climatology (See Chapter 3). In the simulation based on 6K yrs BP forcings where the MLOM is turned on, we find again mostly cooler SSTs, except for a small warming during autumn. Additionally, the pattern of the SST anomalies is quite different from that of the biased SSTs.

We find that the effect of the superposition of the corrected SSTs and the orbitally-induced SST anomalies, is to bring the simulated climate conditions over the current Sahara back again to those of the simulation with fixed NCEP climatology. It is then reasonable to assume that if the validation of our MLOM would have not resulted in any biases, the addition of an oceanic component into Mid-Holocene simulations could have resulted in a more northward position of the southern desert margin even further than that of the simulation with the fixed NCEP climatology (See Chapter 3), bringing our simulations in much better agreement with palaeoclimatic reconstructions. We also understand that the simulated signal in the SSTs is the direct result of orbitally-induced thermal changes in the mixed layer, while possible localized effects

such as upwelling/sinking which we did not account for, could have produced a more complicated signal superimposed on top of the orbitally-induced one.

Chapter 5

Summary and Conclusions

5.1 Summary of Results

The successful simulation of past climate change is a critical component in the process of validating a climate model. It would give us more confidence when attempting to use the model to simulate future climate change. Additionally, it would give us some insights onto the way in which interactions between the components of the climate system (i.e. atmosphere, biosphere, ocean, surface waters) take place. The gained understanding would ultimately allow for model improvements. The Middle Holocene presents a unique opportunity to isolate the effects of insolation on climate since evidence indicates that during this period the ice sheets had already retreated to their current location, and the atmospheric CO_2 concentration was closer to preindustrial levels. During the Middle Holocene (6K yrs BP), an increased seasonality in radiation in the Northern Hemisphere resulted in a stronger West African summer monsoon with the region currently occupied by the Sahara Desert becoming almost completely vegetated. It is our interest to understand the mechanisms through which these insolation changes enhanced the monsoonal climate over West Africa during the period resulting in a significant rainfall increase, as has been widely recorded.

Previous studies using atmospheric general circulation models have significantly underestimated the expected wetter/greener conditions over West Africa during the Middle Holocene. Although the vegetation, soil, lake, wetland, and ocean feedbacks

130

on climate have been omitted in these studies, these have been identified as the possible mechanisms through which orbital forcings could have been enhanced to produce the recorded significant rainfall increase. Here, we have presented the results of several simulations performed with a zonally-symmetric climate model, with the purpose of assessing whether the model is capable of reproducing the main features of the Mid-Holocene climate over West Africa, namely the observed greening of the Sahara during the period. With the objective of assessing the relative contributions of orbitally-induced changes in radiation, vegetation dynamics, the sensitivity to initial vegetation conditions, and ocean dynamics, several experiments based on both current and 6K yrs BP orbital forcings were designed and results are summarized hereafter. Figure 5-1 presents a summary of our findings using the biosphere-atmosphere model in terms of the distribution of moist static energy over the land and ocean, which determines the strength of the monsoon circulation [*Eltahir and Gong*, 1996; *Eltahir*, 1998; *Zheng and Eltahir*, 1998].
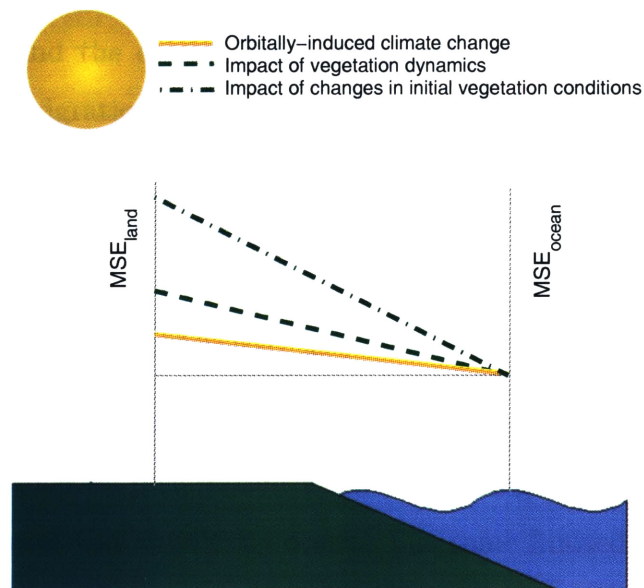
Figure 5-1: Summary of results based on a schematic representation of the distribution of moist static energy over land and ocean. A steeper (flatter) gradient in the moist static energy between the land and the ocean results in a stronger (weaker) monsoon [*Eltahir and Gong*, 1996; *Eltahir*, 1998; *Zheng and Eltahir*, 1998].

131

5.1.1 Orbitally-Induced Climate Change

With the purpose of isolating our model's response to changes in the Earth's orbital configuration, simulations in which vegetation conditions were fixed to the close-to-observed distribution were performed using current and 6K yrs BP orbital forcings. Our results show that an orbitally-induced increase in the solar radiation reaching the top of the Earth's atmosphere alone is insufficient to simulate the expected greener/wetter conditions over West Africa for the Middle Holocene. In the simulation using 6K yrs BP orbital forcings, we found a small increase in precipitation as compared to the simulation with current forcings. However, the increased precipitation is limited to the southern border of the Sahara Desert.

Since in these simulations we have fixed the vegetation to its current distribution, the fixed albedo limits the enhancement of net radiation reaching the land surface. As a consequence of the limited response in the net radiation at the land surface, the energy fluxes (latent and sensible heat fluxes) fed into the land boundary layer do not increase significantly (Figure 5-1, solid line). Therefore, the strength of the monsoon circulation, which is strongly dependent on the differential energy fluxes between the land and the ocean, does not increase significantly, consistent with a limited northward migration of the southern desert margin ($\tilde{}1.1°$). In other words, the limited response simulated is due to the fixed vegetation conditions anchoring the simulated climate to the current climate.

5.1.2 Impact of Vegetation Dynamics

Previous studies using general circulation models have consistently underestimated the extent of the monsoon penetration when prescribing current land surface conditions in simulations of the Middle Holocene. The same limited response is reflected in our results based on changes to the orbital forcings alone. Therefore, in order to allow for a more complete response of the climate system to changes in insolation, we allowed the vegetation in the tropical regions of West Africa to dynamically interact with the climate until an equilibrium was established.

Our results show that when vegetation is allowed to dynamically respond to the slight orbitally-induced increase in precipitation simulated for the Middle Holocene, it becomes greener, which again feeds back into the strength of the monsoon circulation. The main mechanism for the monsoon enhancement results from the lower surface albedo associated to the greener vegetation distribution, which acts by significantly increasing the net radiation reaching the land surface for the Middle Holocene. Since this increase in the net radiation is accompanied by similar increases in the energy fluxes (latent and sensible heat fluxes) fed into the land boundary layer, the resulting steeper gradient of moist static energy (Figure 5-1, dashed line) produces a healthier monsoon circulation. Additionally, we have found that due to the increased soil moisture simulated for the Mid-Holocene, the evapotranspiration increases more significantly than the sensible heating serving as a more significant mechanism for moisture recycling. As a result of these changes, the southern desert margin migrates northward by ˜2.4° (from 15.7° N to 18.1° N). However, the extent of the vegetation expansion is still significantly underestimated compared to palaeoclimatic evidence.

5.1.3   Impact of Changes in Initial Vegetation Conditions

Previous studies have demonstrated the importance of incorporating Mid-Holocene vegetation conditions in order to bring simulations closer to palaeoclimatic reconstructions. Based on the information derived from *Hoelzmann et al.*'s [1998] map of palaeovegetation, we determined the extent of the vegetation belts during the Middle Holocene. When we initialized our model with this greener vegetation distribution on a simulation based on current orbital forcings, we found that it cannot be sustained. The model reaches an equilibrium very similar to the currently observed climate, the same as when it was initialized with the close-to-observed vegetation distribution. However, when using 6K yrs BP orbital forcings, we found that this vegetation distribution can in fact be sustained under Mid-Holocene forcings, except for a small southward retreat of the southern desert margin by ˜2.5° from its originally specified position. Water demanding vegetation types such as dry forest and grassland expand northward by ˜500 km to ˜20.5° N as compared to conditions simulated for

133

the current climate (~15.4° N, defined as location of 200 mm/yr precipitation).

An orbitally-induced increase in top-of-the-atmosphere insolation during the Middle Holocene resulting in a slight increase of the net radiation at the surface, is responsible for the initial enhancement of the West African summer monsoon. As a result of the positive precipitation anomaly simulated over land, moister soil conditions and a greener vegetation distribution are produced. Based on the hypothesis developed by *Eltahir* [1996, 1998] on the soil moisture-rainfall feedback mechanism, these changes to the land surface result in increased net solar radiation. The increased net radiation at the land surface is again balanced by corresponding increases in the total energy fluxes (mostly in the form of latent heat due to decreased Bowen ratio) fed into the land's boundary layer. With conditions over the ocean being fixed by the specified SST climatology, an even steeper gradient of moist static energy between the land and the ocean is produced (Figure 5-1, dashed-dotted line). As a consequence, the summer monsoon circulation is further enhanced until an equilibrium is established in which a significantly stronger monsoon can be sustained under 6K yrs BP orbital forcings.

Contrary to previous studies, which have identified only a single green equilibrium for the West African region during the Middle Holocene, we find multiple equilibria for the period as drawn from the different results obtained when using different initial vegetation conditions corresponding to the current and Mid-Holocene distributions. *Wang and Eltahir* [2000b], demonstrated how climate transitions between different equilibria shape the currently observed low-frequency rainfall variability over the region. Based on this, we hypothesize that similar transitions could have taken place during the Middle Holocene causing the southern desert margin to migrate between 18.1° N and 21.4° N.

5.1.4 Impact of Ocean Dynamics

As part of our research, an interactive mixed layer ocean model (MLOM) has been added to ZonalBAM in order to consider the effect of ocean feedbacks in the dynamics of the West African monsoon. Our validation of the MLOM based on current forcings

resulted in a small cold bias in the simulated SSTs specially during spring/summer. This cold bias in the SSTs results in a lower summer, and consequently, total annual, precipitation over land, and has implications on the accuracy of the MLOM in simulating ocean conditions during the Middle Holocene.

The cold bias in the simulated current SSTs was taken into account by comparing the results obtained from a 6K yrs BP simulation using the interactive MLOM to the results from a "control" simulation with 6K yrs BP orbital forcings in which corrected SSTs (i.e. by including the bias) were fixed. Results from this "control" simulation using the corrected SSTs and 6K yrs BP orbital forcings, again show slightly drier conditions than those of the simulation with fixed current SST climatology.

In the simulation based on 6K yrs BP orbital forcings where the MLOM is turned on, we find again negative SST anomalies during spring/summer when compared to the "control" simulation, consistent with other studies. However, some warming is simulated during autumn, and the pattern of these SST anomalies is quite different from that of the corrected SSTs. The simulated anomaly pattern in the Middle Holocene SSTs by itself, produces a distinct migrational pattern in the precipitation difference field, as well as in other key variables, which is related to a longer-lasting and stronger monsoon. When the effects of the corrected SSTs and the simulated anomaly pattern in the SSTs for 6K yrs BP are superimposed, the simulated year-round increase in precipitation near the coast dominates resulting in increased coastal precipitation. However, near the desert margin, the increase in precipitation resulting from the SST anomalies simulated for the Middle Holocene is counteracted by the precipitation decrease associated with the corrected SSTs. As a consequence, the simulated location of the southern desert margin stays the same as in the simulation with fixed NCEP SST climatology.

It is then reasonable to speculate that if the validation of our MLOM would have not resulted in any biases, the addition of an oceanic component into Mid-Holocene simulations could have resulted in a more northward position of the southern desert margin even further than that of the simulation with the fixed SST climatology, bringing our simulations in much better agreement with palaeoclimatic reconstruc-

tions. We also recognize that the simulated change in the SSTs is the direct result of orbitally-induced thermal changes in the mixed layer, while possible localized effects such as upwelling/sinking which we did not account for, could have produced a more complicated signal superimposed on top of the orbitally-induced one.

5.2 Conclusions

From this modeling study, the complexity and non-linearity of the West African climate is evident. Different feedback mechanisms interact to affect the strength of the close-to-zonally-symmetric monsoon circulation through changes in the moist static energy of the land with respect to the ocean. Our zonally-symmetric climate model, ZonalBAM, has served as a tool to better understand how the inclusion of feedback mechanisms could improve simulations of climate change. Nevertheless, we have found that several limitations arise from ZonalBAM's simplified configuration.

It is evident that zonally-symmetric models are strongly dependent on reliable initial and boundary conditions to accurately reproduce the current and Mid-Holocene climates. For the current climate, this limitation is overcome by the high amount of data available. However, in simulating past climates there is a high degree of uncertainty regarding these conditions (e.g. ocean conditions, vegetation conditions, conditions in mid-latitudes). The importance of having a good idea about the boundary conditions expected under the different climate regime that we are trying to simulate has been demonstrated. It has been shown that due to the multiple equilibria nature of the West African climate during the Middle Holocene, it is important that the vegetation distribution is initialized close to that expected from reconstructions or else the system could evolve into a different equilibrium. We have shown how changes to the ocean conditions during the Middle Holocene could have contributed to a longer-lasting monsoon circulation over West Africa and could have resulted in a more northward location of the southern margin of the Sahara.

Our most realistic results show a northward shift of ~500 km in the southern margin of the Sahara Desert during the Middle Holocene, consistent with palaeoclimatic

reconstructions. However, our model fails to simulate the expected wetter conditions in the region from ~20.5° N-~23° N. The reasons behind this limited response have been identified as:

1. Our zonally-symmetric model cannot simulate the influence of the northwestern polar depressions and Atlantic cyclones, which according to *Petit-Maire and Guo* [1997] were a more important contributor to precipitation in the northern Sahara during the Middle Holocene than currently.

2. Due to our model's zonally-symmetric configuration, additional feedbacks resulting from a significant increase in the area occupied by surface waters during the Middle Holocene have not been included.

3. Due to the simulated cold bias in the current SSTs, the response of the climate system to changes in the ocean conditions was not fully simulated. Additionally, due to our model's zonal symmetry, local changes in SSTs due to localized upwelling/sinking and heat transport by ocean currents, have not been simulated.

However, in spite of all these caveats, it is remarkable that our simple zonally-symmetric model was able to simulate the greening of the Sahara during the Middle Holocene. Additionally, several other studies [*Kutzbach et al.*, 1996; *Doherty et al.*, 2000; *Texier et al.*, 2000; *Carrington et al.*, 2001] suggest the possibility that the distribution of vegetation n of ~20°-25° N was not as spatially continuous as has been inferred from the interpolation between a limited number of sites, and that local moisture recycling may have played an important role in maintaining regional-scale patches of vegetation/lakes/wetlands rather than a uniform continental-scale vegetation shift.

Our results confirm that the same basic mechanisms for monsoon enhancement that have been identified under current forcings can be successfully applied to the understanding of past climates over the region of West Africa. However, care should be exercised by taking into account model limitations, and the high degree of uncertainty in boundary and initial conditions corresponding to past climates. The

understanding gained from this study could be applied to the analysis of future climate changes, such as those expected under increased greenhouse emissions. As an example, *Petit-Maire and Guo* [1997] have stated that the expected greenhouse warming could produce changes in the atmospheric circulation over the Sahara, similar to those that occurred during the Middle Holocene. They have also stated that since the population near the desert margin is expected to double by 2038, there is a fear that the increased water resources probably expected for the region could be counterbalanced by their misuse, as well as other human activities such as deforestation and desertification.

Here, we have shown how increases in the net radiation reaching the land surface, resulting mainly from increased top-of-the-atmosphere insolation and reduced surface albedo, would result in more energy fluxes (latent and sensible heat fluxes) fed into the land boundary layer and a stronger monsoon. The increased greenhouse loading into the atmosphere could similarly increase the net radiation at the surface through additional trapping of the Earth's longwave radiation. With conditions over the ocean being the same, the increased radiation at the land surface could result in a steeper gradient of moist static energy, and consequently, in a stronger monsoon. Associated with the stronger monsoon, vegetation feedbacks could take place resulting in greening of the vegetation and further monsoon enhancement.

5.3   Future Research

The fact that our simple zonally-symmetric climate model was able to reproduce a significant part of the expected greening of the Sahara during the Middle Holocene is remarkable. However, our simulated northward shift of the southern desert margin to ˜20.5° N is still underestimated when compared to reconstructions of palaeovegetation. Several feedback mechanisms which we did not account for, could be the cause for mismatch with palaeodata. Ideally, global climate models with high temporal and spatial resolution in which the atmosphere, biosphere, and ocean are synchronously coupled, would be required to bring palaeoclimate simulations closer to palaeocli-

matic evidence. This will in turn increase our degree of confidence in the model for simulating future climate change. Therefore, the following work is suggested as a continuation of our efforts:

1. Simulations in which vegetation perturbations are introduced in a certain region in order to determine the resilience of the climate system during the Middle Holocene. This could give us some insight into how transitions between the different climate equilibria simulated for the Middle Holocene could have taken place.

2. Sensitivity simulations based on more realistic soil conditions during the Middle Holocene, specifically reflecting the higher organic soil content associated to greener conditions during the period.

3. Simulations in which changes to the atmospheric dust loadings during the Middle Holocene are included.

4. Simulations in which variability in the zonal direction is added to the mixed layer ocean model with the purpose of reducing the bias in the simulated SSTs. This will increase our confidence in the model's ability in simulating the role of ocean dynamics during the Middle Holocene.

5. Simulations using a global climate model with synchronous coupling of the atmosphere-vegetation-ocean system so that we could account for the following processes:

   (a) Changes in the global atmospheric circulation such as those imposed by ENSO, NAO.

   (b) Changes in the global SST distribution resulting from both orbitally-induced direct thermal changes, and changes in the oceanic heat transport and localized upwelling/sinking.

   (c) The inclusion of middle-latitude eddies as an important transport mechanism which could bring moisture to the northern Sahara in the form of northwestern cyclones.

(d) Accounting for surface waters (i.e. wetlands, lakes) as a possible feedback mechanism, specially the contribution of Lake Mega Chad to the local moisture and energy balance during the Middle Holocene.

(e) Accounting for topographically-induced changes in the atmospheric circulation (i.e. gravity waves), especially near the Ahaggar, Tibesti, and Atlas mountain ranges.

(f) Differential expansion of the grassland vegetation between the western, central, and eastern Sahara.

However, until computational constraints, uncertainties in model parameterizations, and the lack of a quantitative set of boundary and initial conditions for the period can be overcome, we will still be dealing with simplification and uncertainty.

References

[1] Adams, J. M. Global Land Environments Since the Last Interglacial. Technical report, Oak Ridge National Laboratory, TN, USA, 1997. http://www.esd.ornl.gov/ern/qen/nerc.html.

[2] Adams, J. M., Faure, H., and QEN members. Review and Atlas of Palaeovegetation: Preliminary Land Ecosystem Maps of the World Since the Last Glacial Maximum. Technical report, Oak Ridge National Laboratory, TN, USA, 1997. http://www.esd.ornl.gov/ern/qen/adams1.html.

[3] Anhuf, D., Schröeder, B., and Motzer, T. Palaeovegetation Maps of Africa. Technical report, Department of Physical Geography. University of Mannheim, Mannheim, Germany, 2000. http://www.uni-mannheim.de/phygeo/palaeo.htm.

[4] Barnola, J. M., Raynaud, D., Korotkevich, Y. S., and Lorius, C. Vostok Ice Core Provides 160,000 Year Record of Atmospheric CO_2. *Nature*, 346:347–349, 1987.

[5] Beerling, D. J. The Role of the Terrestrial Biosphere in Holocene Carbon Cycle Dynamics. *Global Ecol. and Biogeogr.*, 9:421–429, 2000.

[6] Berger, A. L. A Simple Algorithm to Compute Long Term Variations of Daily or Monthly Insolation. Technical Report 18, Institut d'Astronomie et de Geophysique Georges Lemaitre, Université Catholique de Louvain, 1348 Louvain-la-Neuve, Belgium, 1978. a.

[7] Berger, A. L. Long-Term Variations of Daily Insolation and Quaternary Climatic Changes. *J. Atmos. Sci.*, 35(12):2362–2367, 1978. b.

[8] Blunier, T., Chapellaz, J., Schwander, J., Stauffer, B., and Raynaud, D. Variations in the Atmospheric Methane Concentration During the Holocene Epoch. *Nature*, 374:46–49, 1995.

[9] Braconnot, P., Joussaume, S., Marti, O., and de Noblet, N. Synergistic Feedbacks from Ocean and Vegetation on the African Monsoon Response to Mid-Holocene Insolation. *Geophys. Res. Lett.*, 26(16):2481–2484, 1999.

[10] Braconnot, P., Marti, O., Joussaume, S., and Leclainche, Y. Ocean Feedback in Response to 6 kyr BP Insolation. *J. Clim.*, 13:1537–1553, 2000.

[11] Brenner, S. Response of an Ocean Mixed Layer Model in 30-Day December Forecasts with a Coupled Ocean-Atmosphere Model. *J. Clim.*, 9:3337–3356, 1996.

[12] Broström, A., Coe, M., Harrison, S. P., Gallimore, R., Kutzbach, J. E., Foley, J., Prentice, I. C., and Behling, P. Land Surface Feedbacks and Palaeomonsoons in Northern Africa. *Geophys. Res. Lett.*, 25(19):3615–3618, 1998.

[13] Brovkin, V., Claussen, M., Petoukhov, V., and Ganopolski, A. On the Stability of the Atmosphere-Vegetation System in the Sahara/Sahel Region. *J. Geophys. Res.*, 103(D24):31613–31624, 1998.

[14] Bryson, R. A. A Macrophysical Model of the Holocene Intertropical Convergence and Jetstream Positions and Rainfall for the Saharan Region. *Meteor. Atmos. Phys.*, 47:247–258, 1992.

[15] Carrington, D. P., Gallimore, R. G., and Kutzbach, J. E. Climate Sensitivity to Wetlands and Wetland Vegetation in Mid-Holocene North Africa. *Clim. Dyn.*, 17:151–157, 2001.

[16] Charney, J. G. Dynamics of Deserts and Droughts in the Sahel. *Q. J. R. Meteor. Soc.*, 101(428):193–202, 1975.

[17] Cheddadi, R., Lamb, H. F., Guiot, J., and van der Kaars, S. Holocene Climatic Change in Morocco: A Quantitative Reconstruction from Pollen Data. *Clim. Dyn.*, 14:883–890, 1998.

[18] Chou, M.-D., Kratz, D. P., and Ridgway, W. Infrared Radiation Parameterizations in Numerical Climate Models. *J. Clim.*, 4:424–437, 1991.

[19] Claussen, M. and Gayler, V. The Greening of the Sahara During the Mid-Holocene: Results of an Interactive Atmosphere-Biome Model. *Global Ecol. Biogeogr. Lett.*, 6:369–377, 1997.

[20] Claussen, M., Kubatzki, C., Brovkin, V., and Ganopolski, A. Simulation of an Abrupt Change in Saharan Vegetation in the Mid-Holocene. *Geophys. Res. Lett.*, 26(14):2037–2040, 1999.

[21] Coe, M. T. and Bonan, G. B. Feedbacks Between Climate and Surface Water in Northern Africa During the Middle Holocene. *J. Geophys. Res.*, 102(D10):11087–11101, 1997.

[22] COHMAP Members. Climatic Changes of the Last 18,000 Years: Observations and Model Simulations. *Science*, 241:1043–1052, 1988.

[23] COHMAP Members. Oxford Lake Levels Database. IGBP PAGES/World Data Center-A for Paleoclimatology, Data Contribution Series # 94-028. NOAA/NGDC Paleoclimatology Program, Boulder CO, USA, 1994.

[24] Cronin, T. M. *Principles of Paleoclimatology*, chapter IV: Orbital Climate Change, pages 141–148. Columbia University Press, New York Chichester, West Sussex, 1999.

[25] de Menocal, P., Ortiz, J., Guilderson, T., Adkins, J., Sarnthein, M., Baker, L., and Yarusinsky, M. Abrupt Onset and Termination of the African Humid

Period: Rapid Climate Responses to Gradual Insolation Forcing. *Quat. Sci. Rev.*, 19:347–361, 2000.

[26] de Noblet-Ducoudré, N., Claussen, M., and Prentice, C. Mid-Holocene Greening of the Sahara: First Results of the GAIM 6000 Year BP Experiment with Two Asynchronously Coupled Atmosphere/Biome Models. *Clim. Dyn.*, 16:643–659, 2000.

[27] Doherty, R., Kutzbach, J., Foley, J., and Pollard, D. Fully Coupled Climate/Dynamical Vegetation Model Simulations over Northern Africa During the Mid-Holocene. *Clim. Dyn.*, 16:561–573, 2000.

[28] Druyan, L. M. GCM Studies of the African Summer Monsoon. *Clim. Dyn.*, 2(2):117–126, 1987.

[29] Druyan, L. M. Advances in the Study of Sub-Saharan Drought. *Int. J. Climatol.*, 9:77–90, 1989.

[30] Druyan, L. M. and Koster, R. D. Sources of Sahel Precipitation for Simulated Drought and Rainy Seasons. *J. Clim.*, 2:1438–1446, 1989.

[31] Eltahir, E. A. B. The Role of Vegetation in Sustaining Large-Scale Atmospheric Circulations in the Tropics. *J. Geophys. Res.*, 101(D2):4255–4268, 1996.

[32] Eltahir, E. A. B. A Soil Moisture Rainfall Feedback Mechanism 1. Theory and Observations. *Water Resour. Res.*, 34(4):765–776, 1998.

[33] Eltahir, E. A. B. and Bras, R. L. Description of Rainfall Interception over Large Areas. *J. Clim.*, 6:1002–1008, 1993.

[34] Eltahir, E. A. B. and Gong, C. Dynamics of Wet and Dry Years in West Africa. *J. Clim.*, 9:1030–1042, 1996.

[35] Emanuel, K. A Scheme for Representing Cumulus Convection in Large-Scale Models. *J. Atmos. Sci.*, 48:2313–2335, 1991.

[36] Emanuel, K. A. On Thermally Direct Circulations in Moist Atmospheres. *J. Atmos. Sci.*, 52(9):1529–1534, 1995.

[37] Emanuel, K. A., Neelin, J. D., and Bretherton, C. S. On Large Scale Circulations in Convecting Atmospheres. *Q. J. R. Meteor. Soc.*, 120:1111–1143, 1994.

[38] Felzer, B., Webb III, T., and Oglesby, R. J. The Impact of Ice Sheets, CO_2, and Orbital Insolation on Late Quaternary Climates: Sensitivity Experiments with a General Circulation Model. *Quat. Sci. Rev.*, 17:507–534, 1998.

[39] Foley, J. A. The Sensitivity of the Terrestrial Biosphere to Climatic Change: A Simulation of the Middle Holocene. *Global Change Biology*, 8(4):505–525, 1994.

[40] Foley, J. A., Levis, S., Costa, M. H., Cramer, W., and Pollard, D. Incorporating Dynamic Vegetation Cover within Global Climate Models. *Ecol. Appl.*, 10(6):1620–1632, 2000.

[41] Foley, J. A., Levis, S., Prentice, I. C., Pollard, D., and Thompson, S. L. Coupling Dynamic Models of Climate and Vegetation. *Global Change Biology*, 4:561–579, 1998.

[42] Foley, J. A., Prentice, I. C., Ramankutty, N., Levis, S., Pollard, D., Sitch, S., and Haxeltine, A. An Integrated Biosphere Model of Land Surface Processes, Terrestrial Carbon Balance, and Vegetation Dynamics. *Global Biogeochem. Cycles*, 10:603–628, 1996.

[43] Fontes, J. C. and Gasse, F. PALHYDAF (Palaeohydrology in Africa) Program: Objectives, Methods, Major Results. *Palaeogeogr., Palaeoclimatol., Palaeoecol.*, 84:191–215, 1991.

[44] Ganopolski, A., Kubatzki, C., Claussen, M., Brovkin, V., and Petoukhov, V. The Influence of Vegetation-Atmosphere-Ocean Interaction on Climate During the Mid-Holocene. *Science*, 280:1916–1919, 1998.

[45] Gasse, F. and Fontes, J.-C. Palaeoenvironments and Palaeohydrology of a Tropical Closed Lake (Lake Asal, Dibouti) Since 10,000 Yr B.P. *Palaeogeogr., Palaeoclimatol., Palaeoecol.*, 69:67–102, 1974.

[46] Gasse, F. and Van Campo, E. Abrupt Post-Glacial Climate Events in West Asia and North Africa Monsoon Domains. *Earth and Planet. Sci. Lett.*, 126:435–456, 1994.

[47] Gong, C. and Eltahir, E. A. B. Sources of Moisture for Rainfall in West Africa. *Water Resour. Res.*, 32:3115–3121, 1996.

[48] Gornitz, V. and NASA. A Survey of Anthropogenic Vegetation Changes in West Africa During the Last Century – Climatic Implications. *Clim. Change*, 7:285–325, 1985.

[49] Guiot, J. Methodology of the Last Climatic Cycle Reconstruction in France from Pollen Data. *Palaeogeogr., Palaeoclimatol., Palaeoecol.*, 80(1):49–69, 1990.

[50] Hall, N. M. J. and Valdes, P. J. A GCM Simulation of the Climate 6000 Years Ago. *J. Clim.*, 10:3–17, 1997.

[51] Hamilton, A. C. Guenon Evolution and Forest History. In Gautier-Hion, A., Bourliere, F., and Gautier, J.-P., editors, *A Primate Radiation: Evolutionary Biology of the Africa Guenons*, pages 13–34. Cambridge University Press, Cambridge, UK, 1988.

[52] Harrison, S. P., Jolly, D., Laarif, F., Abe-Ouchi, A., Dong, B., Herterich, K., Hewitt, C., Joussaume, S., Kutzbach, J. E., Mitchell, J., de Noblet, N., and Valdes, P. Intercomparison of Simulated Global Vegetation Distributions in Response to 6 kyr BP Orbital Forcing. *J. Clim.*, 11:2721–2742, 1998.

[53] Haynes, C. V. *Natl. Geogr. Soc. Res. Rep.*, 19:269–341, 1985.

[54] Hoelzmann, P., Jolly, D., Harrison, S. P., Laarif, F., Bonnefille, R., and Pachur, H.-J. Mid-Holocene Land-Surface Conditions in Northern Africa and the Ara-

bian Peninsula: A Dataset for the Analysis of Biogeophysical Feedbacks in the Climate System. *Global Biogeochem. Cycles*, 12:35–51, 1998.

[55] Hoelzmann, P., Kruse, H. J., and Rottinger, F. Precipitation Estimates for the Eastern Sahara Palaeomonsoon Based on a Water Balance Model of the West Nubian Palaeolake Basin. *Global Planet. Change*, 26:105–120, 2000.

[56] Holtslag, A. A. M. and Boville, B. A. Local Versus Non-Local Boundary-Layer Diffusion in a Global Climate Model. *J. Clim.*, 6:1825–1842, 1993.

[57] Hooghiemstra, H. Variations of the NW African Trade Wind Regime During the Last 140,000 Years: Changes in Pollen Flux Evidenced by Marine Sediment Records. In Leinen, M. and Sarnthein, M., editors, *Paleoclimatology and Paleometeorology: Modern and Past Patterns of Global Atmospheric Transport, NATO ASI Series. Series C, Mathematical and Physic*, pages 733–770. Kluwer Academic Publishers, Dordrecht, Holland, 1989.

[58] Huntley, B. and Prentice, I. C. Holocene Vegetation and Climates of Europe. In Wright, H. E., editor, *Global Climates since the Last Glacial Maximum*, pages 136–168. University of Minnesota Press, Minneapolis, MN, 1993.

[59] Jolly, D. and 32 co-authors. Biome Reconstruction from Pollen and Plant Macrofossil Data for Africa and the Arabian Peninsula at 0 and 6000 Years. *J. Biogeog.*, 25:1007–1027, 1999.

[60] Jolly, D., Harrison, S. P., Damnati, B., and Bonnefille, R. Simulated Climate and Biomes of Africa During the Late Quaternary: Comparison with Pollen and Lake Status Data. *Quat. Sci. Rev.*, 17:629–657, 1998.

[61] Joussaume, S. and 35 co-authors. Monsson Changes for 6000 Years Ago: Results of 18 Simulations from the Paleoclimate Modeling Intercomparison Project (PMIP). *Geophys. Res. Lett.*, 26(7):859–862, 1999.

[62] Joussaume, S. and Braconnot, P. Sensitivity of Paleoclimate Simulation Results to Season Definitions. *J. Geophys. Res.*, 102(D2):1943–1956, 1997.

[63] Knorr, W., Hoelzmann, P., Pinty, B., Govaerts, Y., and Schnitzler, K.-G. Beyond Charney: Evidence for a Combined Vegetation - Lake Drying Albedo Feedback Amplifying Holocene Climate Changes in North Africa. American Geophysical Union, Fall 2000 Meeting, 2000.

[64] Kohfeld, K. E. and Harrison, S. P. How Well Can We Simulate Past Climates? Evaluating the Models Using Global Palaeoenvironmental Datasets. *Quat. Sci. Rev.*, 19:321–346, 2000.

[65] Kutzbach, J. E. Estimates of Past Climates at Paleolake Chad, North Africa, Based on a Hydrological and Energy-Balance Model. *Quat. Res.*, 14:210–223, 1980.

[66] Kutzbach, J. E. Monsoon Climate of the Early Holocene: Climate Experiment with the Earth's Orbital Parameters for 9000 Years Ago. *Science*, 214:59–61, 1981.

[67] Kutzbach, J. E. and Guetter, P. J. The Influence of Changing Orbital Parameters and Surface Boundary Conditions on Climate Simulations for the Past 18 000 Years. *J. Atmos. Sci.*, 43(16):1726–1760, 1986.

[68] Kutzbach, J. E. and Liu, Z. Response of the African Monsoon to Orbital Forcing and Ocean Feedbacks in the Middle Holocene. *Science*, 278:440–443, 1997.

[69] Kutzbach, J., Bonan, G., Foley, J., and Harrison, S. P. Vegetation and Soil Feedbacks on the Response of the African Monsoon to Orbital Forcing in the Early to Middle Holocene. *Nature*, 384(19/26):623–626, 1996.

[70] Kvamstø, N. G. An Investigation of Diagnostic Relations Between Stratiform Fractional Cloud Cover and Other Meteorological Parameters in Numerical Weather Prediction Models. *J. Appl. Meteor.*, pages 200–216, 1991.

[71] Lamb, H. F., Gasse, F., Benkaddour, A., El Hamouti, N., van der Kaars, S., Perkins, W. T., Pearce, N. J., and Roberts, C. N. Relation Between

Century-Scale Holocene Arid Intervals in Tropical and Temperate Zones. *Nature*, 373(12):134–137, 1995.

[72] Lamb, P. J. Large-Scale Tropical Atlantic Surface Circulation Patterns Associated with Sub-Saharan Weather Anomalies. *Tellus*, 30:240–251, 1978.

[73] Levitus, S. and Boyer, T. World Ocean Atlas 1994. Volume 4: Temperature. Technical report, NOAA/NESDIS, 1994. Facilitated by the LDEO/IRI Data Library.

[74] Lézine, A. M. Late Quaternary Vegetation and Climate of the Sahel. *Quat. Res.*, 32:317–334, 1989.

[75] Lézine, A. M. and Casanova, J. Pollen and Hydrological Evidence for the Interpretation of Past Climate in Tropical West Africa During the Holocene. *Quat. Sci. Rev.*, 8:45–55, 1989.

[76] Liu, Z., Gallimore, R. G., Kutzbach, J. E., Xu, W., Golubev, Y., Behling, P., and Selin, R. Modeling Long-Term Climate Changes with Equilibrium Asynchronous Coupling. *Clim. Dyn.*, 15:325–340, 1999.

[77] Lorius, C., Raynaud, D., Petit, J. R., Jouzel, J., and Merlivate, L. Late-Glacial Maximum-Holocene Atmospheric and Ice-Thickness Changes from Antarctic Ice-Core Studies. *Ann. Glaciol.*, 5:88–94, 1984.

[78] Maley, J. Dust, Clouds, Rain Types and Climatic Variations in Tropical North Africa. *J. Quat. Res.*, 18:1–6, 1982.

[79] Maley, J. Middle to Late Holocene Changes in Tropical Africa and Other Continents: Palaeomonsoon and Sea Surface Temperature Variations. In Nuzhet-Dalfes, H., Kukla, G., and Weiss, H., editors, *Third Millenium BC Climate Change and Old World Collapse*, volume 149 of *NATO ASI Series. Series I, Global Environment*, pages 611–640. Springer-Verlag, 1997.

[80] Martin, P. H. Land-Surface Characterization in Climate Models: Biome-Based Parameter Inference Is Not Equivalent to Local Direct Estimation. *J. Hydrol.*, 212–213:287–303, 1998.

[81] Masson, V. and Joussaume, S. Energetics of the 6000-Yr BP Atmospheric Circulation in Boreal Summer, from Large-Scale to Monsoon Areas: A Study with Two Versions of the LMD AGCM. *J. Clim.*, 10:2888–2903, 1997.

[82] Middleton, N. Desertification and Wind Erosion in the Western Sahel: The Example of Mauritania. Technical Report 40, School of Geography. University of Oxford, 1987.

[83] Morley, J. J. and Dworetzky, B. A. Holocene Temperature Patterns in the South Atlantic, Southern and Pacific Oceans. In Wright, H. E., editor, *Global Climates since the Last Glacial Maximum*, pages 125–135. University of Minnesota Press, Minneapolis, MN, 1993.

[84] Moulin, C., Lambert, C., Dulac, F., and Dayan, U. Control of Atmospheric Export of Dust from North Africa by North Atlantic Oscillation. *Nature*, 387:691–694, 1997.

[85] Neftel, A., Oeschger, H., Schwander, J., Stauffer, B., and Zumbrunn, R. Ice Core Sample Measurements Give Atmospheric CO_2 Content During the Past 40,000 Yr. *Nature*, 295:220–223, 1982.

[86] Otto-Bliesner, B. L. El Niño/La Niña and Sahel Precipitation During the Middle Holocene. *Geophys. Res. Lett.*, 26(1):87–90, 1999.

[87] Pachur, H.-J. and Altmann, N. The Quaternary (Holocene, ca., 8,000 a BP). *Palaeogeographic-Palaeotectonic Atlas of Northeastern Africa, Arabia and Adjacent Areas*, pages 111–125, 1997.

[88] Pachur, H.-J. and Hoelzmann, P. Paleoclimatic Implications of Late Quaternary Lacustrine Sediments in Western Nubia, Sudan. *Quat. Res.*, 36:257–276, 1991.

[89] Pachur, H.-J. and Rottinger, F. Evidence for a Large Extended Palaeolake in the Eastern Sahara as Revealed by Spaceborne Radar Lab Images. *Remote Sens. Environ.*, pages 437–440, 1997.

[90] Palmer, T. N. Influence of the Atlantic, Pacific and Indian Oceans on Sahel Rainfall. *Nature*, 322:251–253, 1986.

[91] Park, J. and Oglesby, R. J. A Comparison of Precession and Obliquity Effects in a Cretaceous Palaeoclimate Simulation. *Geophys. Res. Lett.*, 17(11):1929–1932, 1990.

[92] Peltier, W. Time Dependent Topography Through Glacial Cycle. IGBP PAGES/World Data Center-A for Paleoclimatology, Data Contribution Series # 93-015. NOAA/NGDC Paleoclimatology Program, Boulder CO, USA, 1993.

[93] Petit-Maire, N. Le Sahara á l'Holocene: Mali, scale 1:1,000,000, CCGM. Technical report, Inst. Géogr. Nat., Oarus, 1988.

[94] Petit-Maire, N. Interglacial Environments in Presently Hyperarid Sahara: Palaeoclimatic Implications. In Leinen, M. and Sarnthein, M., editors, *Paleoclimatology and Paleometeorology: Modern and Past Patterns of Global Atmospheric Transport, NATO ASI Series. Series C, Mathematical and Physic*, pages 637–661. Kluwer Academic Publishers, Norwell MA, USA, 1989.

[95] Petit-Maire, N. The Sahara in the Holocene. IGBP PAGES/World Data Center-A for Paleoclimatology Data Contribution Series # 94-002. NOAA/NGDC Paleoclimatology Program, Boulder CO, USA, 1994.

[96] Petit-Maire, N., Commelin, D., Fabre, J., and Fontugne, M. First Evidence for Holocene Rainfall in the Tanezrouft Hyperdesert and its Margins. *Palaeogeogr., Palaeoclimatol., Palaeoecol.*, 79:333–338, 1990.

[97] Petit-Maire, N., Fontugne, M., and Rouland, C. Atmospheric Methane Ratio and Environmental Changes in the Sahara and Sahel During the Last 130 Kyrs. *Palaeogeogr., Palaeoclimatol., Palaeoecol.*, 86:197–204, 1991.

[98] Petit-Maire, N. and Guo, Z. Holocene Palaeoprecipitation over the Present-Day Sahara Desert: Implications for the Future. *Episodes*, 20(4):232–234, 1997.

[99] Petit-Maire, N. and Riser, J. Sahara ou Sahel? Quaternaire Récent du Bassin de Taoudenni (Mali). Lamy, Marseille, 1983.

[100] Petit-Maire, N. and Riser, J. Holocene Palaeohydrology of the Niger. *Palaeoecol. Afr.*, 18:135–141, 1987.

[101] Phillips, P. J. and Held, I. M. The Response of Orbital Perturbations in an Atmospheric Model Coupled to a Slab Ocean. *J. Clim.*, 7:767–782, 1994.

[102] Pinty, B., Roveda, F., Verstraete, M. M., Gobron, N., Govaerts, Y., Martonchik, J. V., Diner, D. J., and Kahn, R. A. Surface Albedo Retrieval from Meteosat: 1. Theory. *J. Geophys. Res.*, 105(D14):18099–18112, 2000. a.

[103] Pinty, B., Roveda, F., Verstraete, M. M., Gobron, N., Govaerts, Y., Martonchik, J. V., Diner, D. J., and Kahn, R. A. Surface Albedo Retrieval from Meteosat: 2. Applications. *J. Geophys. Res.*, 105(D14):18113–18134, 2000. b.

[104] Plumb, R. A. and Hou, A. Y. The Response of a Zonally Symmetric Atmosphere to Subtropical Thermal Forcing: Threshold Behaviour. *J. Atmos. Sci.*, 49:1790–1799, 1992.

[105] Prell, W. L. and Kutzbach, J. E. Monsoon Variability over the Past 150,000 Years. *J. Geophys. Res.*, 92(D7):8411–8425, 1987.

[106] Prentice, I. C., Cramer, W., Harrison, S. P., Leemans, R., Monserud, R. A., and Solomon, A. M. A Global Biome Model Based on Plant Physiology and Dominance, Soil Properties and Climate. *J. Biogeog.*, 19:117–134, 1992.

[107] Prentice, I. C. and Thompson, W. I. BIOME 6000: Reconstructing Global Mid-Holocene Vegetation Patterns from Palaeoecological Records. *J. Biogeog.*, 25:997–1005, 1998.

[108] Prospero, J. M. and Nees, R. T. Dust Concentration in the Atmosphere of the Equatorial North Atlantic; Possible Relationship to Sahelian Drought. *Science*, 196:1196–1198, 1977.

[109] Raynaud, D., Jouzel, J., Barnola, J. M., Chappelaz, J., Delmas, R. J., and Lorius, C. The Ice Record of Greenhouse Gases. *Science*, 259:926–934, 1993.

[110] Ritchie, J. C., Eyles, C. H., and Haynes, C. V. Sediment and Pollen Evidence for an Early to Mid-Holocene Humid Period in the Eastern Sahara. *Nature*, 314:352–354, 1985.

[111] Rossignol-Strick, M. Mediterranean Quaternary Sapropels and Immediate Response of the African Monsoon to Variations in Insolation. *Palaeogeogr., Palaeoclimatol., Palaeoecol.*, 49:237–263, 1985.

[112] Rossignol-Strick, M. and Duzer, D. West African Vegetation and Climate Since 22,000 BP from Deep-Sea Cores Palynology. *Plant Ecol.*, 11(2):105–134, 1979.

[113] Rossignol-Strick, M., Nesteroff, V., Olive, P., and Vergnand-Grazzini, C. After the Deluge: Mediterranean Stagnation and Sapropel Formation. *Nature*, 295:105–110, 1982.

[114] Ruddiman, W. F. and Mix, A. C. The North and Equatorial Atlantic at 9000 and 6000 Yr B.P. In Wright, H. E., editor, *Global Climates since the Last Glacial Maximum*, pages 94–124. University of Minnesota Press, Minneapolis, MN, 1993.

[115] Sandweiss, D. H., Richardson, J. B., Reitz, E. J., Rollins, H. B., and Maasch, K. A. Geoarchaeological Evidence from Peru for a 5000 years B.P. Onset of El Niño. *Science*, 273:1531–1533, 1996.

[116] Saravanan, R. and Chang, P. Oceanic Mixed Layer Feedback and Tropical Atlantic Variability. *Geophys. Res. Lett.*, 26(24):3629–3632, 1999.

[117] Saravanan, R. and McWilliams, J. C. Advective Ocean-Atmosphere Interaction: An Analytical Stochastic Model with Implications for Decadal Variability. *J. Clim.*, 11:165–188, 1998.

[118] Sarnthein, M. Sand Deserts During Glacial Maximum and Climatic Optimum. *Nature*, 272:43–46, 1978.

[119] Schneider, J. L. Evolution du Dernier Lacustre et Peuplements Préhistoriques aux Bas-Pays du Tchad. *Bulletin. Association Sénégalaise pour l' Etude du Quaternaire en Afrique*, pages 18–23, 1967.

[120] Shuttleworth, W. J. Evaporation from Amazonia Rainforest. *Proc. Roy. Soc. (B)*, 233:321–346, 1988.

[121] Smith, T. M. and Reynolds, R. W. A High Resolution Global Sea Surface Temperature Climatology for the 1961-90 Base Period. *J. Clim.*, 11:3320–3323, 1998.

[122] Street, F. A. and Grove, A. T. Environmental and Climatic Implications of Late Quaternary Lake-Level Fluctuations in Africa. *Nature*, 261:385–390, 1976.

[123] Street-Perrott, F. A. and Perrott, R. A. Holocene Vegetation, Lake Levels, and Climate of Africa. In Wright, H. E., editor, *Global Climates since the Last Glacial Maximum*, pages 318–352. University of Minnesota Press, Minneapolis, MN, 1993.

[124] Sutton, R. T., Jewson, S. P., and Rowell, D. P. The Elements of Climate Variability in the Tropical Atlantic Region. *J. Clim.*, 13:3261–3284, 2000.

[125] Texier, D., de Noblet, N., and Braconnot, P. Sensitivity of the African and Asian Monsoons to Mid-Holocene Insolation and Data-Inferred Surface Changes. *J. Clim.*, 13(1):164–181, 2000.

[126] Texier, D., de Noblet, N., Harrison, S. P., Haxeltine, A., Jolly, D., Joussaume, S., Laarif, F., Prentice, I. C., and Tarasov, P. Quantifying the Role of Biosphere-Atmosphere Feedbacks in Climate Change: Coupled Model Simulations for 6000

Years BP and Comparison with Palaeodata for Northern Eurasia and Northern Africa. *Clim. Dyn.*, 13:865–882, 1997.

[127] Tucker, C. J. and Nicholson, S. E. Variations in the Size of the Sahara Desert from 1980 to 1997. *Ambio*, 28(7):587–591, 1999.

[128] UNESCO. When the Sahara Desert Was a Blooming Garden. *The UNESCO Courier*, XV(5):16–17, 1962.

[129] USGS Global Land Cover Characterization Data. USGS EROS Data Center. Distributed Active Archive Center. http://edcdaac.usgs.gov/glcc/glcc.html.

[130] Vincens, A., Chalie, F., Bonnefille, R., Guiot, J., and Tiercelin, J. J. Pollen-Derived Rainfall and Temperature Estimates from Lake Tanganyika and Their Implication for Late Pleistocene Water Levels. *Quat. Res.*, 40(3):343–350, 1993.

[131] Wang, G. *The Role of Vegetation Dynamics in the Climate of West Africa.* PhD thesis, MIT, 2000.

[132] Wang, G. and Eltahir, E. A. B. Biosphere-Atmosphere Interactions over West Africa. 1: Development and Validation of a Coupled Dynamic Model. *Q. J. R. Meteor. Soc.*, 126(565):1239–1260, 2000. a.

[133] Wang, G. and Eltahir, E. A. B. Biosphere-Atmosphere Interactions over West Africa. 2: Multiple Climate Equilibria. *Q. J. R. Meteor. Soc.*, 126(565):1261–1280, 2000. b.

[134] Wang, G. and Eltahir, E. A. B. Ecosystem Dynamics and the Sahel Drought. *Geophys. Res. Lett.*, 27(6):795–798, 2000. c.

[135] Wang, G. and Eltahir, E. A. B. Role of Vegetation Dynamics in Enhancing the Low-Frequency Variability of the Sahel Rainfall. *Water Resour. Res.*, 36(4):1013–1022, 2000. d.

[136] Xue, Y. and Shukla, J. The Influence of Land Surface Properties on Sahel Climate. Part I: Desertification. *J. Clim.*, 6:2232–2245, 1993.

[137] Yu, G. and Harrison, S. P. An Evaluation of the Simulated Water Balance of Eurasia and Northern Africa at 6000 Yr BP Using Lake Status Data. *Clim. Dyn.*, 12:723–735, 1996.

[138] Zheng, X. *Moist Zonally-Symmetric Models and Their Applications to West African Monsoons*. PhD thesis, MIT, 1997.

[139] Zheng, X. and Eltahir, E. A. B. The Role of Vegetation in the Dynamics of West African Monsoons. *J. Clim.*, 11:2078–2096, 1998.

[140] Zheng, X., Eltahir, E. A. B., and Emanuel, K. A. A Mechanism Relating Tropical Atlantic Spring Sea Surface Temperature and West African Rainfall. *Q. J. R. Meteor. Soc.*, 125:1129–1163, 1999.